Investigation of Atomic Clusters in Ion Traps

I n a u g u r a l d i s s e r t a t i o n

zur

Erlangung des akademischen Grades eines

Doktors der Naturwissenschaften

der

Mathematisch-Naturwissenschaftlichen Fakultät

der

Ernst-Moritz-Arndt-Universität Greifswald

vorgelegt von

Franklin Leon Martinez

geboren am 28.11.1977

in Berlin

Greifswald, 15. Juni 2012

Dekan:	Prof. Dr. Klaus Fesser
1. Gutachter:	Prof. Dr. Lutz Schweikhard
2. Gutachter:	Prof. Dr. Karl-Heinz Meiwes-Broer
Tag der Promotion:	02. November 2012

Contents

List of Figures

List of Abbreviations and Notations

ET ..... electron tunneling
FT-ICR ..... Fourier transform ion cyclotron resonance
ICR ..... ion cyclotron resonance
PES ..... photoelectron spectroscopy
RF ..... radio frequency
SWIFT ..... stored waveform inverse Fourier transform
ToF ..... time of flight

α ..... scaling factor
δ ..... electron spill-out
ϵ_0 ..... vacuum permittivity
τ ..... lifetime
Φ ..... potential height
Φ_0 ..... electric potential difference
ω ..... angular frequency
ω_+ ..... reduced cyclotron frequency
ω_- ..... magnetron frequency
ω_c ..... cyclotron frequency
ω_p ..... parametric frequency
ω_z ..... axial (trapping) frequency
Ω ..... frequency of driving field

$a, a_{[i]}$ ... storage parameter ([i]:index)
A ..... relative ion abundance
A_0 ..... maximum ion abundance
$\vec{B}$ ..... magnetic field strength, $B = |\vec{B}|$
d_0 ..... parameter of trap geometry
e ..... Euler´s number
e ..... elementary charge
$\vec{E}$ ..... electric field strength, $E = |\vec{E}|$
E_e ..... electron energy
EA .... electron affinity (index EA)
h, $\hbar$ .... Planck constant, $\hbar = h/2\pi$
J ..... electron current density
k_B ..... Boltzmann constant

m ..... mass of an ion
m_e ..... mass of the electron
n ..... cluster size (number of atoms)
n_{exp} .... experimental appearance size
$n_{[i]}$ ..... predicted appearance size
n_{min} ... smallest observed cluster size
P ..... tunneling probability
$q, q_{[i]}$ ... storage parameter
Q ..... electric charge of an ion
r_0 ..... smallest trap radius
r_1, r_2 ... turning points (Coulomb pot.)
R ..... cluster radius
R_a ..... atomic radius
t ..... time
t_{obs} ..... observation time
T ..... temperature
U_0 ..... trapping voltage
U_{dc} ..... direct-current voltage
U_{ac} ..... alternating-current voltage
U_T ..... trapping potential depth
v ..... classical electron velocity
V_C ..... Coulomb potential (index VC)
$V_{C,max}$. height of Coulomb potential
W ..... (bulk) work function
z ..... absolute value of charge state
z_0 ..... smallest axial trap-size

1 Introduction: Cluster Research

Oh, this is elementary, my dear fellow! – This well-known saying of a fictitious criminologist, considering logical conclusions to be simple and obvious, reflects the objective of any physicist studying nature. One of many roads to reach this state of understanding is the ongoing search for "elementary" particles. On the way down to the smallest one passes the range of nanoscopic systems, the *atomic clusters*. Too small to be adequately characterized by concepts of solid state physics, but yet too large to fit into models describing single atoms, clusters fill the gap between both research areas. Accordingly, their physical properties are dominated by the number of their constituents, being referred to as the cluster size.
The interatomic bonding determines their properties, too, thus having clusters being categorized accordingly. However, this classification varies from author to author. There is consent that "metal clusters" (e.g. Au, Cu, Al) and "ionic clusters" (NaCl, MgO, KF) are hold together by the respective bond types [RECK95, HABE95, JOHN02, REIN04, ALON05]. In addition, clusters made of e.g. carbon, silicon and germanium may be referred to as "covalent clusters" [RECK95, HABE95, REIN04], "semiconductor clusters" [JOHN02], or "network clusters" [ALON05]. Clusters made of water molecules exhibit hydrogen-bonds and are sometimes considered as an own class of "H-bond-clusters" [RECK95, HABE95]. Finally, rare-gas atoms form clusters due to weak induced dipole forces ("van-der-Waals clusters" or "rare-gas clusters"). Sharing the same bonding type, "molecular clusters" are either considered as an own class [RECK95, JOHN02], or are classed with the "van-der-Waals clusters" [REIN04, ALON05]. Despite this categorization, clusters might exhibit different properties than indicated by the bulk behavior of their atoms, e.g. for some metal clusters a transition from metallic to insulator-like behavior is observed with decreasing cluster size [ISSE05].

Beyond academic interest, atomic clusters entered a wide field of applications. Clusters made of coinage metals are responsible for stained glass windows used in architecture for centuries, while e.g. silver clusters played an important role in analog photography [FAYE86, LEIS96, KELL03]. Today, carbon clusters are in use as reference masses for precision mass spectrometry of heavy nuclides [BLAU03, CHAU07, KETE10] and help to understand growing processes of carbon(-hydrogen) structures in astro-chemistry [SAVI05]. Clusters serve as model systems for catalytic reactions [BOND02, DOPF03, HEIZ04, JENA06, ZHAI10], support the research of biological processes on the molecular level [STAR11, ARIG12] and are of interest in the physics of the earth´s atmosphere [JETZ04, GOKE10]. Deposited on surfaces clusters can self-organize, allowing for nano-engineering [CARU01, BART07]. Finally, clusters are considered as building blocks for new materials [EBER02, CAST09, CLAR09, SCHU11].

For their investigation, clusters are either deposited on a surface [HEIZ04, MEIW07, YOUN08, KULK10, POPO11], dissolved in a liquid or liquid crystal [DUPO10, HEGM07], embedded in helium droplets [TIGG07], or dealt with as free systems in the gas phase [CAST86, KAPP88]. Depending on their environment, clusters may also occur positively or negatively charged. In particular, cluster ions in the gas phase can be manipulated by means of electric and magnetic fields, e.g. being steered as ion beams [MART86, SCOL88, REIS94, PAUL00] or stored in ion traps [GHOS95, MAJO04, BRED09] as discussed in the present thesis. Properties of clusters are extracted from processes like ionization, electron de- and attachment, charge transfer, and fragmentation, mostly in response to photo-, collisional or chemical activation. Detection and analysis of charged reaction products is obtained by several techniques, e.g. by time-of-flight (ToF)[WILE55, MAMY73, WOLL93, MAMY01] or Fourier transform ion cyclotron resonance (FT-ICR) mass spectrometry [COMI74, MARS92, MARS98], ion mobility spectrometry [KANU08] or photoelectron spectroscopy (PES)[KRUI83, GANT88, NEUM01, WANG09, ROHM10].

The size-dependency of the cluster properties is mainly determined by their electronic and geometrical structure. According to their geometrical shapes, in particular for van-der-Waals clusters, shell-closing effects are observed for some cluster sizes, giving rise to enhanced stability with respect to fragmentation [ECHT81]. Likewise, closed electronic shells can stabilize metal clusters [KNIG84]. However, the number of (valence) electrons is not only given by the number of atoms, i.e. the cluster size, but also by the charge state, with attachment or removal of electrons changing the cluster structure. This affects its properties, e.g. the geometrical shape, ionization potential, polarizability, or dissociation energy, making the charge state of a cluster a crucial parameter.

The cluster group in Greifswald investigates charged clusters stored in different types of ion traps. The cluster species studied range from small metal clusters, to carbon clusters (fullerenes), and to microdroplets. Ion storage tools include ion cyclotron resonance (ICR) traps [BROW86, GHOS95, MAJO04, WALS09, ROSE12], radio-frequency (RF) traps [PAUL53, GHOS95, MAJO04, BAND11], electro-static ion-beam traps [ZAJF97, ZAJF04, BRED09, WOLF12], and an electron beam ion trap [MARR88, LEVI88, BEIE01].
The present work comprises recent modifications of the ICR setup ClusterTrap [BECK95, SCHW03], the manipulation of trapped clusters by electric RF-excitation fields, and improvement of trapping techniques regarding production of multiply negatively charged clusters (poly-anionic clusters). The setup has been complemented by a quadrupole ion deflector, and a RF quadrupole trap, including rearrangement of previous components (Article I). Ion storage has been investigated with respect to the unintended removal of a cluster species from an ICR trap upon manipulation of the same or another species. This removal has been ascribed to a particularity of the applied RF-excitation field (Article II). The method of poly-anion production in an ICR trap has been further developed: The switching of the trapping voltage during cluster-ion storage and repeated application of electron attachment extends

the range of accessible cluster sizes and charge states (Article III). This allowed the production of penta-anionic aluminum clusters, which have been investigated with respect to their appearance as a function of cluster size (Article IV).[1]

[1] The references given are only a small selection out of available literature on cluster science. For thesis articles I to IV see Chapter 7.

2 Experimental Tool: Ion Traps

Charged particles can be manipulated by means of electric and magnetic fields, both being of static or dynamic nature, and thus be brought into interaction with other charged or neutral particles or with photons. In crossed-beam experiments the interaction region is well defined, however reaction and observation times are very short due to the relatively high velocities of the particles involved and thus the short duration of the passage through the interaction region. In ion-storage rings, the ion confinement time after an interaction is increased, allowing the observation of delayed reactions. However, ion confinement yet requires high particle velocities, i.e. respectively high kinetic energies of the ions.
In contrast, in an ion trap charged particles can be stored at relatively low kinetic energies. Their motion is restricted to a small, well-defined volume in space, allowing for long reaction and observation times. Localization is demonstrated by the ongoing miniaturization of ion traps within the last years [STIC06]. Ion traps can be operated under vacuum conditions and at atmospheric pressure, and ions can be stored in principle for arbitrarily long times, e.g. for weeks or month [GABR90, DEVO02]. However, in reality the storage duration is limited by experimental conditions, e.g. by perturbation of ion trajectories or by loss of ionic charge, both due to collisions with background gas. Ion loss may also be caused by trapping field perturbations due to trap-electrode imperfections or due to external fields.

Two basic trapping concepts can be distinguished. Either static electric and magnetic fields (e.g. ICR trap, electrostatic trap, Orbitrap, magnetic bottle) are used or electro-dynamic fields (RF trap). Both concepts, and their combinations, allow for a wide range of trap types. On the one hand they differ in their storage restrictions with respect to the ions´ mass, charge sign and energy range. On the other hand they vary with respect to their spatial construction, which affects access to the trap, and size and mobility of experimental setups. For example, ICR traps have only an upper mass limit, thus allowing simultaneous storage over a wide mass range, e.g. from electrons up to large cluster ions, but only as long as all particles have the same charge sign. In RF traps the range of simultaneously storable masses is limited, however ions of positive and negative charge signs are trapped at the same time. Both, an ICR trap and a RF quadrupole trap are involved in this work. They are briefly described in the following sections.

2.1 The ClusterTrap experiment

The ClusterTrap [BECK95, SCHW95, SCHW99] is a setup developed for the production, storage, manipulation and mass-resolved detection of cluster ions. In the original configuration (Fig. 2.1) cluster ions were produced in an external laser-ablation source [WEID91], transferred to and stored in an ICR trap, and there manipulated by collisions with electrons, gas or by laser radiation. Ionic reaction products were subsequently detected and analyzed in a ToF mass spectrometer.

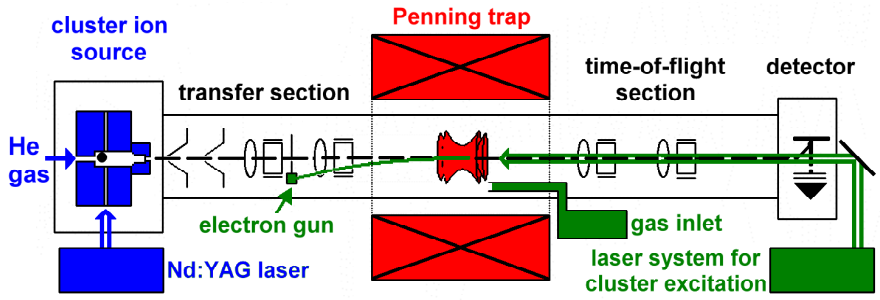

Figure 2.1: Schematic of the ClusterTrap setup, with cluster ion source (left, blue), Penning trap (middle, red) with ion manipulation equipment (middle, green) and ToF mass-spectrometer (right, black). Figure adapted from [HILD98, SCHW03].

The ClusterTrap setup has contributed for almost two decades to the research of metal clusters, including production of poly-cationic and -anionic clusters [SCHW96, KRÜC97, HERL03, WALS10], collision-induced dissociation [SCHW97, KRÜC97b], photofragmentation [HILD98, VOGE01, VOGE03, SCHW03b] and chemical reactions [DIET96, DIET00]. A second research topic has been the investigation and improvement of trapping techniques, including e.g. FT-ICR detection [SCHW90, SCHW90b, BREI07], ion cooling [HASS94], trapping instabilities [SCHW95b], motion of trapped ions [HERL04], and elliptical trapping fields [BREI08]. Of course, both research fields complement each other [SCHW05, WALS09].

The main tool for these investigations, the ICR trap, also called Penning trap, is briefly introduced at this point. Ion confinement is realized by a homogeneous static magnetic field ($B = 5$ T), produced by a super-conducting magnet, and superimposed by a quadrupolar electro-static field supplied by the trapping voltage U_0, which is applied between a hyperbolically shaped ring and two endcap electrodes [BROW86, SCHW03]. The superposition of both fields causes a cyclotron motion of trapped ions at a reduced (angular) cyclotron frequency ω_+, whose center is moving around the trap axis due to an $\vec{E} \times \vec{B}$-drift at the (angular) magnetron frequency ω_-, with

$$\omega_\pm = \frac{\omega_c}{2} \pm \sqrt{\frac{\omega_c^2}{4} - \frac{\omega_z^2}{2}} \qquad \text{and} \qquad \omega_z = \sqrt{\frac{QU_0}{md_0^2}} \quad . \tag{2.1}$$

The "true" angular cyclotron frequency $\omega_c = QB/m$ is given by the ion mass m and charge Q, which also determine the ions´ oscillation perpendicular to the gyration plane at the axial trapping frequency ω_z (Eq. 2.1). The geometry parameter $d_0^2 = r_0^2/4 + z_0^2/2$ is given by the smallest distances of the ring and endcap electrodes to the center of the trap, r_0 and z_0, respectively [BROW86]. In the case of ClusterTrap the electrode geometry is asymptotically symmetric, i.e. $z_0 = r_0/\sqrt{2}$, with a corresponding axial trapping potential depth $U_T = U_0/2$ [KNIG83]. The ring electrode has an inner radius of $r_0 = 20$ mm and is radially divided into 8 segments, which are used for manipulation of the radial ion motion by means of radio-frequency excitation fields, and for ion detection by FT-ICR mass spectrometry [SCHW90]. Manipulation of the ion motion is an important tool for ion preparation in the cluster experiments. But before this technique is described in more detail in Sect. 2.3, the modification of the ClusterTrap, including the implementation of a linear RF trap, is discussed in the next section.

2.2 The new ClusterTrap setup.....Article I

The ClusterTrap setup has been constantly improved and extended, however, only on a minor scale, with respect to the local conditions and the efforts required to access and change interior parts. Thus, some weak points remained throughout time. Only when the setup was disassembled and transferred to the new building of the Institute of Physics, some major changes were introduced. A few previous shortcomings and resulting rearrangements are described below to illustrate the modifications.

Two major additions to the setup are the implementation of a linear radio-frequency quadrupole trap and of an electro-static quadrupole ion deflector between the cluster ion source and the ICR trap, including relocation of the cluster ion source from on-axis to now perpendicular to the main beamline of the experiment (Fig. 2.2). With the quadrupole deflector acting as a "crossing" for ions, further cluster sources and ion detection devices can be added, improving the versatility of the setup. In particular, a detector has been installed upstream the beamline (at the former location of the cluster source), relocating the time-of-flight section to the other side of the superconducting magnet. Thus, access to the ICR trap has been separated according to functionality. Through one endcap electrode, cluster ions are transferred into and extracted from the trap. Through the opposite endcap electrode the guidance of e.g. electron or ion beams or of laser radiation into the trap is realized (Fig. 2.2). Thus, a problem of the old setup, the interference between cluster ion transfer and electron guidance into the Penning trap (Fig. 2.1), has been overcome.

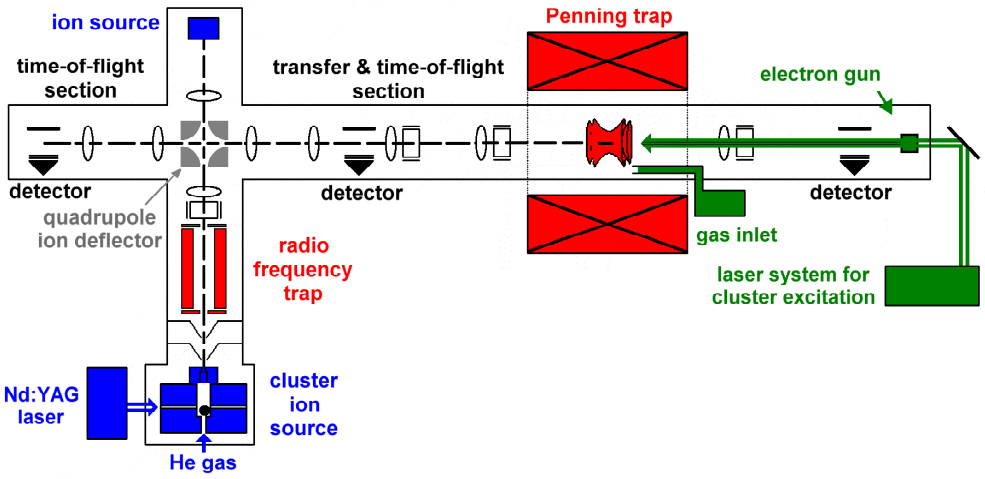

Figure 2.2: Modified ClusterTrap setup, including a quadrupole ion deflector and a radio-frequency trap. Figure adapted from Article I.

The linear RF quadrupole trap, a typical representative of dynamic traps, is shortly introduced at this point. It is based on the RF quadrupole mass-filter, where ions traverse parallel to four RF-electrodes with hyperbolic cross section [GHOS95, MAJO04]. Between pairs of opposite RF-electrodes, an alternating potential difference $\Phi_0(t) = U_{ac} \cos \Omega t + U_{dc}$ is applied (Fig. 2.3a, circular rods are shown instead of hyperbolic electrodes). The corresponding alternating electric field limits the ion trajectories in the plane perpendicular to the rods direction, but there is no axial ion confinement. By use of further electrodes at each end of the rod array, which produce an additional axial trapping field, a linear RF trap is obtained [GHOS95, MAJO04].

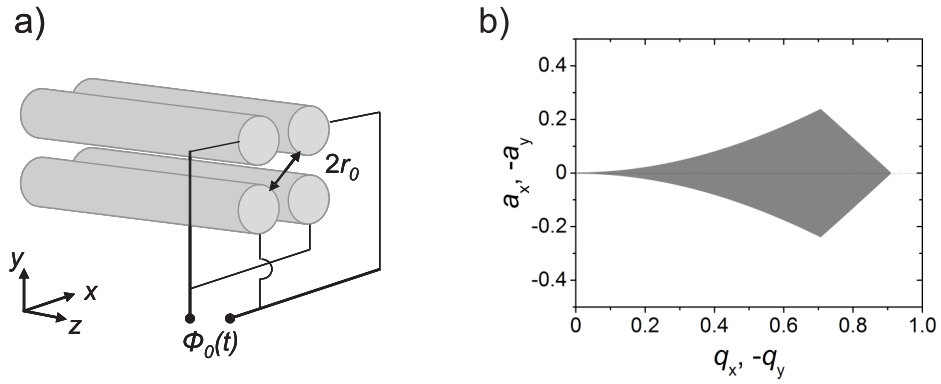

Figure 2.3: (a) Schematic of a quadrupole RF mass-filter, (b) corresponding a-q-stability diagram.

Ion trajectories in the radial plane are obtained by solving the Mathieu-equation for both spatial coordinates, x and y, for which the trapping parameters

$$a_x = -a_y = \frac{4U_{dc}}{r_0^2\Omega^2} \cdot \frac{Q}{m} \qquad \text{and} \qquad q_x = -q_y = -\frac{2U_{ac}}{r_0^2\Omega^2} \cdot \frac{Q}{m} \tag{2.2}$$

are introduced. For a certain range of (a, q)-pairs, i.e. certain combinations of trap values $r_0, U_{dc}, U_{ac}, \Omega$ and ion values m and Q, the solutions of the Mathieu equation correspond to ion trajectories of limited amplitude. If the respective (a_x, q_x)- and (a_y, q_y)-regions overlapp, ion storage in the radial plane is possible [GHOS95, MAJO04]. In a "stability diagram" the overlapp of the respective (a, q)-pairs is visualized (gray-shaded area in Fig. 2.3b). Note, that ion confinement can also be achieved in linear multipole RF traps, e.g. 22-pole traps, requiring a more elaborate description [GERL92].

At ClusterTrap the linear RF quadrupolar trap continuously accumulates ion bunches, which are provided by the pulsed laser ion source. Being equipped with a continuous buffer gas inlet and a set of four additional electrodes, the RF trap cools and bunches the ions in front of its exit endcap [ARND11]. Furthermore, where required a preselection of particular cluster sizes can be realized in the RF trap, e.g. by means of stored waveform inverse Fourier transform (SWIFT) excitation [MARS85]. Eventually, the ion bunch is extracted and transferred into the ICR trap for further experiments. Thus, ion preparation steps are taken away from the ICR trap, and its loading with a sufficient amount of size-selected ions becomes more efficient. In addition, time consumption has been reduced, because the next ion bunch can already be prepared in the RF trap, while the previous ion bunch is still under investigation in the ICR trap.

Further major modifications include the use of a potential lift at the relocated time-of-flight section, and replacement of the complete experimental control and data acquisition system by a new, more sophisticated one [ZIEG12]. With the potential lift, ion energies of several hundreds of electron volts can be used for time-of-flight analysis, without the need to have all ion-optical elements of the respective section on correspondingly high electric potentials.
The previous experiment control system was outdated and therefore had to be replaced. However, one of its special features, namely to perform a reference measurement alternating with the "experiment" measurement, was transferred into the new system and extended to the use of more than two alternating cycles. In addition, the new control system introduces automated scanning of several parameters, e.g. duration of experimental steps, frequency and amplitude of excitation fields, or variation of the potentials applied to several electrodes [ZIEG12].

2.3 Unintended ejection of cluster ions.....Article II

The main tool for cluster investigations at ClusterTrap is the ICR trap. Even though its trapping principle is well known (Sect. 2.1), continuous efforts are made to further develop the techniques for manipulation of trapped ions. This includes the excitation of the radial ion motion, which is briefly introduced in this section.

The motional frequencies of ions in an ICR trap depend on their charge-over-mass ratio Q/m (Sect. 2.1), allowing to selectively address ion species by application of respective RF electric fields. The spatial configuration of the fields and the RF frequency determine their effect on the motion of trapped ions [SCHW93], ranging from ion centering up to ion removal from the trap. For practical use, ICR traps typically feature a ring electrode that is radially divided into at least four segments.[1] Thus, different electric field configurations can be realized for the application of RF fields (Fig. 2.4). The resulting electric fields are either one of three basic types (parametric, dipolar and quadrupolar), or are combinations of those, all with correspondingly different effects on the ion motion.

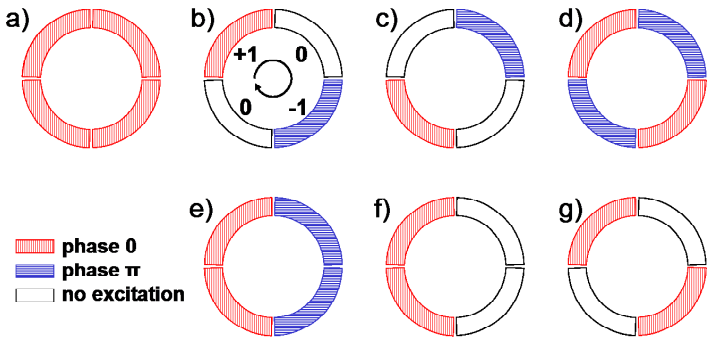

Figure 2.4: Different schemes for radial excitation at a quarter-segmented ring electrode: parametric (a), dipolar (b, c, e), quadrupolar (d), asymmetric dipolar (f) and asymmetric quadrupolar (g).

For parametric excitation, the field-generating RF-signal is applied to the entire ring electrode (i.e. no segmentation required, Fig. 2.4a), resulting in a variation of the trapping potential U_0. It affects the axial ion motion, if applied at the axial parametric frequency $2\omega_z$ (also referred to as axial quadrupolar excitation). If applied at the radial parametric frequency, $\omega_p = \omega_+ - \omega_-$, the radius of both, cyclotron and magnetron motion, is increased (also referred to as radial monopolar excitation) [SCHW93].
For dipolar excitation, two phases of the RF-signal, shifted by π, are applied to halves of the ring, i.e. to pairs of adjacent quarter segments (Fig. 2.4e). Alternatively, they may be applied only to two opposite quarter segments (Fig. 2.4b and c),

[1] In cases where Fourier-Transform ICR detection is used, the number of segments might be increased, as it is the case if higher-order electric fields are to be applied [BREI07, ROSE12].

with correspondingly increased RF-amplitude. Excitation at the frequencies ω_+ or ω_- will increase the radius of the cyclotron or magnetron motion, respectively, until the addressed ions are eventually removed from the trap by hitting the ring electrode [SCHW93]. The dipolar excitation is suitable for ion selection, often used in combination with broad-band SWIFT excitation, where all trapped species within specified cyclotron frequency ranges (respectively mass ranges) are simultaneously removed [MARS85].
For quadrupolar excitation, the RF-signal and its π-shifted counterpart are applied each to a pair of opposite quarter segments, respectively (Fig. 2.4d). Once more, cyclotron and magnetron radius are increased, albeit for application of the doubled frequencies, $2\omega_+$ and $2\omega_-$, respectively. Furthermore, application of the sum frequency, $\omega_+ + \omega_- = \omega_c$ (Eq. 2.1) causes a periodic conversion of kinetic energy between both motions [BOLL90, SCHW93]. In combination with buffer-gas cooling, this excitation scheme is used for selective centering of ions in the trap [SAVA91, SCHW92].

A dipolar and a quadrupolar excitation field can both also be realized in an "asymmetric" fashion, by application of a RF-signal to only one pair of adjacent or opposite segments, respectively, leaving the other segments without excitation signal (Fig. 2.4f and g). However, in those cases the trapping potential at the trap center is varied, as observed for parametric excitation. Thus, the asymmetric dipolar and asymmetric quadrupolar excitation schemes include monopolar terms.
Such combination of two basic excitation fields realized by one excitation scheme can be described and analyzed in a vector model. A vector represents an excitation scheme, with the number of vector components being given by the number of ring segments. The values of the vector components represent the relative RF-signal strength applied to the respective segment. A positive or negative sign indicates the phase of the RF-signal, being 0 or π, respectively (Fig. 2.4b). In the case of a quarter-segmented ring, a set of base vectors can be given by those four excitation schemes, which include all three basic excitation fields mentioned above (Fig. 2.4a–d). From decomposition of an arbitrary vector into this set of base vectors, a quick analysis of the involved basic excitation fields can be obtained. For example, application of an RF-signal to only one of the quarter segments results in an excitation scheme, which includes all three basic excitation modes.

In two specific settings, the effects of asymmetric quadrupolar excitation (Fig. 2.4g) have been experimentally investigated at ClusterTrap. The cyclotron frequency ω_c is independent of the trapping voltage U_0. However, at a particular value of U_0 it coincides with twice the axial frequency $2\omega_z$, which does depend on U_0 (Eq. 2.1). In this case ($\omega_c = 2\omega_z$), a monopolar component contributes to the excitation, causing a loss of ions, as shown for gold clusters, Au_{51}^-.
In another example, aluminum cluster anions, Al_n^- ($n \approx 20 - 75$) were stored at a trapping voltage of $U_0 = 26$ V. Upon centering of Al_{70}^-, a loss of the smaller clusters Al_{29}^- and Al_{63}^- was observed. Again, the monopolar contribution caused this loss, when twice the axial frequency, $2\omega_z$, of Al_{29}^-, and when the parametric frequency ω_p of Al_{63}^- happened to coincide with the cyclotron frequency ω_c of Al_{70}^-.

3 Clusters in Ion Traps: Production of Poly-Anionic Clusters

Poly-anionic clusters are not as well investigated as their positively charged counterparts. In contrast to poly-cations, which are relatively stable in the gas phase with respect to their charge, poly-anions may decay by electron emission. Furthermore, attachment of electrons for the production of poly-anions requires more sophisticated techniques than the production of poly-cations by photoionization[NÄHE92, KÖLL99], electron-impact [VÖLP93, KRÜC97] or ion-impact ionization [CHAN95].

3.1 Electron-bath technique

Most cluster ion sources provide singly negatively charged clusters. In some cases also di-anionic clusters can be produced [SCHA90, LIMB91, HETT91, WANG99, STOE01, HAMP02]. However, production of higher poly-anionic species is unlikely, due to the extreme conditions present in most cluster ion sources (heat, carrier gas, electric fields). Therefore, specific methods for electron attachment had to be developed.

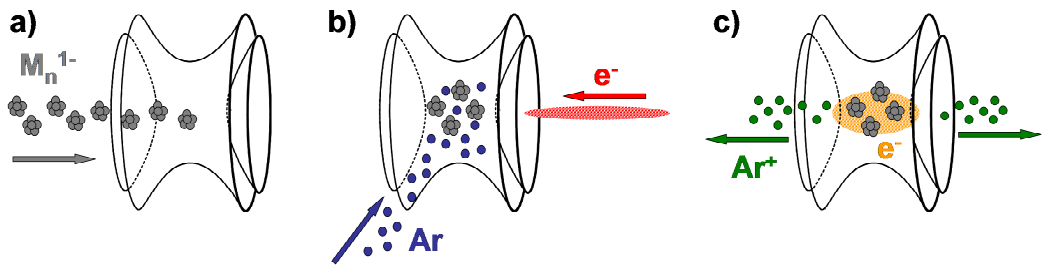

Figure 3.1: Schematic of the electron-bath technique: (a) capture of cluster mono-anions, (b) electron-impact ionization of argon gas inside the trap, (c) withdrawal of argon cations and trapping of low-energy secondary electrons and cluster mono-anions.

One of these methods is the "electron-bath technique" [HERL02, WALS10]. It uses the wide mass range of ICR traps for simultaneous storage of cluster anions

and electrons, and is realized in the following way: After capture of cluster mono-anions (Fig. 3.1a), argon gas is pulsed into the trap volume and there ionized by an electron beam, which is guided through the trap (Fig. 3.1b). While the resulting argon cations leave the trap immediately, the low-energy secondary electrons remain trapped, and may attach to the cluster anions (Fig. 3.1c), thus producing higher charge states.

3.2 The modified electron-bath.....Article III

For the production of poly-anionic clusters, two basic requirements need to be fulfilled. On the one hand, the cluster needs to be big enough, to accommodate a certain number of excess electrons. This issue is discussed in more detail in Chap. 4. On the other hand, the trapped electrons need sufficient energy to overcome the Coulomb potentials of the already negatively charged clusters, in order to attach.

For a given trapping voltage U_0, the ICR trap has an upper limit of the mass-over-charge ratio m/Q for ion trapping. This "mass-limit" corresponds to an upper limit of U_0, for trapping of an ion with a given mass-over-charge ratio. This upper limit of U_0 decreases with increasing ion mass, i.e. cluster size. In addition, it is further lowered if space-charge effects have to be taken into account, as it is the case during application of an electron bath. The production of higher charge states requires bigger clusters, which in turn require lower trapping voltages U_0, because the starting points for the electron bath are always mono-anionic clusters.

At the same time, the trapping potential defines an energy limit for trapped electrons. With such an energy limit, the electrons can only overcome Coulomb potentials of a certain height. But as the Coulomb potential increases with the number of excess electrons already attached to the cluster, the negative charge state that can be produced is limited, too. Evaluation of experimental data showed, that for efficient production of poly-anions, the height of the Coulomb potential should not exceed a fraction of the trapping potential. This behavior is understood by means of the trapped-electron energy distribution, having only a few electrons with the maximum possible energy. Furthermore, the cyclotron motion of the trapped electrons in the magnet field of the ICR trap causes an energy loss due to synchrotron radiation, decreasing the mean electron energy with time.

This means in conclusion, that (a) for a mono-anion of a given cluster size there is a corresponding upper limit of the trapping voltage. And (b), this maximum voltage limits the energy of co-trapped electrons and in this way also the anionic charge state that can be produced by the electron-bath technique. For aluminum cluster poly-anions produced at the ClusterTrap setup, this limit is encountered when heading for the fifth anionic charge state.
As shown in the present study, a way to circumvent this limit is the application of two electron baths, with an intermediate increase of the trapping voltage. During the first electron bath, low charge states, e.g. doubly and triply charged clusters, are

produced. They have a lower mass-over-charge ratio than the mono-anions, with a correspondingly higher limit of the trapping voltage. Thus the trapping voltage can be raised, and while the singly charged clusters are lost, the "pre-charged" clusters remain trapped. They are then subjected to the second electron bath and brought to higher charge states.

This modified electron-bath technique has been applied for the production of the fifth anionic charge state of aluminum clusters. The upper limit of the trapping voltage for storage of the required cluster mono-anions in the size range of about 445 atoms (Sect. 4.1) interferes with the minimum trapping voltage required for electrons to overcome the Coulomb potential of the respective tetra-anionic clusters. This minimum trapping voltage has been determined experimentally, and found to be in good agreement with the trend indicated by previous measurements for lower charge states. Furthermore, the dependency of the upper storage limit of the trapping voltage on space charge effects can be utilized to estimate the electron density of the electron bath [WALS09].

As indicated above, the size of a cluster is important for the production of higher negative charge states. After penta-anionic aluminum clusters had been produced by application of the modified electron bath, the dependency of their production on the cluster size has been investigated and is addressed in the next chapter.

4 Negatively Charged Clusters: Investigation of Appearance Sizes

The amount of electric charge that can be stored by a macroscopic capacitor is limited by its geometrical dimensions. This limit is given by critical electric field strengths that develop upon charging and eventually cause a voltage breakdown. Such a kind of size restriction also applies to the charging limit of atomic clusters with respect to electron emission at a critical electric field strength at the cluster surface. Therefore, a minimum cluster size is required to carry a certain number of excess electrons. This size limit is referred to as the *appearance size*, and depends on element-specific properties. In this chapter, a simple approach to estimate the appearance size of poly-anionic clusters is outlined. Furthermore, a new method for evaluation of experimental data with respect to the appearance size is introduced and applied to poly-anionic aluminum clusters.

4.1 Stability of poly-anionic clusters

For the determination of the appearance size, the stability of poly-anionic clusters with respect to electron emission is considered. For this purpose, the poly-anionic cluster with z excess electrons ($Q = -ze$) is assumed to be composed of a poly-anion with $z-1$ excess electrons (the "precursor" cluster, with respect to electron attachment) and another excess electron (Fig. 4.1a). The appearance size is estimated in three steps, considering the electron affinity, the Coulomb potential, and electron tunneling.

In the conducting-sphere model [JACK98], the cluster is assumed to be spherically shaped. Its radius $R = R_a n^{1/3}$ is given by a sphere, whose volume equals the sum of the volumina of its n atomic constituents. In a classical approach, the electron affinity of a cluster carrying $z-1$ excess electrons, is given by [HERR78, PERD88, SEID94]

$$EA = W - \left[(z-1) + \frac{1}{2}\right] \frac{e^2}{4\pi\epsilon_0 R} \quad , \tag{4.1}$$

with the bulk work function W. Equation (4.1) describes the general trend of the electron affinity. It neglects odd-even-size oscillations that are observed at small clusters due to spin effects [EKAR84]. However, for the estimation of appearance sizes, Eq. (4.1) is adequate, in particular for the larger cluster sizes involved at higher

charge states.
There has been some discussion in literature about Eq. (4.1). First calculations yielded a term of 5/8 (instead of 1/2) [SMIT65, WOOD81, STAV87, BREC95, HALA03], which also better described experimental results with small clusters [WOOD81, KAPP88, BREC89, BREC95]. Later these results were explained by quantum-mechanical effects, and the factor 1/2 is now widely accepted [HERR78, MAKO88, PERD88, HEER90, SEID91, SEID94, MEIW94, ISSE05, SVAN10]. One of the microscopic effects is the electron density reaching beyond the cluster radius [SNID83]. It is taken into account by adding an electron spill-out δ to the cluster radius, $R = R_a n^{1/3} + \delta$. However, for consistent approach, $\delta = 0$ is assumed for the moment.

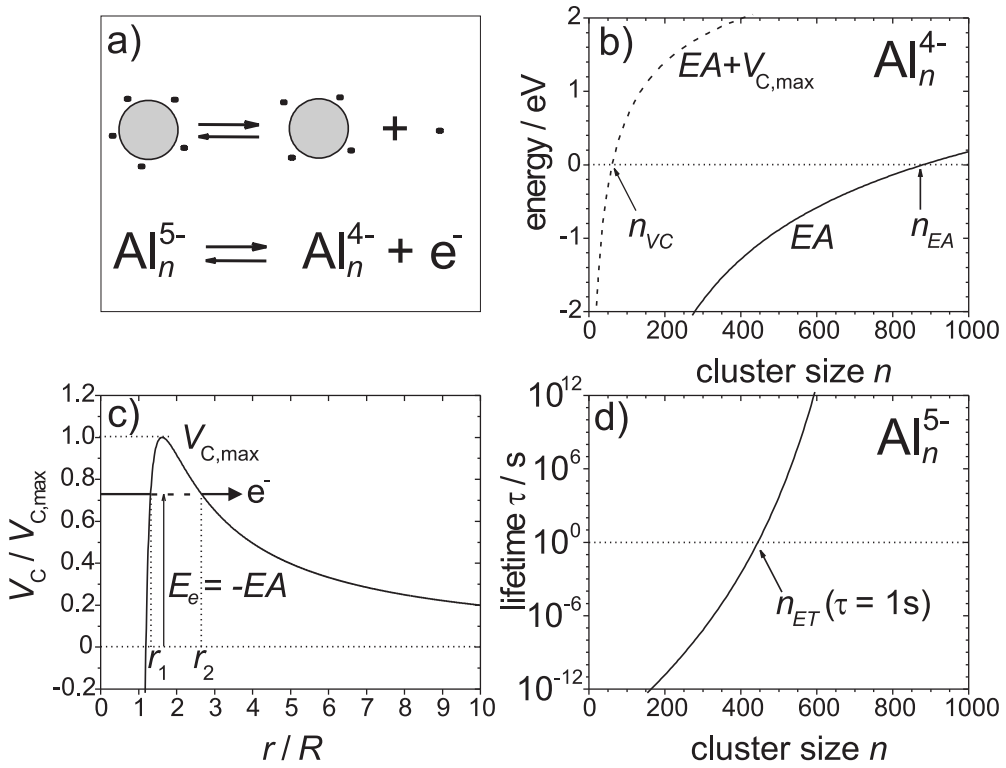

Figure 4.1: (a) Schematic of electron attachment and detachment of Al_n^{4-} and Al_n^{5-}, respectively. (b) Electron affinity of Al_n^{4-} as a function of the cluster size n. (c) Normalized Coulomb potential V_C as a function of the electron distance from the cluster center. (d) Calculated lifetime τ of Al_n^{5-} with respect to electron detachment as a function of the cluster size n. See text for details.

For very large clusters ($R \to \infty$ in Eq. 4.1), the electron affinity approaches the bulk work function W. With decreasing cluster size the electron affinity decreases as well and becomes negative at some cluster size n_{EA} (solid line in Fig. 4.1b). As only clusters with a positive electron affinity can stably bound another excess electron,

n_{EA} defines a lower size limit.
However, the size limit n_{EA} is actually an overestimation of the appearance size, because a poly-anionic cluster exhibits a Coulomb potential (Fig. 4.1c),

$$V_C(r) = \frac{e^2}{4\pi\epsilon_0}\left[\frac{z-1}{r} - \frac{R^3}{2r^2(r^2-R^2)}\right] \quad , \tag{4.2}$$

as given by the image-potential approach [JACK98]. For smaller clusters, for which the electron affinity is already negative ($EA < 0$), the Coulomb potential stabilizes another excess electron as long as the (negative) electron affinity is below the potential maximum, $-EA \leq V_{C,max}$. A corresponding size limit n_{VC} is given by $-EA = V_{C,max}$ (Fig. 4.1b).
Now again, the size limit n_{VC} is underestimating the appearance size, because such a "stabilized" anion is actually meta-stable with respect to electron tunneling (ET) through the Coulomb potential (Fig. 4.1c). A corresponding lifetime estimation of

$$\tau(n,z) = \frac{2r_1}{P \cdot v} \quad , \tag{4.3}$$

can be calculated from the classical electron velocity $v = \sqrt{2E_e/m_e}$, which leads to the "knocking frequency" $v/2r_1$, and from the tunneling probability per try, e.g. given by the Wentzel-Kramers-Brillouin (WKB) approximation,

$$P = exp\left[-\frac{2}{\hbar}\int_{r_1}^{r_2}\sqrt{2m_e(V_C(r)-E_e)}dr\right] \quad , \tag{4.4}$$

with the electron mass m_e. The energy E_e of the electron defines the integration limits r_1 and r_2 (Fig. 4c) as solutions of $V_C(r) = E_e$. In recent publications, E_e is set to $E_e = -EA$ (Fig. 4.1c) [HERL03, WALS09b, WALS10].
For meta-stable clusters ($n_{VC} < n < n_{EA}$), the lifetime increases by orders of magnitude as a function of the cluster size n (Fig. 4.1d). The smallest cluster size, for which the poly-anion has a given lifetime τ, e.g. of the order of 1 s as in typical ion storage experiments, again defines a lower size limit n_{ET} (Fig. 4.1d). Based on the assumption that electron tunneling is the dominant decay channel for poly-anionic clusters, the size limit n_{ET} is considered to be the appearance size.

In recent electron-bath experiments, di-, tri- and tetra-anions of aluminum clusters were produced and observed to increase in abundance as a function of cluster size [WALS07, WALS09b, WALS10]. In the case of the tri- and tetra-anions, the smallest anions observed were below the calculated appearance sizes [WALS09b, WALS10]. For adaption of the calculations, electron affinities of neutral clusters determined in photoelectron spectroscopy experiments were considered, as well as a correction for the electron spill-out [SNID83].

4.2 Appearance size of poly-anionic clusters .....Article IV

With the production of penta-anionic aluminum clusters (Sect. 3.2), the investigation of the appearance cluster size has been extended to the fifth charge state. The penta-anion abundance has been measured as a function of the cluster size in a range around $n = 445$, which is the appearance size n_{ET} estimated from Eqs. (4.1 − 4.4, without spill-out correction). Indeed, a significant increase of the penta-anion abundance has been observed, covering about 100 cluster sizes. The smallest observed penta-anion, Al_{390}^{5-}, is clearly below the estimated appearance size, continuing the trend observed for tri- and tetra-anions [WALS09b, WALS10].

In previous investigations, for a given charge state the smallest poly-anion cluster size observed in experiments, n_{min}, was called the appearance size and compared to the calculated value n_{ET}. In a new approach, the relative abundance of the measured poly-anions is considered for determination of the experimental value of the appearance size, n_{exp}.
Relative ion abundances $A(n)/A_0$ are assumed to depend on the observation time t_{obs} and on the size-dependent lifetimes $\tau(n)$ of the poly-anionic clusters (Eq. 4.3), by means of an exponential decay law, $A(n)/A_0 = \mathrm{e}^{-t_{obs}/\tau(n)}$. As the poly-anion lifetime is expected to increase as a function of the cluster size, also the relative abundance does increase. In other words, smaller poly-anionic clusters appear in lower abundances, in agreement with the observations [WALS07, WALS09b, WALS10].
For the determination of the appearance size with regard to some certain lifetime, the observation time in the experiment is accordingly chosen, e.g. $t_{obs} = 1$ s [WALS07, WALS09b, WALS10]. If the lifetime of the experimental appearance-size cluster fulfills the condition $\tau(n_{exp}) = t_{obs}$, its relative abundance is expected to be $A(n_{exp})/A_0 = 1/\mathrm{e}$. All cluster poly-anions that show smaller abundances do have lifetimes $\tau < t_{obs}$. This is in particular valid for the smallest poly-anion cluster size observed, if it appears in very low abundances [WALS07, WALS09b, WALS10].

The new evaluation method has been applied to the exerimental penta-anion results, as well as to the data of the previously measured tri- and tetra-anionic aluminum clusters [WALS09b, WALS10]. Additionally, the size-dependence of the dianion abundance has been remeasured, as previously suggested [WALS10]. All poly-anion abundances observed (symbols in Fig. 4.2, for Al_n^{3-} and Al_n^{4-}) share a common feature, namely a significantly smaller increase as a function of cluster size than predicted from the lifetime estimations (dotted lines). Furthermore, the onset of the experimental abundance curves is found at smaller sizes than predicted. As mentioned above, this shift has been dealt with before, by inclusion of the electron spill-out δ (dashed lines in Fig. 4.2)[WALS10].
The observed lower increase of the poly-anion abundance indicates an overestimation of the lifetimes by the prediction. This might be explained by the fact, that the calculations neglect any internal excitation of the clusters, assuming "cold" clusters. But as the clusters are most probably at room temperature in the experiments, the

corresponding thermal energy may increase the tunneling probabilities P (Eq. 4.4), and thus decrease the poly-anion lifetimes τ (Eq. 4.3) with respect to electron loss.

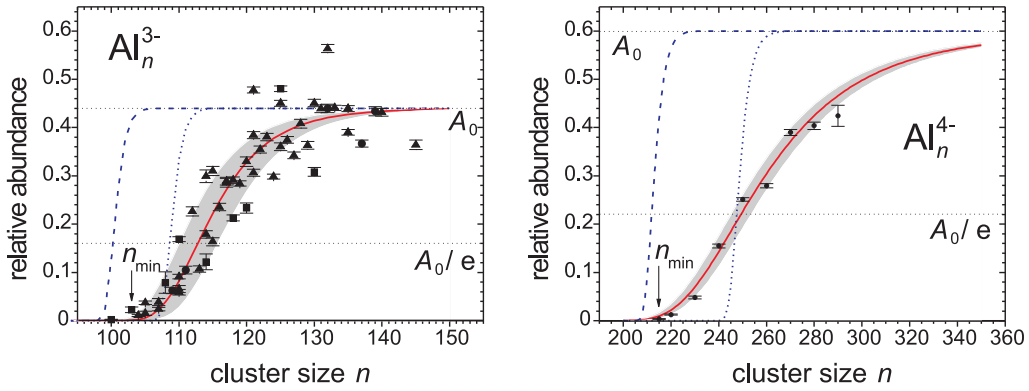

Figure 4.2: Measured tri- and tetra-anion abundances of aluminum clusters (symbols), and model predictions (lines). Experimental data reproduced from [WALS09b, WALS10]. See text for details.

In order to account for the thermal energy an alternative approach has now been introduced based on thermionic electron emission. The Richardson-Dushman equation describes the current density,

$$J = \frac{2\pi m_e (k_B T)^2}{h^3} \cdot exp\left[-\frac{\Phi}{k_B T}\right] \quad , \tag{4.5}$$

of electrons emitted from bulk [DUSH23]. Besides the temperature T, the current density is determined by the potential height Φ, which the electrons have to overcome in order to escape. For bulk material the potential is given by the work function, $\Phi = W$. For the adaption of the Richardson-Dushman equation to poly-anionic clusters, the work function is replaced by the energy difference between the maximum of the Coulomb potential and the electron affinity, $\Phi = V_{C,max} + EA$ (i.e. for negative electron affinities $\Phi < V_{C,max}$). Including the surface area of a spherically-shaped cluster, the current density is transformed into respective lifetimes for electron emission.
However, in contrast to classical thermionic emission, the electrons may be emitted by tunneling through the Coulomb potential before they overcome it. This effect is taken into account by reducing the potential height by a factor α, yielding an "effective" potential height, $\Phi = \alpha(V_{C,max} + EA)$. This factor has been chosen to reproduce the observed ion abundances (solid lines in Fig. 4.2). The same factor is applied to all cluster sizes for a given poly-anionic charge state.

Obviously, the internal energy of clusters decreases their stability, thus increasing the appearance size for a given charge state. Therefore, the cluster sizes with a relative abundance of 1/e in the experimental data represent the appearance sizes n_{exp} of room-temperature poly-anionic aluminum clusters (1/e-levels of solid lines

in Fig. 4.2). In contrast, the appearance sizes n_{ET} predicted from Eqs. (4.1 − 4.4), which neglect any internal energy, refer to "cold" poly-anionic clusters (1/e-levels of dashed lines in Fig. 4.2). In conclusion, the sizes n_{min} of the smallest observed poly-anionic clusters of a given charge state turn out to be a better indicator for the "cold" appearance sizes, than the room temperature appearance sizes.

5 Summary and Outlook

5.1 Summary

This thesis describes investigations of metal clusters stored in an ion-cyclotron-resonance (ICR) trap, as well as corresponding trap research and development. Charged clusters are produced and investigated in the experimental setup ClusterTrap, comprising a cluster-ion source, an ICR trap and a time-of-flight (ToF) mass spectrometer.

In the framework of its move to the new building of the Institute of Physics, new components have been added to the ClusterTrap setup. A radio-frequency ion trap is now used for cluster ion preparation prior to the performance of cluster experiments in the ICR trap. A quadrupole ion deflector allows an optimized usage of the ICR trap, as well as simultaneous use of several ion sources and detectors. The implementation of a potential lift at the ToF mass spectrometer enables a more flexible operation of the setup with ion energies up to several hundreds of electron volts. The new components have been tested and characterized, and the experimental procedures have been adapted.

An important aspect of cluster investigations is the manipulation of trapped ions by application of appropriate excitation fields. For the ICR trap, a vector representation model has been developed for quick analysis of radial excitation fields, applied to the quarter-segmented ring electrode of an ICR trap. Its application has been demonstrated for asymmetric radial quadrupolar excitation of stored cluster ions, confirming the observation of unintended ion ejection from the trap.

Investigation of multiply negatively charged metal clusters at ClusterTrap has been continued. By the "electron-bath" technique, i.e. simultaneous storage of cluster mono-anions and electrons in the ICR trap, high charge states are produced up to a limit which arises from restrictions for ion trapping. A modification of the electron bath, which bypasses this limit, has been introduced and demonstrated by the first-time production and detection of aluminum cluster anions carrying five excess electrons (penta-anions). Results of the penta-anion production as a function of the trapping voltage relate to the Coulomb potentials of the cluster anions involved, in agreement with previous findings.

The observed poly-anionic clusters are meta-stable and their abundance as a function of the cluster size is determined by their lifetimes. Observed poly-anion abundances are described by a thermionic-emission approach, by means of the Richardson-

Dushman formula. The height of the Coulomb potential in the formula is decreased to match experimental data, thus accounting for electron tunneling.
Poly-anions are observed only above a minimum cluster size, the appearance size. To determine this limit from experimental results, a new data evaluation method has been introduced, which considers the poly-anion lifetimes and respective abundances of a range of cluster sizes. As a result, the experimental appearance size is larger than the smallest poly-anionic cluster observed, in contrast to previous approaches.

5.2 Outlook

The production and investigation of high-state poly-anionic clusters resulted in the need to go to larger and larger clusters. However, the mass limit of the ICR trap restricts the experimental possibilities. Obviously, the cluster mass increases with the cluster size, i.e. the number of atoms. Note, that in addition it depends on the choice of element the clusters are made of.
The mass limit has been circumvented for the production of Al_n^{5-}, but for future experiments further increased mass range for ion storage may be desirable. Given by its B^2-dependency, the mass limit of the ICR trap can be increased by use of magnetic fields that are higher than the 5 T of the recent experiments. Indeed, in the meantime, ClusterTrap has been equipped with a 12 T super-conducting magnet.
In a complementary approach, poly-anion production in radio-frequency traps is under investigation. Due to the different trapping principles in ICR and RF traps, new methods for poly-anion production have to be developed, e.g. the use of a digital ion trap [DING02, DING06, BAND12].

With these new ion trapping tools at hand, not only the production, but also the stability of poly-anionic clusters will be investigated by means of collision-induced and photoexcitation. In contrast to their positively charged congeners, poly-anionic clusters may decay not only by fragmentation, but also by charge loss, i.e. emission of electrons. Occurrence and dominance of either decay channel is determined by the strengths of the atomic and the electron bounds, which again depend on the cluster size and the charge state. Determination of respective threshold energies, e.g. for electrons by means of photoelectron spectroscopy [WANG09], promises further inside into physical properties of clusters (electron affinity respective ionization potential, Coulomb barrier).
Of special interest for poly-anionic clusters is the investigation of correlated electron emission. Although not directly observed yet, earlier laser experiments on dianionic metal clusters indicate such a simultaneous emission of two electrons [HERL12]. In those cases sequential electron emission has been excluded by verifying that respective mono-anions decay by fragmentation, rather than electron emission. However, the products of double electron emission from a di-anion are neutral clusters, which can not be stored in an ion trap, and thus not be detected at ClusterTrap. But for higher-charged poly-anions, the products would remain charged, and thus correlated electron emission might be confirmed more clearly.

For appropriate description of the experimental findings regarding the appearance size of a poly-anionic cluster, a model has to be applied, which combines quantum-mechanical electron tunneling with thermionic electron emission. Similarly, performance of the poly-anion experiments with defined internal cluster energies, e.g. by use of temperature-controlled ion traps, may give insight in the combination of both effects of thermionic emission and electron tunneling.

6 Bibliography

[ALON05] J.A. Alonso, *Structure and Properties of Atomic Nanoclusters*, Imperial College Press, London (2005).

[ARIG12] K. Ariga et al., Inorganic Nanoarchitectonics for Biological Applications, *Chem. Mater.*, **24** (2012) 728, DOI:10.1021/cm202281m.

[ARND11] M. Arndt, *An ion-trap setup for interaction studies of clusters with intense laser light*, PhD-thesis, Greifswald (2011).

[ASTR02] M. Astruc Hoffmann et al., Photoelectron spectroscopy of Al^-_{32000}: Observation of a "Coulomb staircase" in a free cluster, *Phys. Rev. B*, **66** (2002) 041404(R), DOI:10.1103/PhysRevB.66.041404.

[BAND11] S. Bandelow et al., A split-ring Paul trap for dipolar excitation of the radial ion motion and ellipticity studies, *Eur. Phys. J. D*, **61** (2011) 315, DOI:10.1140/epjd/e2010-10467-5.

[BAND12] S. Bandelow et al., *in preparation.*

[BART07] J.V. Barth, Molecular Architectonic on Metal Surfaces, *Annu. Rev. Phys. Chem.*, **58** (2007) 375, DOI:10.1146/annurev.physchem.56.092503.141259.

[BECK95] S. Becker et al., A Penning trap mass spectrometer for the study of cluster ions, *Rev. Sci. Instrum.*, **66** (1995) 4902, DOI:10.1063/1.1146172.

[BEIE01] P. Beiersdorfer et al., Current Research with Highly Charged Ions in EBIT-II and SuperEBIT, *Phys. Scr.*, T**92** (2001) 268, DOI:10.1238/Physica.Topical.092a00268.

[BLAU03] K. Blaum et al., Laser desorption/ionization cluster studies for calibration in mass spectrometry, *Eur. Phys. J. D*, **24** (2003) 145, DOI:10.1140/epjd/e2003-00131-8.

[BOLL90] G. Bollen et al., The accuracy of heavy-ion mass measurements using time of flight-ion cyclotron resonance in a Penning trap, *J. Appl. Phys.*, **68** (1990) 4355, DOI:10.1063/1.346185.

[BOND02] V. E. Bondybey, M. K. Beyer, How many molecules make a solution?, *Int. Rev. Phys. Chem.*, **21** (2002) 277, DOI:10.1080/01442350210132741.

[BREC89] C. Brechignac et al., Photoionization of mass-selected K_n^+ ions: A test for the ionization scaling law, *Phys. Rev. Lett.*, **63** (1989) 1368, DOI:10.1103/PhysRevLett.63.1368.

[BREC95] C. Brechignac, *Alkali Clusters*, in [HABE95].

[BRED09] R. Bredy et al., An introduction to the trapping of clusters with ion traps and electrostatic storage devices, *J. Phys. B*, **42** (2009) 154023, DOI: 10.1088/0953-4075/42/15/154023.

[BREI07] M. Breitenfeldt et al., Simultaneous monitoring of the radial modes of the ion motion and their manipulation in Penning traps by FT-ICR mass spectrometry, *Int. J. Mass Spectrom.*, **263** (2007) 94, DOI:10.1016/j.ijms.2007.01.003.

[BREI08] M. Breitenfeldt et al., The elliptical Penning trap: Experimental investigations and simulations, *Int. J. Mass Spectrom.*, **275** (2008) 34, DOI:10.1016/j.ijms.2008.05.008.

[BROW86] L.S. Brown and G. Gabrielse, Geonium theory: Physics of a single electron or ion in a Penning trap, *Rev. Mod. Phys.*, **58** (1986) 233, DOI:10.1103/RevModPhys.58.233.

[CARU01] F. Caruso, Nanoengineering of Particle Surfaces, *Adv. Mat.*, **13** (2001) 11, DOI:10.1002/1521-4095(200101)13:1<11::AID-ADMA11>3.0.CO;2-N.

[CAST86] A.W. Castleman Jr., R.G. Keese, Clusters: Bridging the Gas and Condensed Phases, *Acc. Chem. Res.*, **19** (1986) 413, DOI:10.1021/ar00132a006.

[CAST09] A.W. Castleman Jr., S.N. Khanna, Clusters, Superatoms, and Building Blocks of New Materials, *J. Phys. Chem. C*, **113** (2009) 2664, DOI:10.1021/jp806850h.

[CHAN95] F. Chandezon et al., Critical Sizes against Coulomb Dissociation of Highly Charged Sodium Clusters Obtained by Ion Impact, *Phys. Rev. Lett.*, **74** (1995) 3784, DOI:10.1103/PhysRevLett.74.3784.

[CHAU07] A. Chaudhuri et al., Carbon-cluster mass calibration at SHIPTRAP, *Eur. Phys. J. D*, **45** (2007) 47, DOI:10.1140/epjd/e2007-00001-5.

[CLAR09] S.A. Claridge et al., Cluster-Assembled Materials, *ACS Nano*, **3** (2009) 244, DOI:10.1021/nn800820e.

[COMI74] M.B. Comisarow, A.G. Marshall, Fourier Transform Ion Cyclotron Resonance Spectroscopy, *Chem. Phys. Lett.*, **25** (1974) 282, DOI:10.1016/0009-2614(74)89137-2.

[DEVO02] R.G. DeVoe, C. Kurtsiefer, Experimental study of anomalous heating and trap instabilities in a microscopic ^{137}Ba ion trap, *Phys. Rev. A*, **65** (2002) 063407, DOI:10.1103/PhysRevA.65.063407.

[DIET96] G. Dietrich et al., Chemisorption of hydrogen on a V_5^+ cluster, *Chem. Phys. Lett.*, **252** (1996) 141, DOI:10.1016/S0009-2614(96)00130-3.

[DIET00] G. Dietrich et al., The interaction of gold clusters with methanol molecules: Infrared photodissociation of mass-selected $Au_n^+(CH_3OH)_m$, *J. Chem. Phys.*, **112** (2000) 752, DOI:10.1063/1.480718.

[DING02] L. Ding et al., A simulation study of the digital ion trap mass spectrometer, *Int. J. Mass Spectrom.*, **221** (2002) 117, DOI:10.1016/S1387-3806(02)00921-1.

[DING06] L. Ding, F.L. Brancia, Electron Capture Dissociation in a Digital Ion Trap Mass Spectrometer, *Anal. Chem.*, **78** (2006) 1995, DOI:10.1021/ac0519007.

[DOPF03] O. Dopfer, Spectroscopic and theoretical studies of CH_3^+-Rg_n clusters (Rg=He, Ne, Ar): From weak intermolecular forces to chemical reaction mechanisms, *Int. Rev. Phys. Chem.*, **22** (2003) 437, DOI:10.1080/0144235031000112878.

[DUPO10] J. Dupont, J.D. Scholten, On the structural and surface properties of transition-metal nanoparticles in ionic liquids, *Chem. Soc. Rev.*, **39** (2010) 1780, DOI:10.1039/b822551f.

[DUSH23] S. Dushman, Electron Emission from Metals as a Function of Temperature, *Phys. Rev.*, **21** (1923) 623, DOI:10.1103/PhysRev.21.623.

[EBER02] W. Eberhardt, Clusters as new materials, *Surf. Sci.*, **500** (2002) 242, DOI:10.1016/S0039-6028(01)01564-3.

[ECHT81] O. Echt et al., Magic Numbers for Sphere Packings: Experimental Verification in Free Xenon Clusters, *Phys. Rev. Lett.*, **47** (1981) 1121, DOI:10.1103/PhysRevLett.47.1121.

[EKAR84] W. Ekardt, Work function of small metal particles: Self-consistent spherical jellium-background model, *Phys. Rev. B*, **29** (1984) 1558, DOI:10.1103/PhysRevB.29.1558.

[FAYE86] P. Fayet et al., The Role of Small Silver Clusters in Photography, *Z. Phys. D*, **3** (1986) 299, DOI:10.1007/BF01384819.

[GABR90] G. Gabrielse et al., Thousandfold Improvement in the Measured Antiproton Mass, *Phys. Rev. Lett.*, **65** (1990) 1317, DOI:10.1103/PhysRevLett.65.1317.

[GANT88] G. Ganteför et al., Photoelectron spectroscopy of jet-cooled aluminium cluster anions, *Z. Phys. D*, **9** (1988) 253, DOI:10.1007/BF01438297.

[GERL92] D. Gerlich, Inhomogenous RF fields: A versatile tool for the study of processes with slow ions, *Adv. Chem. Phys.*, **82** (1992) 1, DOI:10.1002/9780470141397.ch1.

[GOKE10] E.G. Goken, A.W. Castleman, Reactions of formic acid with protonated water clusters: Implications of cluster growth in the atmosphere, *J. Geophys. Res.*, **115** (2010) D16203, DOI:10.1029/2009JD013249.

[GHOS95] P.K. Ghosh, *Ion Traps*, Clarendon, Oxford (1995).

[HABE95] H. Haberland (ed.), *Clusters of Atoms and Molecules I*, Springer Series in Chemical Physics, Vol. 52, Springer-Verlag, Berlin (1995).

[HALA03] S. Halas, Ionization potential of large metallic clusters: explanation for the electrostatic paradox, *Chem. Phys. Lett.*, **370** (2003) 300, DOI:10.1016/S0009-2614(03)00027-7.

[HAMP02] O. Hampe et al., On the generation and stability of isolated doubly negatively charged fullerenes, *Chem. Phys. Lett.*, **354** (2002) 303, DOI:10.1016/S0009-2614(02)00124-0.

[HASS94] H.-U. Hasse et al., External-ion accumulation in a Penning trap with quadrupole excitation assisted buffer gas cooling, *Int. J. Mass Spectrom. Ion Proc.*, **132** (1994) 181, DOI:10.1016/0168-1176(93)03924-B.

[HEER90] W.A. de Heer, P. Milani, Comment on "Photoionization of mass-selected K_n^+ ions: A test for the ionization scaling law", *Phys. Rev. Lett.*, **65** (1990) 3356, DOI:10.1103/PhysRevLett.65.3356.

[HEGM07] T. Hegmann et al., Nanoparticles in Liquid Crystals: Synthesis, Self-Assembly, Defect Formation and Potential Applications, *J. Inorg. Organomet. Polym.*, **17** (2007) 483, DOI:10.1007/s10904-007-9140-5.

[HEIZ04] U. Heiz, E.L. Bullock, Fundamental aspects of catalysis on supported metal clusters, *J. Mater. Chem.*, **14** (2004) 564, DOI:10.1039/B313560H.

[HERL02] A. Herlert et al., The influence of the trapping potential on the attachment of a second electron to stored metal cluster and fullerene anions, *Int. J. Mass. Spectrom.*, **218** (2002) 217, DOI:10.1016/S1387-3806(02)00723-6.

[HERL03] A. Herlert, L. Schweikhard, Production of dianionic and trianionic noble metal clusters in a Penning trap, *Int. J. Mass Spectrom.*, **229** (2003) 19, DOI:10.1016/S1387-3806(03)00251-3.

[HERL04] A. Herlert, L. Schweikhard, The influence of spontaneous m/z-changes on the ion motion in an ion cyclotron resonance trap, *Int. J. Mass Spectrom.*, **234** (2004) 161, DOI:10.1016/j.ijms.2004.02.017.

[HERL06] A. Herlert, L. Schweikhard, First observation of delayed electron emission from dianionic metal clusters, *Int. J. Mass Spectrom.*, **252** (2006) 151, DOI:10.1016/j.ijms.2006.01.051.

[HERL12] A. Herlert, L. Schweikhard, Two-electron emission after photoexcitation of metal-cluster dianions, *New J. Phys.*, **14** (2012) 055015, DOI:10.1088/1367-2630/14/5/055015.

[HERR78] A. Herrmann et al., Preparation and photoionization potentials of molecules of sodium, potassium, and mixed atoms, *J. Chem. Phys.*, **68** (1978) 2327, DOI:10.1063/1.436003.

[HETT91] R.L. Hettich et al., Doubly charged negative ions of Carbon-60, *Phys. Rev. Lett.*, **67** (1991) 1242, DOI:10.1103/PhysRevLett.67.1242.

[HILD98] U. Hild et al., Time-resolved photofragmentation of stored silver clusters Ag_n^+ ($n = 8 - 21$), *Phys. Rev. A*, **57** (1998) 2786, DOI:10.1103/PhysRevA.57.2786.

[ISSE05] B. von Issendorff, O. Cheshnovsky, Metal to insulator transitions in clusters, *Annu. Rev. Phys. Chem.*, **56** (2005) 549, DOI:10.1146/annurev.physchem.54.011002.103845.

[JACK98] J. D. Jackson, *Classical Electrodynamics*, 3rd ed., Wiley, New York (1998).

[JENA06] P. Jena, A.W. Castleman, Clusters: A bridge across the disciplines of physics and chemistry, *Proc. Natl. Acad. Sci. USA*, **103** (2006) 10560, DOI:10.1073/pnas.0601782103.

[JETZ04] M. Jetzki et al., Vibrational delocalization in ammonia aerosol particles, *J. Chem. Phys.*, **120** (2004) 11775, DOI:10.1063/1.1752889.

[JOHN02] R.L. Johnston, *Atomic and Molecular Clusters*, Taylor & Francis, London (2002).

[KANU08] A.B. Kanu et al., Ion mobility–mass spectrometry, *J. Mass Spectrom.*, **43** (2008) 1, DOI:10.1002/jms.1383.

[KAPP88] M.M. Kappes, Experimental Studies of Gas-Phase Main-Group Metal Clusters, *Chem. Rev.*, **88** (1988) 369, DOI:10.1021/cr00084a002.

[KELL03] K.L. Kelly et al., The Optical Properties of Metal Nanoparticles: The Influence of Size, Shape, and Dielectric Environment, *J. Phys. Chem. B*, **107** (2003) 668, DOI:10.1021/jp026731y.

[KETE10] J. Ketelaer et al., Accuracy studies with carbon clusters at the Penning trap mass spectrometer TRIGA-TRAP, *Eur. Phys. J. D*, **58** (2010) 47, DOI:10.1140/epjd/e2010-00092-9.

[KNIG83] R.D. Knight, The general form of the quadrupole ion trap potential, *Int. J. Mass Spectrom. Ion Phys.*, **51** (1983) 127, DOI:10.1016/0020-7381(83)85033-5.

[KNIG84] W.D. Knight et al., Electronic Shell Structure and Abundances of Sodium Clusters, *Phys. Rev. Lett.*, **52** (1984) 2141, DOI:10.1103/PhysRevLett.52.2141.

[KÖLL99] L. Köller et al., Plasmon-Enhanced Multi-Ionization of Small Metal Clusters in Strong Femtosecond Laser Fields, *Phys. Rev. Lett.*, **82** (1999) 3783, DOI:10.1103/PhysRevLett.82.3783.

[KRÜC97] S. Krückeberg et al., First Observation of Multiply Charged Vanadium Clusters in a Penning Trap, *Rap. Comm. Mass Spectrom.*, **11** (1997) 455, DOI:10.1002/(SICI)1097-0231(199703)11:5<455::AID-RCM887>3.0.CO;2-Y.

[KRÜC97b] S. Krückeberg et al., Collision induced dissociation of doubly charged silver clusters Ag_n^{2+}, $n = 21, 22, 23$, *Hyp. Inter.*, **108** (1997) 107, DOI:10.1023/A:1012634023288.

[KRUI83] P. Kruit, F.H. Read, Magnetic field paralleliser for 2π electron-spectrometer and electron-image magnifier, *J. Phys. E*, **16** (1983) 313, DOI:10.1088/0022-3735/16/4/016.

[KULK10] A. Kulkarni et al., Metal clusters on supports: synthesis, structure, reactivity, and catalytic properties, *Chem. Commun.*, **46** (2010) 5997, DOI:10.1039/c002707n.

[LASS05] A. Lassesson et al., Formation of fullerene dianions in a Penning trap, *Eur. Phys. J. D*, **34** (2005) 73, DOI:10.1140/epjd/e2005-00122-9.

[LEIS96] T. Leisner et al., The catalytic role of small coinage-metal clusters in photography, *Surf. Rev. Lett.*, **3** (1996) 1105, DOI:10.1142/S0218625X96001972.

[LEVI88] M.A. Levine et al., The Electron Beam Ion Trap: A New Instrument for Atomic Physics Measurements, *Physica Scripta*, T**22** (1988) 157, DOI:10.1088/0031-8949/1988/T22/024.

[LI98] X. Li et al., s−p Hybridization and Electron Shell Structures in Aluminum Clusters: A Photoelectron Spectroscopy Study, *Phys. Rev. Lett.*, **81** (1998) 1909, DOI:10.1103/PhysRevLett.81.1909.

[LIMB91] P.A. Limbach et al., Observation of the doubly charged, gas-phase fullerene anions C_{60}^{2-} and C_{70}^{2-}, *J. Am. Chem. Soc.*, **113** (1991) 6795, DOI:10.1021/ja00018a012.

[MAJO04] F.G. Major, V.N. Gheorghe, G. Werth, *Charged Particle Traps: The Physics and Techniques of Charged Particle Field Confinement*, Springer, Berlin (2004).

[MAKO88] G. Makov et al., On the ionization potential of small metal and dielectric particles, *J. Chem. Phys.*, **88** (1988) 5076, DOI:10.1063/1.454661.

[MAMY73] B.A. Mamyrin et al., Mass reflection: A new nonmagnetic time-of-flight high resolution mass-spectrometer, *Zh. Eksp. Teor. Fiz.*, **64** (1973) 82, OSTI:4560209.

[MAMY01] B.A. Mamyrin, Time-of-flight mass spectrometry (concepts, achievements, and prospects), *Int. J. Mass Spectrom.*, **206** (2001) 251, DOI:10.1016/S1387-3806(00)00392-4.

[MARR88] R.E. Marrs et al., Measurement of Electron-Impact-Excitation Cross Sections for Very Highly Charged Ions, *Phys. Rev. Lett.*, **60** (1988) 1715, DOI:10.1103/PhysRevLett.60.1715.

[MARS85] A.G. Marshall et al., Tailored Excitation for Fourier Transform Ion Cyclotron Resonance Mass Spectrometry, *J. Am. Chem. Soc.*, **107** (1985) 7893, DOI:10.1021/ja00312a015.

[MARS92] A.G. Marshall, L. Schweikhard, Fourier transform ion cyclotron resonance mass spectrometry: technique developments, *Int. J. Mass Spectrom. Ion Proc.*, **118/119** (1992) 37, DOI:10.1016/0168-1176(92)85058-8.

[MARS98] A.G. Marshall et al., Fourier transform ion cyclotron resonance mass spectrometry: A primer, *Mass Spectrom. Rev.*, **17** (1998) 1, DOI:10.1002/(SICI)1098-2787(1998)17:1<1::AID-MAS1>3.0.CO;2-K.

[MART86] T.P. Martin, Cluster Beam Chemistry - from Atoms to Solids, *Angew. Chem.*, **25** (1986) 197, DOI:10.1002/anie.198601973.

[MEIW94] K.-H. Meiwes-Broer, Work functions of metal clusters, *Hyp. Inter.*, **89** (1994) 263, DOI:10.1007/BF02064511.

[MEIW07] K.-H. Meiwes-Broer, R. Berndt (Eds.), Topical Issue on Atomic Clusters at Surfaces and in Thin Films, *Eur. Phys. J. D*, **45** (2007) 399, DOI:10.1140/epjd/e2007-00321-4.

[NÄHE92] U. Näher et al., Observation of Highly Charged Sodium Clusters, *Phys. Rev. Lett.*, **68** (1992) 3416, DOI:10.1103/PhysRevLett.68.3416.

[NEUM01] D.M. Neumark, Time-resolved photoelectron spectroscopy of molecules and clusters, *Annu. Rev. Phys. Chem.*, **52** (2001) 255, DOI:10.1146/annurev.physchem.52.1.255.

[PAUL53] W. Paul, H. Steinwedel, Ein neues Massenspektrometer ohne Magnetfeld, *Z. Naturfor. A*, **8** (1953) 448.

[PAUL00] H. Pauly, *Atom, Molecule, and Cluster Beams I*, Springer, Berlin (2000).

[PERD88] J.P. Perdew, Energetics of charged metallic particles: From atom to bulk solid, *Phys. Rev. B*, **37** (1988) 6175, DOI:10.1103/PhysRevB.37.6175.

[POPO11] V.N. Popok et al., Cluster–surface interaction: From soft landing to implantation, *Surf. Sci. Rep.*, **66** (2011) 347, DOI:10.1016/j.surfrep.2011.05.002.

[RECK95] E. Recknagel, *Clusterphysik*, lecture notes, Universität Konstanz (1995).

[REIN04] P.-G. Reinhard, E. Suraud, *Introduction to Cluster Dynamics*, Wiley-VCH, Weinheim (2004).

[REIS94] M. Reiser, *Theory and design of charged particle beams*, Wiley, New York (1994).

[ROHM10] M. Rohmer et al., Time-resolved photoelectron nano-spectroscopy of individual silver particles: Perspectives and limitations, *Phys. Status Solidi B*, **247** (2010) 1132, DOI:10.1002/pssb.200945479.

[ROSE12] M. Rosenbusch et al., A study of octupolar excitation for mass-selective centering in Penning traps, *Int. J. Mass Spectrom.*, **314** (2012) 6, DOI:10.1016/j.ijms.2012.01.002.

[SAVA91] G. Savard et al., A new cooling technique for heavy ions in a Penning trap, *Phys. Lett. A*, **158** (1991) 247, DOI:10.1016/0375-9601(91)91008-2.

[SAVI05] I. Savic, D. Gerlich, Temperature variable ion trap studies of $C_3H_n^+$ with H_2 and HD, *Phys. Chem. Chem. Phys.*, **7** (2005) 1026, DOI:10.1039/B417965J.

[SCHA90] S.N. Schauer et al., Production of small doubly charged negative carbon cluster ions by sputtering, *Phys. Rev. Lett.*, **65** (1990) 625, DOI:10.1103/PhysRevLett.65.625.

[SCHU11] U. Schubert, Cluster-based inorganic–organic hybrid materials, *Chem. Soc. Rev.*, **40** (2011) 575, DOI:10.1039/C0CS00009D.

[SCHW90] L. Schweikhard et al., Quadrupole-detection FT-ICR mass spectrometry, *Int. J. Mass Spectrom Ion Proc.*, **98** (1990) 25, DOI:10.1016/0168-1176(90)85045-4.

[SCHW90b] L. Schweikhard et al., Parametric-mode-excitation/dipole-mode-detection Fourier-transform–ion-cyclotron-resonance spectrometry, *Rev. Sci. Instr.*, **61** (1990) 1055, DOI:10.1063/1.1141475.

[SCHW92] L. Schweikhard et al., Quadrupolar excitation and collisional cooling for axialization and high pressure trapping of ions in Fourier transform ion cyclotron resonance mass spectrometry, *Int. J. Mass Spectrom. Ion Proc.*, **120** (1992) 71, DOI:10.1016/0168-1176(92)80053-4.

[SCHW93] L. Schweikhard, A.G. Marshall, Excitation modes for Fourier transform-ion cyclotron resonance mass spectrometry, *J. Am. Soc. Mass Spectrom.*, **4** (1994) 433, DOI:10.1016/1044-0305(93)80001-F.

[SCHW95] L. Schweikhard et al., Trapped metal cluster ions, *Physica Scripta*, T**59** (1995) 236, DOI:10.1088/0031-8949/1995/T59/032.

[SCHW95b] L. Schweikhard et al., The trapping condition and a new instability of the ion motion in the ion cyclotron resonance trap, *Int. J. Mass Spectrom. Ion Proc.*, **141** (1995) 77, DOI:10.1016/0168-1176(94)04092-L.

[SCHW96] L. Schweikhard et al., Production and investigation of multiply charged metal clusters in a Penning trap, *Hyp. Inter.*, **99** (1996) 97, DOI:10.1007/BF02274913.

[SCHW97] L. Schweikhard et al., Collision Induced Dissociation of Doubly Charged Stored Metal Cluster Ions, *Rap. Comm. Mass Spectrom.*, **11** (1997) 1592, DOI:10.1002/(SICI)1097-0231(199709)11:14<1592::AID-RCM996>3.0.CO;2-1.

[SCHW99] L. Schweikhard et al., The Mainz Cluster Trap: Ion storage techniques at work in atomic cluster research, *Eur. Phys. J. D*, **9** (1999) 15, DOI:10.1007/s100530050391.

[SCHW03] L. Schweikhard et al., New approaches to stored cluster ions: The determination of dissociation energies and recent studies on dianionic metal clusters, *Eur. Phys. J. D*, **24** (2003) 137, DOI:10.1140/epjd/e2003-00181-x.

[SCHW03b] L. Schweikhard et al., Laser Investigations of Stored Metal Cluster Ions, *Hyp. Inter.*, **146/147** (2003) 275, DOI:10.1023/B:HYPE.0000004234.96012.06.

[SCHW05] L. Schweikhard et al., Atomic clusters and ion-cyclotron-resonance mass spectrometry: a fruitful combination, *Eur. J. Mass Spectrom.*, **11** (2005) 457, DOI:10.1255/ejms.744.

[SCOL88] G. Scoles (Ed.), *Atomic and Molecular Beam Methods, Vol. I*, Oxford University Press, Oxford and New York (1988).

[SEID91] M. Seidl et al., Finite-size effects in ionization potentials and electron affinities of metal clusters, *J. Chem. Phys.*, **95** (1991) 1295, DOI:10.1063/1.461111.

[SEID94] M. Seidl, P. Perdew, Size-dependent ionization energy of a metallic cluster: Resolution of the classical image-potential paradox, *Phys. Rev. B*, **50** (1994) 5744, DOI:10.1103/PhysRevB.50.5744.

[SMIT65] J.M. Smith, Nonequilibrium lonization in Wet Alkali Metal Vapors, *AAIA J.*, **3** (1995) 648, OSTI:4628995.

[SNID83] D.R. Snider, R.S. Sorbello, Density-functional calculation of the static electronic polarizability of a small metal sphere, *Phys. Rev. B*, **28** (1983) 5702, DOI:10.1103/PhysRevB.28.5702.

[STAR11] W.J. Stark, Nanoparticles in Biological Systems, *Angew. Chem. Int. Ed.*, **50** (2011) 1242, DOI:10.1002/anie.200906684.

[STAV87] M.P.J. van Staveren et al., Energetics of charged small metal particles, *Phys. Rev. B*, **35** (1987) 7749, DOI:10.1103/PhysRevB.35.7749.

[STIC06] D. Stick et al., Ion trap in a semiconductor chip, *Nature Physics*, **2** (2006) 36, DOI:10.1038/nphys171.

[STOE01] C. Stoermer et al., Observation of multiply charged cluster anions upon pulsed UV laser ablation of metal surfaces under high vacuum, *Int. J. Mass Spectrom.*, **206** (2001) 63, DOI:10.1016/S1387-3806(00)00390-0.

[SVAN10] M. Svanqvist, K. Hansen, Non-jellium scaling of metal cluster ionization energies and electron affinities, *Eur. Phys. J. D*, **56** (2010) 199, DOI:10.1140/epjd/e2009-00298-x.

[TIGG07] J. Tiggesbäumker, F. Stienkemeier, Formation and properties of metal clusters isolated in helium droplets, *Phys. Chem. Chem. Phys.*, **9** (2007) 4725, DOI:10.1039/b703575f.

[VÖLP93] R. Völpel et al., Ionization and Fragmentation of Fullerene Ions by Electron Impact, *Phys. Rev. Lett.*, **71** (1993) 3439, DOI:10.1103/PhysRevLett.71.3439.

[VOGE01] M. Vogel et al., Model-Free Determination of Dissociation Energies of Polyatomic Systems, *Phys. Rev. Lett.*, 87 (2001) 013401, DOI:10.1103/PhysRevLett.87.013401.

[VOGE03] M. Vogel et al., Model-independent determination of dissociation energies: method and applications, *J. Phys. B*, **36** (2003) 1073, DOI:10.1088/0953-4075/36/5/326.

[WALS07] N. Walsh et al., Multiply negatively charged aluminium clusters: Production of Al_n^{2-} in a Penning trap, *Eur. Phys. J. D*, **43** (2007) 241, DOI:10.1140/epjd/e2007-00114-9.

[WALS09] N. Walsh et al., Atomic clusters in a Penning trap: Investigation of their properties and utilization as diagnostic tools, *J. Phys. B*, **42** (2009) 154024, DOI:10.1088/0953-4075/42/15/154024.

[WALS09b] N. Walsh et al., Multiply negatively charged aluminium clusters II: Production of Al_n^{3-}, *Eur. Phys. J. D*, **52** (2009) 27, DOI:10.1140/epjd/e2008-00255-3.

[WALS10] N. Walsh et al, First observation of a tetra-anionic metal cluster, Al_n^{4-}, *J. Chem. Phys.*, **132** (2010) 014308, DOI:10.1063/1.3270153.

[WANG99] X.B. Wang, L.S. Wang, Experimental Search for the Smallest Stable Multiply Charged Anions in the Gas Phase, *Phys. Rev. Lett.*, **83** (1999) 3402, DOI:10.1103/PhysRevLett.83.3402.

[WANG09] X.B. Wang, L.S. Wang, Photoelectron Spectroscopy of Multiply Charged Anions, *Annu. Rev. Phys. Chem.*, **60** (2009) 105, DOI:10.1146/annurev.physchem.59.032607.093724.

[WEID91] R. Weidele et al., Production of "cold/hot" metal cluster ions: A modified laser vaporization source, *Z. Phys. D*, **20** (1991) 425, DOI:10.1007/BF01544024.

[WILE55] W.C. Wiley, I.H. McLaren, Time-of-Flight Mass Spectrometer with Improved Resolution, *Rev. Sci. Instrum.*, **26** (1955) 1150, DOI:10.1063/1.1715212.

[WOLF12] R.N. Wolf et al., Static-mirror ion capture and time focusing for electrostatic ion-beam traps and multi-reflection time-of-flight mass analyzers by use of an in-trap potential lift, *Int. J. Mass Spectrom.*, **313** (2012) 8, DOI:10.1016/j.ijms.2011.12.006.

[WOLL93] H. Wollnik, Time-of-flight mass analyzers, *Mass Spectrom. Rev.*, **12** (1993) 89, DOI:10.1002/mas.1280120202.

[WOOD81] D.M. Wood, Classical Size Dependence of the Work Function of Small Metallic Spheres, *Phys. Rev. Lett.*, **81** (1981) 749, DOI:10.1103/PhysRevLett.46.749.

[YOUN08] N. P. Young et al., Weighing Supported Nanoparticles: Size-Selected Clusters as Mass Standards in Nanometrology, *Phys. Rev. Lett.*, **101** (2008) 246103, DOI:10.1103/PhysRevLett.101.246103.

[ZAJF97] D. Zajfman et al., Electrostatic bottle for long-time storage of fast ion beams, *Phys. Rev. A*, **55** (1997) R1577, DOI:10.1103/PhysRevA.55.R1577.

[ZAJF04] D. Zajfman et al., Dynamics of stored ions in an electrostatic ion beam trap, *Nucl. Instr. Meth. Phys. Res. A*, **532** (2004) 196, DOI:10.1016/j.nima.2004.06.045.

[ZHAI10] H.-J. Zhai, L.-S. Wang, Probing the electronic structure of early transition metal oxide clusters: Molecular models towards mechanistic insights into oxide surfaces and catalysis, *Chem. Phys. Lett.*, **500** (2010) 185, DOI:10.1016/j.cplett.2010.10.001.

[ZIEG12] F. Ziegler et al., A new Pulse-Pattern Generator based on LabVIEW FPGA, *Nucl. Instr. Meth. Phys. Res. A*, **679** (2012) 1, DOI:10.1016/j.nima.2012.03.010.

7 Thesis Articles

Author Contribution

Article I: The new ClusterTrap setup
F. Martinez, G. Marx, L. Schweikhard, A. Vass, F. Ziegler, *Eur. Phys. J. D* **63**, 255-262 (2011)
F.M. had the main responsibility for the move of the ClusterTrap setup from the IPP building to its new location. He designed (together with G.M. and L.S.), and he prepared and realized the hardware modifications (with the help of the other co-authors). F.M. was also in charge of the tests and characterizations of the new setup. F.M. and L.S. wrote the manuscript. It was edited by all co-authors.

Article II: Unintended parametric ejection of ions from ion cyclotron resonance trap by two-electrode axialization
F. Martinez, A. Herlert, G. Marx, L. Schweikhard, N. Walsh, *Eur. J. Mass Spectrom.* **15**, 283-291 (2009)
L.S. conceived the idea. The measurements on aluminum clusters were performed by N.W. and F.M. with equal contributions. The measurements on gold clusters were performed by A.H. The vector model was developed by L.S. and F.M. The manuscript was written by F.M. and L.S. and edited by all co-authors.

Article III: Lifting of the trapping potential during ion storage for multi-anion production in a Penning trap
F. Martinez, S. Bandelow, C. Breitenfeldt, G. Marx, L. Schweikhard, F. Wienholtz, F. Ziegler, *Int. J. Mass Spectrom.* **313**, 30-35 (2012)
F.M. and L.S. developed the idea of the modified electron-bath technique. F.M. was in charge of the planning and realization of the setup modifications. He also performed the measurements with the help of the co-authors. Furthermore, F.M. evaluated the data. F.M. and L.S. wrote the manuscript, which all co-authors edited.

Article IV: Appearance size of poly-anionic aluminum clusters, Al_n^{z-}, $z = 2 - 5$
F. Martinez, S. Bandelow, C. Breitenfeldt, G. Marx, L. Schweikhard, F. Wienholtz, F. Ziegler, submitted to *Eur. Phys. J. D* (2012)
F.M. prepared and performed the measurements. F.M. and L.S. developed the new approaches for data evaluation and interpretation. F.M. evaluated the data. F.M. and L.S. wrote the manuscript, which all co-workers edited.

Confirmed:

Greifswald, den Lutz Schweikhard

Article I

EPJ D
Atomic, Molecular, Optical and Plasma Physics
EPJ.org
your physics journal

Eur. Phys. J. D **63**, 255–262 (2011) DOI: 10.1140/epjd/e2011-10528-3

The new ClusterTrap setup

F. Martinez, G. Marx, L. Schweikhard, A. Vass and F. Ziegler

EDP SCIENCES
Società Italiana di Fisica
Springer

Eur. Phys. J. D **63**, 255–262 (2011)
DOI: 10.1140/epjd/e2011-10528-3

THE EUROPEAN PHYSICAL JOURNAL D

Regular Article

The new ClusterTrap setup

F. Martinez[a], G. Marx, L. Schweikhard, A. Vass, and F. Ziegler

Ernst-Moritz-Arndt University, 17487 Greifswald, Germany

Received 19 September 2010 / Received in final form 27 January 2011
Published online 17 May 2011 – © EDP Sciences, Società Italiana di Fisica, Springer-Verlag 2011

Abstract. ClusterTrap has been designed to investigate properties of atomic clusters in the gas phase with particular emphasis on the dependence on the cluster size and charge state. The combination of cluster source, Penning trap and time-of-flight mass spectrometry allows a variety of experimental schemes including collision-induced dissociation, photo-dissociation, further ionization by electron impact, and electron attachment. Due to the storage capability of the trap extended-delay reaction experiments can be performed. Several recent modifications have resulted in an improved setup. In particular, an electrostatic quadrupole deflector allows the coupling of several sources or detectors to the Penning trap. Furthermore, a linear radio-frequency quadrupole trap has been added for accumulation and ion bunching and by switching the potential of a drift tube the kinetic energy of the cluster ions can be adjusted on their way towards or from the Penning trap. Recently, experiments on multiply negatively charged clusters have been resumed.

1 Introduction

The ClusterTrap experiment [1–4] has been designed and built for the investigation of atomic (metal) clusters by means of ion-storage techniques [5–7]. The evolution of properties of clusters as a function of the cluster size and the charge state has been investigated by numerous groups [8–11]. In contrast to experiments using cluster ion beams, confinement of cluster ions in storage devices allows extended observation times and multiple-step operation at one location in space, including multiple preparation and reaction steps.

The ClusterTrap setup utilizes a Penning trap for cluster research. A superconducting magnet provides a 5-T magnetic field, which in combination with an electrostatic field confines ions to a defined volume [5–7]. Cluster ions are produced by an external source, transferred to and captured in the Penning trap, and after storage and reaction steps are ejected and mass-analyzed by time-of-flight (ToF) mass spectrometry. While the mass resolving power of this detection mode is low as compared to the alternative FT-ICR method, even very low ion intensities can still be observed.

Recently, the ClusterTrap setup has been modified, in particular by implementation of an electrostatic quadrupole deflector [12–15] and a radio-frequency quadrupole (RFQ) ion trap [16–19]. Both devices are versatile tools in cluster research, e.g. as ion guide and energy filter [20–28] and as ion storage device [29,30], respectively. Additionally, the experiment-control and data-acquisition system has been replaced. Details on the previous setup have been described elsewhere [1,2,4,31]. In this contribution a general overview of the new setup and preliminary results of recent measurements are presented.

[a] e-mail: franklin.martinez@physik.uni-greifswald.de

2 Overview of the new setup

The new ClusterTrap setup is schematically shown in Figure 1. Cluster ions are produced in a laser ablation source [32]. In a linear RFQ trap the cluster-ion ensemble is prepared by accumulation, bunching and where required by size selection. A quadrupole deflector connects the cluster ion source/RFQ, the Penning trap, detector 1 and a second ion source. Alternatively, the latter device can be replaced by another ion detector, such as a Faraday cup, a collector for the neutral clusters, or a second RFQ trap for further ion preparation. In the Penning trap the ions are stored for up to seconds and exposed to e.g. electrons, neutral gas atoms or laser radiation. The remaining cluster and reaction-product ions are then extracted towards detector 1 and mass-analyzed by the ToF method. Detectors 2 and 3 are mainly used for optimization of the ion transfer.

3 Details of the new elements

3.1 Control of experimental sequence and data acquisition

As the hardware of the old control system was outdated and had to be replaced a modern experiment-control and

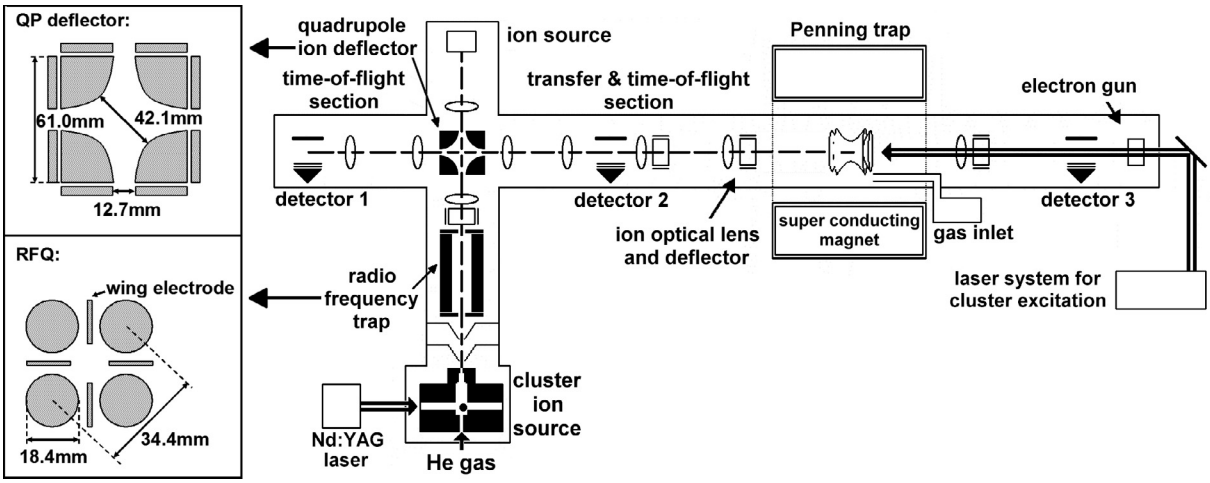

Fig. 1. Overview of the modified ClusterTrap setup (right) and cross-sectional views of the quadrupole deflector and the linear RFQ (left top and bottom, respectively).

data-acquisition system has been implemented. The new system was developed within LabVIEW [33,34] and is based on the CS Framework developed and maintained by the experiment electronics department (EE) of the GSI Helmholtzzentrum für Schwerionenforschung GmbH in Darmstadt, Germany [35]. As the new system is a further development of the old one which, however, has not yet been described in detail, we include such a description. In short, the old control system, originally developed for the ISOLTRAP [36,37] experiment at CERN/Geneva, was running on a VME-bus with Motorola E6 CPU. The software was developed with GNU C and executed within the real-time operating system OS-9 from Eltec. The graphical user interface (GUI) for the configuration of the experimental parameters and visualisation of the data (written in Borland C++) was outsourced (connection via TCP/IP) to a PC with operating system Windows 3.11 [35]. For the data acquisition a transient recorder (model TR8818A, LeCroy) embedded in a CAMAC-bus system was employed, i.e. a VME-CAMAC interface was required. For the timing and device triggering three home-build time-pattern modules ("memory modules") were used. Each of these was addressed and programmed individually with an user-defined timing structure with a precision of four microseconds. One of the modules was used for all preparation steps within a measurement cycle, in particular the accumulation of clusters by repeated transfer of ion bunches from the source to the Penning trap by use of the same memory-module loop for several times. The other two modules were used for the triggering of all subsequent experimental steps. These two modules were running simultaneously and an additional switch controlled which module was actually connected to the hardware devices. Thus, it was possible to alternately (and therefore quasi-simultaneously) execute two different cycles [1]. While in the "measurement cycle" a certain parameter of interest was varied, the same parameter remained constant in the "reference cycle". Thus, changes in the ion signal over time due to causes different from the parameter varied for the particular experiments could be monitored and compensated in the data evaluation. Typical cases for such applications are drifts of the cluster ion source accompanied by changes in the cluster production.

The new control system for ClusterTrap has been designed such that it includes and extends the functionality of the old system. Many impractical peculiarities of both hardware and software due to the adaption from the ISOLTRAP system have been removed. In particular, commercially available hardware has replaced the obsolete home-built electronics components (e.g. the memory modules). The most important extension is the implementation of automated scans of device parameters.

In the new system, the timing pattern of the experiment is controlled by a Field-Programmable-Gate-Array (FPGA) card (model NI7811R, National Instruments) which is programmed as a pulse-pattern generator [38]. Different devices at the experiment like power supplies or arbitrary function generators are now connected via USB, GPIB, PCI and allow remote controlling of many experimental parameters.

The data acquisition is implemented in the experiment-control system. The signal from the ion detector is fed into a multi-channel scaler (model MSA300, Becker & Hickl). For achievement of a high signal-to-noise ratio, a cycle sequence is repeated several times (iteration loop). The ToF spectrum of each cycle is recorded and saved to a separate file. Thus, a later shot-to-shot evaluation of the spectra is possible. (In the old system, due to data-rate limitations the spectra had to be accumulated in the CAMAC-based transient recorder with no possibility to disentangle individual measurement cycles during data evaluation.) If required, additional multi-channel-scaler cards can be added, and the signals from two or more detectors can be recorded simultaneously.

By implementation of the RFQ trap and the quadrupole deflector the original experimental cycle

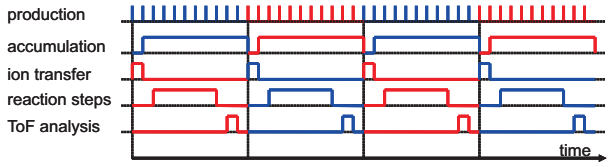

Fig. 2. (Color online) Event sequence of an experimental cycle; "reaction steps" can mean a combination of several steps at the Penning trap. For details see text.

including preparation and reaction steps has now been split into two independent, simultaneously running subcycles (Fig. 2). In the preparation subcycle cluster ions are produced at a rate of, e.g., 10 Hz in the source and several ion bunches are accumulated in the RFQ trap (lines 1 and 2 in Fig. 2). The main trigger for this subcycle is provided by the laser system of the cluster source. In the reaction subcycle the cluster ions are transferred from the RFQ trap into the Penning trap, undergo reactions, and are analyzed by ToF mass spectrometry (lines 3 to 5 in Fig. 2). The reaction subcycle is triggered by the experiment-control system at a typical rate of about one per second.

The new experiment-control system allows an automatic scanning of experiment parameters, like voltages, frequencies or the length of reaction or delay times. It can be chosen between two different modes: either for a given scan value a preset number of iteration loops is executed before stepping forward to the next scan value. Or the whole scan range is executed with only one measurement cycle at each scan value, but the scan is repeated several times, as preset by the number of scan iterations.

3.2 Linear RFQ trap

The radio-frequency trap is of linear geometry, i.e. four copper-rod electrodes with a length of 250 mm (for further dimensions see Fig. 1) are oriented parallel to the cluster-beam axis. Between adjacent rods a radiofrequency potential of typically 400 V at a frequency of 0.5 MHz provides a radial confinement of ions (principle of the quadrupole ion guide, i.e. the DC term is kept at 0 V). Axial confinement of cations (or anions) is achieved by application of a DC-potential to endcap electrodes at each end of the trap, e.g. +25 V (or –25 V) with respect to the average rod potentials (typically +100 V or –100 V). While this restricts the trapping to ions with one charge sign at a time, the same restriction already applies to the Penning trap where the actual measurements are performed.

Each endcap has a bore of 8 mm in diameter for axial entrance and exit of ions. For extraction the endcap potential is switched to –10 V (or +10 V) with respect to the average rod potential. The ions pass the endcap and are then further accelerated by the potential difference between the endcap and an adjacent grounded transfer electrode. The RFQ trap is mounted inside a CF-100 standard 6-way cross, with pumping barriers at the position of the endcaps. Through a needle valve a continuous flow of argon provides a buffer-gas environment with a pressure of the order of 10^{-4} mbar.

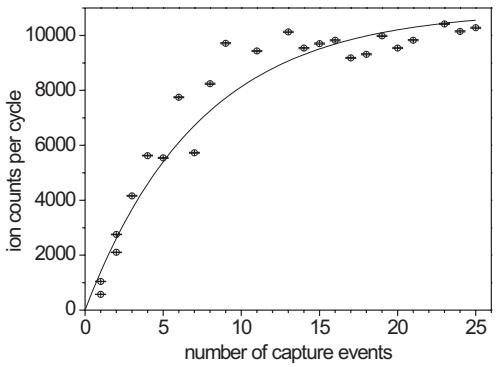

Fig. 3. Cluster-ion counts at detector 1 after extraction from the RFQ trap as a function of the number of capture events (line to guide the eye).

Accumulation of cluster ions is achieved by repeated capture of clusters, i.e. pulsing down of the source-side endcap potential. Once captured, the motion of the ions is cooled by collisions with the buffer gas, such that during the next opening of the entrance endcap the ions do not escape. Figure 3 shows the number of cluster ions extracted from the RFQ trap and counted at detector 1 as function of the number of capture events. For the specific parameters of this measurement up to about 10 ion bunches can be accumulated before saturation sets in. Thus, typically 10 to 15 capture events are applied to load the RFQ trap. At a bunch rate of 10/s from the source this is well-adjusted to the typical storage of cluster-ion manipulation and reaction at the Penning trap of about one second.

Between each pair of adjacent rods additional "plate electrodes" [39] are mounted (see Fig. 1, left side, bottom) to which a DC voltage U_{PE} is applied. As the distance of these electrodes from the trap axis is varied linearly along the axial direction from 6 mm to 14 mm, a potential minimum is created at the exit endcap of the trap. In Figure 4 the time-of-flight spectra of an aluminum-cluster bunch is shown for $U_{PE} = 0$ V, 10 V and 90 V for extraction from the RFQ trap and deflection towards detector 1. While without bunching ($U_{PE} = 0$ V) the ions' time of flight is spread over more than 2 ms, the ion ensemble becomes compressed for $U_{PE} > 0$ with a pulse width of $t_{FWHM} \simeq 55$ μs for $U_{PE} = 90$ V. For comparison, when arriving at the entry endcap of the RFQ trap the cluster distribution from the source has a spread of about 1.5 ms.

The frequencies of the secular (macro) motion depend on the ions' mass-over-charge ratio. Thus, particular ion species can be addressed by application of dipolar excitation fields, causing an increase of the amplitude and eventually the removal of these ions from the trap. For selection of ions of a single cluster size all but one ion species can be removed from the trap, simultaneously, by application of the stored waveform inverse Fourier transform (SWIFT) excitation [40–42]. In 3-dimensional ion traps, SWIFT dipolar excitation is preferably applied between the two endcap electrodes, causing excitation of

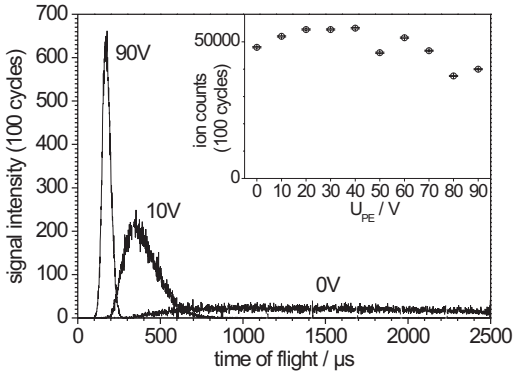

Fig. 4. Intensity of the aluminum cluster anion signal (Al_n^{1-}, $n \approx 50$ to 200) observed at detector 1 as a function of time after ejection from the RFQ trap for $U_{PE} = 0$ V, 10 V and 90 V. The inset shows the ion counts as function of U_{PE}.

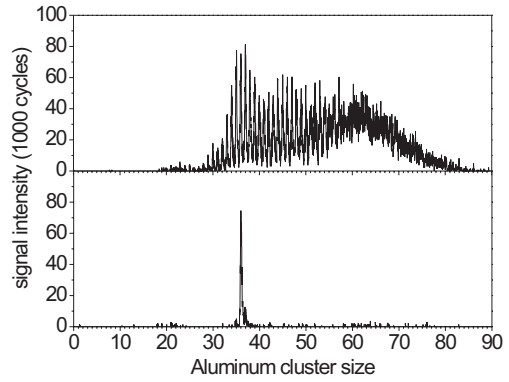

Fig. 5. Abundance spectrum of aluminum cluster anions. Top: after accumulation in the RFQ trap, transfer to the Penning trap, storage and ToF mass spectrometry by use of detector 1. Bottom: as top but with Al_{36}^- selection by radial SWIFT excitation at the RFQ trap.

the axial ion motion [43,44]. In linear quadrupole ion traps the radial ion motion can be addressed by applying a SWIFT dipolar excitation between two opposing quadrupole rods [45,46]. At the present setup each phase of the dipolar SWIFT excitation signal is applied to two adjacent plate electrodes. As the strength of the radial excitation field varies along the axial direction due to the triangularly shaped plate electrodes, the ions were bunched before exposure to the excitation field. As an example, Figure 5 demonstrates the size selection of Al_{36}^-.

3.3 Quadrupole deflector

The "quadrupole deflector/energy filter" (Extrel CMS, LLC) serves as a switch yard between different devices as the ions are transferred towards and from the Penning trap. The quadrupole deflector consists mainly of four hyperbolically shaped deflector electrodes. Their outer edges form a cube (for dimensions see Fig. 1 left, top). A potential difference U_{QP} (quadrupole deflector voltage) applied between the two pairs of opposing quadrupole electrodes generates an electric field which deflects passing ions [15].

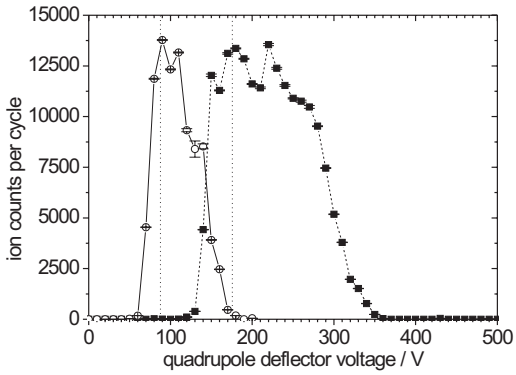

Fig. 6. Number of cluster cations as a function of the applied quadrupole-deflector voltage. The ions are extracted from the radio-frequency trap, being at a potential of +50 V (open circles) and +100 V (filled squares), respectively. The dotted lines indicate the expected deflector voltages, $U_{QP} = 88.4$ V and 176.8 V, respectively.

Each side of the cubic electrode array is screened by a grounded electrode, supplied with an aperture for ions to enter and exit the deflector.

For ion transfer from the cluster source or RFQ trap in the Penning trap, the corresponding deflector voltage is applied to the quadrupole electrodes thus deflecting the ion beam by an angle of 90°. Similarly, the ions can be guided into the opposite direction, i.e. towards detector 1. For ToF mass spectrometry after storage in the Penning trap, the ions are ejected and drift to detector 1 while U_{QP} is switched off to allow the ions to pass in a straight line.

When switched on, i.e. operated as a deflector, the quadrupole acts as an energy filter. For a given deflector voltage only ions of charge Q with the corresponding kinetic energy E_{kin} are following the ideal trajectory, independent of the ions' masses. The relation between the quadrupole deflector voltage and the kinetic energy is given by [15],

$$U_{QP} = 2\left(\frac{2r_0}{\beta_0 D}\right)^2\left(\frac{E_{kin}}{Q}\right), \qquad (1)$$

with $D = 61.0$ mm, $2r_0 = 42.1$ mm (Fig. 1) and $\beta_0 \cong 0.734$ [15]. Figure 6 shows the signal of cluster ions ejected from the RFQ trap and detected at detector 1 as a function of the deflector voltage U_{QP}.

Note, that cluster ions that are extracted from the RFQ trap have the same kinetic energy, independent of their mass. Thus, all cluster sizes can be guided towards the Penning trap without need to change ion-optical settings of the transfer section. This is an improvement with respect to the original ClusterTrap setup (without RFQ trap and quadrupole deflector), when cluster ions coming directly from the cluster source had to be captured in the Penning trap. The clusters leave the source with roughly the same velocity, namely that of the helium gas flow through the nozzle, and thus have different kinetic energies according to their cluster size [1]. This in turn required adjustment of ion-optical parameters along the

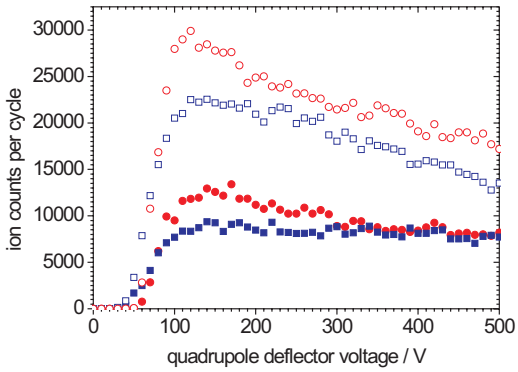

Fig. 7. (Color online) Number of cluster ions as a function of the applied quadrupole voltage. The ions are extracted from the cluster source and charge separated by the deflector. Positively (red circles) and negatively (blue squares) charged clusters are counted at detector 1 (filled symbols) and detector 2 (open symbols).

whole transfer section at the original setup, when changing the range of cluster sizes to be investigated.

3.4 Ion detection

The new ClusterTrap setup (Fig. 1) is provided with three conversion-electrode single-ion-counting detectors where the photo-multiplier tube of a Daly configuration [47] has been replaced by a set of two MCPs in Chevron-arrangement. Detector 1 is part of the ToF-spectrometer for mass analysis of the content of the Penning trap. Furthermore, it is used to detect and monitor ion bunches extracted from the RFQ trap. Detectors 2 and 3 are used mainly to optimize the ion transfer towards, respectively through the Penning trap, by adjusting the ion-optical elements. Additionally, when the RFQ is not used as a trap but as an ion guide, detectors 1 and 2 can be used simultaneously to characterize the cluster-ion source by detection of the ions after charge-sign separation by the quadrupole deflector. As an example, Figure 7 shows the deflection of aluminum cluster ions, as a function of U_{QP}.

As described above, clusters leaving the source have different kinetic energies according to their cluster size. Larger clusters are transmitted at higher deflection voltages than smaller clusters. In principle this opens up the possibility to analyse the cluster-size distribution of the source (roughly Al_{50} to Al_{700} for Fig. 7). Furthermore, the simultaneous detection of charge separated clusters leads to a comparison of the production between positive and negative clusters and, at the same time, of the detection-efficiencies of the two detectors.

The DC-offset potential of the Penning trap is in general the same as that of the RFQ trap, typically 100 V. For an improved transmission and resolving power of the ToF spectrometer several hundreds of volts of acceleration potential are recommended. However, this would require either an increase of the DC offset of the Penning trap prior to ion extraction, or a floating of the complete drift tube of the ToF-spectrometry section. As both options are technically difficult to realize, a "potential lift" has been implemented, instead. Ions are extracted from the Penning trap into the first drift tube of the ToF-section. This tube is floated and thus accelerates the ions by a potential difference of typically 400 V (Fig. 8a). While the ions pass this tube, its potential is switched back to ground by means of fast high-voltage switches (model NIM-AMX500-3, CGC Instruments) at the lift time t_{lift} after ejection (Fig. 8b). Thus, the ions keep their kinetic energy when leaving the first drift tube and continue through the grounded parts of the ToF section towards detector 1 (Fig. 8c).

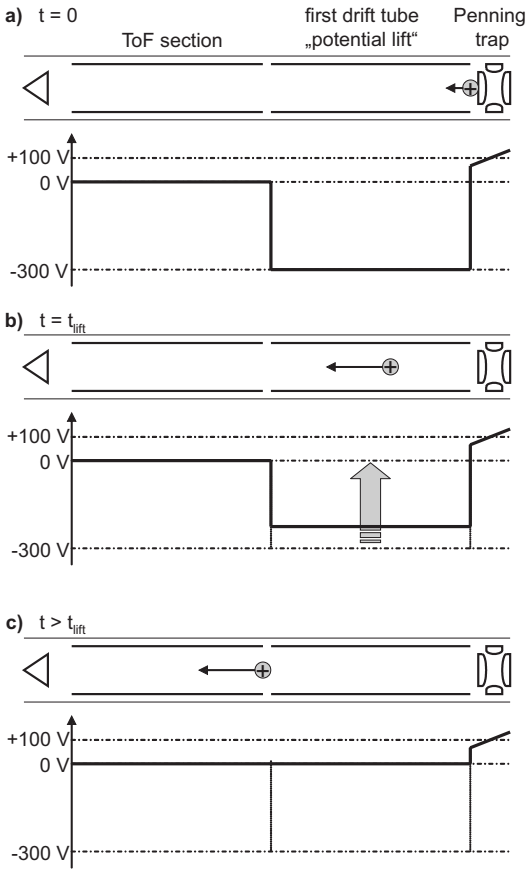

Fig. 8. Principle of the potential lift, shown for positively charged ions. (a) The first drift tube is kept at a potential of –300 V. At extraction ions are accelerated to a kinetic energy of 400 eV. (b) At the time t_{lift} the first drift tube is switched back to ground potential. (c) The ions keep their kinetic energy when leaving the first drift tube.

The lift time is a crucial parameter for an ion mass distribution to be ToF-analyzed. If t_{lift} is chosen too short, slow ions, i.e. with a high mass-over-charge ratio, have not yet entered the first drift tube and are thus not accelerated properly to reach the detector. On the other hand, if t_{lift} is chosen too long, fast ions, i.e. with a low mass-over-charge ratio, reach the end of the first drift tube, when the tube potential is not yet switched back to ground. Thus, these ions, which are too fast, encounter an electric field due to the potential difference of 300 V between the

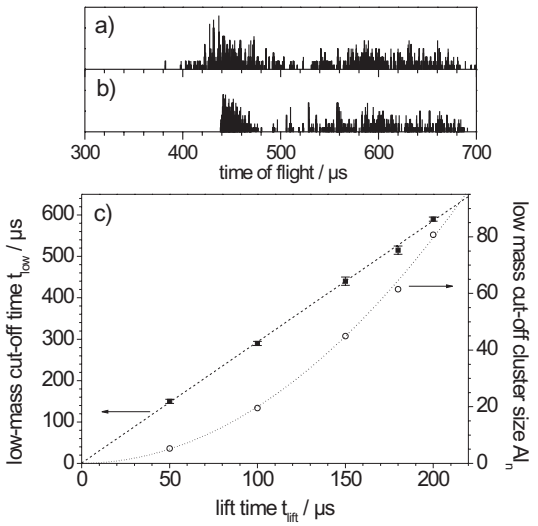

Fig. 9. ToF spectrum by use of detector 1 of residual-gas ions for (a) $t_{lift} = 100$ μs and for (b) $t_{lift} = 150$ μs. (c) Low-mass cut-off times t_{low} (filled squares) and corresponding aluminum cluster sizes Al_n (open circles, for singly charged clusters) as a function of the lift time t_{lift} (lines to guide the eye). For details see text.

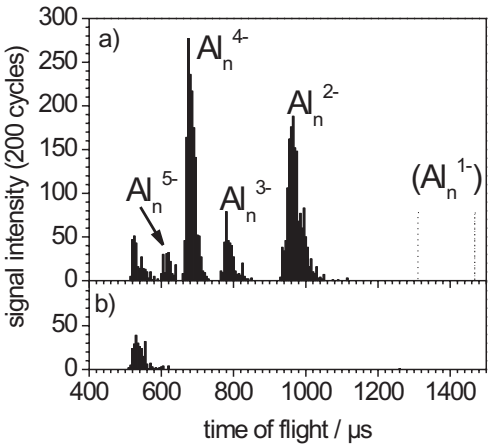

Fig. 10. (a) ToF spectrum (recorded with detector 1) of aluminum cluster anions Al_n, $n = 400$ to 500, as extracted from the Penning trap. After application of an electron bath to Al_n^{1-} the higher charged species Al_n^{2-}, Al_n^{3-}, Al_n^{4-} and Al_n^{5-} are observed. The ion signal for $t_{ToF} < 600$ μs is due to residual-gas ions, which have been produced during application of the electron bath. (b) The reference cycle shows a ToF spectrum without clusters after application of the electron bath.

tube and the adjacent grounded transfer electrode. The ions are retarded, and more important, are deflected from the ideal path and do not reach the detector at all. This causes a cut-off of the ion signal at the time-of-flight value t_{low} in the ToF-spectra, as it can be observed in Figure 9b, with $t_{low} = 440$ μs, for $t_{lift} = 150$ μs. (For comparison, a ToF spectrum with a properly chosen value $t_{lift} = 100$ μs is given in Fig. 9a.) Thus, for a given lift time only ions with a limited range of mass-over-charge ratios can be analyzed. For more extended ranges the spectrum can be reconstructed from repeated measurements with corresponding switch times.

Figure 9c shows the low-mass cut-off times t_{low} which appear in respective ToF spectra (filled squares) as experimentally determined from measurements with cluster and residual gas ions. The right-hand ordinate shows the respective low-mass cut-off cluster sizes (open circles) for singly-charged aluminum clusters. Calibration of the mass-over-charge scale (i.e. cluster size over charge state) is realized by means of ion-selective resonant radial dipolar excitation at the reduced cyclotron frequency in the Penning trap. Single ion species are removed from the trap prior to the ToF analysis, thus indicating the corresponding mass-over-charge ratio as a gap in the ions' ToF distribution.

4 A first experiment with the new setup

Recently, experiments on the production of multiply negatively charged clusters [31,48–52] have been resumed. In short, cluster mono-anions and electrons are stored simultaneously in the Penning trap (electron-bath technique [48]), for attachment of electrons to the already negatively charged clusters. In a first experiment aluminum cluster mono-anions Al_n^{1-}, with a size distribution of $n = 400$ to 500, have been stored in the Penning trap and exposed to two electron baths. As shown in Figure 10, aluminum cluster anions Al_n^{2-}, Al_n^{3-} and Al_n^{4-} have been produced. In addition, aluminum cluster penta-anions Al_n^{5-} have been observed for the first time. The differences in abundance of the several charge states mainly depend on the cluster size and have been observed before [51,52]. In the ToF-spectrum di-, tri-, tetra- and penta-anions are shown, but no mono-anions. The latter ones were removed from the Penning trap during the penta-anion production cycle, due to a variation of the electrostatic trapping potential between the two periods of electron-bath exposure. This is required to match two contrary effects. On the one hand the trapping of ions with high mass-over-charge ratio (e.g. large, singly-charged clusters) requires low trapping potentials due to storage conditions for the Penning trap [53]. On the other hand, attachment of additional electrons to already negatively charged clusters requires a high trapping potential [52,54]. Details of the penta-anion production of size-selected aluminum clusters will be published elsewhere.

5 Summary

Modifications of the ClusterTrap setup which facilitate and extend its potential for investigation of stored clusters have been presented. A new LabVIEW-based experiment-control and data-acquisition system includes automated setting of several hardware parameters. Thus, automated scans instead of manual step-by-step variation of experimental parameters can be realized. Furthermore, scans of

two or more parameters can be performed automatically, as well as a simultaneous variation of two parameters.

With the newly implemented electrostatic quadrupole deflector the number of (cluster) ion sources and detection devices being attached simultaneously to the setup has been increased. Furthermore, positively and negatively charged clusters can now be monitored simultaneously and thus will allow a better characterization of the cluster source. With the implementation of a linear RFQ trap cluster-preparation steps like accumulation and cluster-size selection can be performed prior to transfer to the Penning trap. Thus, the count rates per cycle can be increased. In addition, the cycle repetition rate of the experiment has doubled, since cluster preparation steps and cluster measurements are now realized in two simultaneously running subcycles. Furthermore, by adding the linear RFQ trap the cluster-ion transfer from the source to the Penning trap has been facilitated, as all clusters can be ejected from the RFQ trap with the same energy regardless of their size and thus the same ion-optical settings can be used.

Last but not least the rearrangement of the setup allows one to perform the ToF mass analysis with ion ejection from the Penning trap back in the direction towards the cluster source, i.e. to use the transfer section as the ToF drift section, too. This opens up the option to install further interaction or analysis devices at the other side of Penning trap or, alternatively, to shorten the apparatus on that side of the superconducting magnet.

As a first test application with the new setup, aluminum clusters in the size range between about 400 and 500 have been trapped and exposed to two subsequent electron baths between which the trapping voltage was increased. With this new technique, to be reported elsewhere in more detail, multiply negatively charged metal clusters have been observed up to the penta-anions for the first time.

The authors thank the Collaborative Research Centre SFB 652 of the DFG for financial support. F.M. has received a postgraduate stipend from the state of Mecklenburg-Vorpommern in the framework of the International Max Planck Research School on Bounded Plasmas. Special thanks go to Martin Arndt for the design of the linear RFQ trap, and to Steffi Bandelow for her support with respect to measurements with this device.

References

1. L. Schweikhard et al., Phys. Scr. T **59**, 236 (1995)
2. S. Becker, K. Dasgupta, G. Dietrich, H.J. Kluge, S. Kuznetsov, M. Lindinger, K. Lützenkirchen, L. Schweikhard, J. Ziegler, Rev. Sci. Instrum. **66**, 4902 (1995)
3. L. Schweikhard, S. Krückeberg, K. Lützenkirchen, C. Walther, Eur. Phys. J. D **9**, 15 (1999)
4. L. Schweikhard, K. Hansen, A. Herlert, G. Marx, M. Vogel, Eur. Phys. J. D **24**, 137 (2003)
5. L.S. Brown, G. Gabrielse, Rev. Mod. Phys. **58**, 233 (1986)
6. F.G. Major, V.N. Gheorghe, G. Werth, *Charged Particle Traps: The Physics and Techniques of Charged Particle Field Confinement* (Springer, Berlin 2004)
7. P.K. Ghosh, *Ion Traps* (Clarendon, Oxford, 1995)
8. *Clusters of Atoms and Molecules*, edited by H. Haberland (Springer Series of Chemical Physics, Springer, Berlin, 1994), Vols. 52, 56
9. R.L. Johnston, *Atomic and Molecular Clusters* (Taylor and Francis, London, 2002)
10. J.-P. Connerade, A.V. Solov'yov, *Latest Advances in Atomic Cluster Collisions: Fission, Fusion, Electron, Ion and Photon Impact* (Imperial College Press, London, 2004)
11. P.-G. Reinhard, E. Suraud, *Introduction to Cluster Dynamics* (Wiley-VCH, Weinheim, 2004)
12. L. Assoufid, V.O. Kostroun, Nucl. Instr. Methods B **69**, 492 (1992)
13. P.R. Mahaffy, K. Lai, J. Vac. Sci. Technol. A **8**, 3244 (1990)
14. J.W. Farley, Rev. Sci. Instrum. **56**, 1834 (1985)
15. H.D. Zeman, Rev. Sci. Instrum. **48**, 1079 (1977)
16. R. Bredy, J. Bernard, L. Chen, G. Montagne, B. Li, S. Martin, J. Phys. B **42**, 154023 (2009)
17. H. Wunderlich, C. Wunderlich, K. Singer, F. Schmidt-Kaler, Phys. Rev. A **79**, 052324 (2009)
18. D.J. Douglas, Mass Spectrom. Rev. **28**, 937 (2009)
19. F. Herfurth, J. Dilling, A. Kellerbauer, G. Bollen, S. Henry, H.-J. Kluge, E. Lamour, D. Lunney, R.B. Moore, C. Scheidenberger, S. Schwarz, G. Sikler, J. Szerypo, Nucl. Instrum. Methods **469**, 254 (2001)
20. F. Bulut, W. Rosellen, M. Getzlaff, Appl. Phys. A **97**, 185 (2009)
21. R. Alayan, L. Arnaud, M. Broyer, E. Cottancin, J. Lerme, S. Marhaba, J.L. Vialle, M. Pellarin, Phys. Rev. B **76**, 075424 (2007)
22. M. Hillenkamp, G. Domenicantonio, C. Felix, Rev. Sci. Instrum. **77**, 025104 (2006)
23. R. Alayan, L. Arnaud, A. Bourgey, M. Broyer, E. Cottancin, J.R. Huntzinger, J. Lerme, J.L. Vialle, M. Pellarin, G. Guiraud, Rev. Sci. Instrum. **75**, 2461 (2004)
24. M.O. Watanabe, N. Uchida, T. Kanayama, Eur. Phys. J. D **9**, 571 (1999)
25. B. Plastridge, K.A. Cowen, D.A. Wood, M.H. Cohen, M.H.J.V. Coe, Surf. Rev. Lett. **3**, 655 (1996)
26. J. Tiggesbäumker, L. Köller, H.O. Lutz, K.H. Meiwes-Broer, Chem. Phys. Lett. **190**, 42 (1992)
27. C.W. Walter, Y.K. Bae, D.C. Lorents, J.R. Peterson, Chem. Phys. Lett. **195**, 543 (1992)
28. T. Dresch, H. Kramer, Y. Thurner, R. Weber, Z. Phys. D **18**, 391 (1991)
29. S. Wolf, G. Sommerer, S. Rutz, E. Schreiber, T. Leisner, L. Wöste, R.S. Berry, Phys. Rev. Lett. **74**, 4177 (1995)
30. H. Hiura, T. Kanayama, Chem. Phys. Lett. **328**, 409 (2000)
31. N. Walsh, A. Herlert, F. Martinez, G. Marx, L. Schweikhard, J. Phys. B **42**, 154024 (2009)
32. R. Weidele, U. Frenzel, T. Leisner, D. Kreisle, Z. Phys. D **20**, 411 (1991)
33. R. Jamal, Nucl. Instrum. Methods **352**, 438 (1994)
34. C. Elliott, V. Vijayakumar, W. Zink, R. Hansen, J. Assoc. Lab. Automat. **12**, 17 (2007)

35. D. Beck, K. Blaum, H. Brand, F. Herfurth, S. Schwarz, Nucl. Instrum. Methods **527**, 567 (2004)
36. G. Bollen, S. Becker, H.-J. Kluge, M. König, R.B. Moore, T. Otto, H. Raimbault-Hartmann, G. Savard, L. Schweikhard, H. Stolzenberg, the ISOLDE Collaboration, Nucl. Instrum. Methods **368**, 675 (1996)
37. M. Mukherjee, D. Beck, K. Blaum, G. Bollen, J. Dilling, S. George, F. Herfurth, A. Herlert, A. Kellerbauer, H.-J. Kluge, S. Schwarz, L. Schweikhard, C. Yazidjian, Eur. Phys. J. A **35**, 1 (2008)
38. D. Beck, H. Brand, H. Hahn, F. Herfurth, S. Koszudowski, G. Marx, L. Schweikhard, F. Ziegler, *Proceedings of ICALEPCS 2009* (Kobe, Japan, 2010), p. 215, ISBN 978-4-9905391-0-8
39. A. Loboda, A. Krutchinsky, O. Loboda, J. McNabb, V. Spicer, W. Ens, K. Standing, Eur. J. Mass Spectrom. **6**, 531 (2000)
40. A.G. Marshall, T.-C.L. Wang, T.L. Ricca, J. Am. Chem. Soc. **107**, 7893 (1985)
41. S. Guan, A.G. Marshall, Anal. Chem. **65**, 1288 (1993)
42. S. Krückeberg, D. Schooss, M. Maier-Borst, J.H. Parks, Phys. Rev. Lett. **85**, 4494 (2000)
43. R.K. Julian, Jr., R.G. Cooks, Anal. Chem. **65**, 1827 (1993)
44. S. Guan, A.G. Marshall, Int. J. Mass Spectrom. Ion Proc. **157/158**, 5 (1996)
45. M.E. Belov, E.N. Nikolaev, K. Alving, R.D. Smith, Rapid. Commun. Mass Spectrom. **15**, 1172 (2001)
46. D.J. Douglas, A.J. Frank, D. Mao, Mass Spectrom. Rev. **24**, 1 (2005)
47. N.R. Daly, Rev. Sci. Instrum. **31**, 264 (1960)
48. A. Herlert, S. Krückeberg, L. Schweikhard, M. Vogel, C. Walther, Phys. Scr. T **80**, 200 (1999)
49. A. Lassesson, N. Walsh, F. Martinez, A. Herlert, G. Marx, L. Schweikhard, Eur. Phys. J. D **34**, 73 (2005)
50. N. Walsh, F. Martinez, G. Marx, L. Schweikhard, Eur. Phys. J. D **43**, 241 (2007)
51. N. Walsh, F. Martinez, G. Marx, L. Schweikhard, F. Ziegler, Eur. Phys. J. D **52**, 27 (2009)
52. N. Walsh, F. Martinez, G. Marx, L. Schweikhard, F. Ziegler, J. Chem. Phys. **132**, 014308 (2010)
53. L. Schweikhard, J. Ziegler, H. Bopp, K. Lützenkirchen, Int. J. Mass Spectrom. Ion Proc. **141**, 77 (1995)
54. A. Herlert, R. Jertz, J. Alonso Otamendi, A.J. Gonzalez Martinez, L. Schweikhard, Int. J. Mass Spectrom. **218**, 217 (2002)

Article II

Received: 10 June 2008 ■ *Revised: 20 October 2008* ■ *Accepted: 29 October 2008* ■ *Publication: 20 November 2008*

EJMS EUROPEAN JOURNAL OF MASS SPECTROMETRY

Dedicated to Peter Derrick in recognition of his contributions to mass spectrometry

Unintended parametric ejection of ions from an ion cyclotron resonance trap by two-electrode axialization

Franklin Martinez, Alexander Herlert, Gerrit Marx, Lutz Schweikhard and Noelle Walsh

Institut für Physik, Ernst-Moritz-Arndt-Universität Greifswald, D-17487 Greifswald, Germany. E-mail: martinez@physik.uni-greifswald.de

Azimuthal quadrupolar excitation is a commonly used technique in the field of ion cyclotron resonance mass spectrometry, in particular in combination with buffer-gas collisions to achieve axialization of the stored ions. If the quadrupolar excitation is applied with only one phase to a set of two opposing ring segments (rather than the "regular" method where two sets of electrodes are addressed with opposite polarities), parametric resonance effects at the frequencies $2\nu_z$ and $\nu_p=\nu_+-\nu_-$ can lead to unintended ejection of ions from the trap. These parametric resonances have been revisited both theoretically and experimentally: multipole components of different azimuthal excitation schemes are derived by a simple vector representation of the excitation signal applied to the ring segments. Thus, parametric contributions can be easily identified, as demonstrated for the two-electrode and the four-electrode quadrupolar excitation schemes as well as further examples. In addition, the effect of the single-phase two-electrode quadrupolar excitation is demonstrated for storage and axialization of cluster ions.

Keywords: ion cyclotron resonance, Penning trap, axialization, buffer-gas cooling, ion ejection

Introduction

Ion traps[1,2] are particularly suitable devices to confine charged particles for extended periods of time. They facilitate the manipulation of ion motion to allow the removal of unwanted ions and the preparation of ions before a particular interaction is investigated. Manipulation of the ion motional modes is achieved by application of additional rf-fields, with the geometric arrangement of the excitation electrodes and the applied frequency determining the nature of excitation and the kind of ions being affected. Penning traps [i.e. ion cyclotron resonance (ICR) cells] are particularly suitable for this purpose and a number of excitation methods are currently in use.[3]

The technique of dipolar radial excitation is of particular importance in Penning trap mass spectrometry. It is achieved by application of rf-excitation signals of opposite polarity (i.e. a phase shift of 180° w.r.t. each other) to two opposing trap electrodes. When the excitation is applied at the reduced cyclotron frequency, ν_+, or the magnetron frequency, ν_-, the corresponding amplitudes of the motional modes are increased or decreased, depending on the phase relation between the excitation signal and the ion motion. Such an excitation scheme allows the excitation of stored ions to higher kinetic energies, for example, for collision studies, for mass selection by radial ejection of all unwanted species and by excitation to a coherent motion at large radii for the observation of the image–charge signal induced in ring electrodes in Fourier transform ICR mass spectrometry (FT-ICR MS).[4–7] Similarly, a dipolar excitation can be applied in the axial direction, but as the trapping motion is independent of the magnetic field, this mode is rarely used.

Contribution for special issue in honor of Peter J. Derrick

ISSN: 1469-0667
doi: 10.1255/ejms.962

© IM Publications LLP 2009
All rights reserved

After its introduction in the early 90s in the framework of precision mass-spectrometry experiments of short-lived radio isotopes,[8,9] the azimuthal quadrupolar excitation[10] has found widespread use, in particular in combination with buffer-gas collisions.[11,12] Two effects are brought together: Interconversion between magnetron and cyclotron motional modes and buffer-gas damping of the ion motion. The latter would lead to ion loss due to the metastability of the magnetron motion with respect to frictional forces. However, since the damping of the cyclotron motion is faster than the magnetron blow-up, the additional coupling between the two motional modes leads to an overall decrease of the extension of the radial ion motion.

Thus, by combining buffer-gas damping with quadrupolar excitation, an effective technique of radial centering, also called "axialization" or simply "cooling", had been found, which has been further developed, described and made use of extensively.[12–17]

The present cluster experiments were performed with a Penning trap, i.e. with hyperbolically shaped electrodes. However, this poses no restriction of the methods described in the following, with respect to the applicability to other electrode arrangements, as frequently employed for FT-ICR MS, such as the cubic and the cylindrical ion trapping cell. All three trap types have two "end-cap electrodes", or trapping plates that define the trapping volume in axial direction. There is at least a third electrode between them which will be referred to as "ring electrode" (and for both the hyperbolical and the cylindrical trap it is indeed circular in shape) and is generally split into several segments. In the case of the cubic trap, the "ring" electrode is realized by four additional plates. Thus it is automatically split into four electrodes as will be the case for the ring electrode in most of what follows below. In FT-ICR MS, one pair of opposing electrodes is usually referred to as excitation plates, while the other pair is called detection plates, due to their purpose. For metal-cluster research with FT-ICR MS see, for example, Anderson *et al.*[18]

As the ring-electrode segments are in general used for several excitation schemes, the application of quadrupolar excitation often requires switching between different electrical connections,[19] in particular, if the ring electrode is segmented into only four pieces. However, it was realized soon after the introduction of the method, that azimuthal quadrupolar excitation is also possible by application of the rf-signal (of equal polarity) to only two opposing segments of a four-segment ring.[20] (Note in passing that splitting the ring into two pieces of 180° is not sufficient, but would correspond to parametric excitation, see below).

As already mentioned by Hendrickson *et al.*,[20] the two-electrode quadrupolar excitation does have a drawback: in addition to the (usually desired) conversion resonance at the sum frequency $\nu_+ + \nu_- = \nu_c$ [10] and the (unwanted) resonances at $2\nu_-$ and $2\nu_+$, it includes a further resonance where the ions are driven out of the trap, namely at the axial parametric frequency, $2\nu_z$. In addition to the axial one there is also a radial parametric resonance at $\nu_p = \nu_+ - \nu_-$.[21] As it is based on the same parameter (most commonly represented by the trapping voltage), it is expected that this resonance can be addressed by the two-electrode quadrupolar excitation, too. Jackson *et al.* have shown that this is indeed the case and derived the details of these excitation forms in great detail,[22] based on the method of known ion trajectories and instantaneous power absorption, as described earlier.[3]

The two investigations on unipolar (i.e. one-phase) quadrupolar excitation mentioned above are mainly concerned with the application in FT-ICR MS**.** In this field, the implication of the unwanted resonances are only minor, maybe with the exception that, due to the $2\nu_+$–resonances, one should restrict the range of axialization to "an octave in [excitation] frequency",[22] i.e. a mass range spanning a maximum spread of two. (Note that this is a limit of axialization, only, not of the trapping range, where the mass-over-charge ranges can exceed a factor of 10^7.)[23]

In this contribution, examples from atomic-cluster studies in a Penning trap are shown, where the additional resonances mentioned above lead to the ejection of particular cluster sizes,[24] which—depending on the investigation—may be unwanted. Furthermore, an alternative approach to derive the effects is described (see next section), where, instead of recalculating the ion motion from first principles,[22] the two-electrode excitation is decomposed into its "natural components" which can be immediately related to the resonance frequencies as derived previously.[3]

Theoretical considerations

Without repeating the derivations and details, the following is recalled from an earlier review of the most important resonances in an ICR trap:[3]

Resonant dipolar excitation can be applied axially at ν_z or radially at either ν_- or ν_+. Thus, the amplitudes of the trapping, the magnetron and the cyclotron motion, respectively, are affected. When the corresponding motion has no finite initial amplitude, i.e. the trapping mode amplitude or the radii of the radial circular motions are zero, the amplitude increases linearly as a function of time (where excitation during many periods is assumed and the effect is averaged).

Azimuthal quadrupolar excitation leads to a resonance phenomenon at $\nu_+ + \nu_- = \nu_c = qB/(2\pi m)$: The magnetron and the cyclotron motional modes are coupled and continuously interconverted into one another.[10] At $2\nu_-$ and $2\nu_+$, the amplitude of the magnetron and the cyclotron motion, respectively, increases exponentially as a function of time.

Parametric resonances occur at twice the trapping frequency, $2\nu_z$, and at the "parametric frequency", $\nu_p = \nu_+ - \nu_-$. In the first case, the amplitude of the trapping motion increases exponentially as a function of time, in the second both the magnetron and the cyclotron radii increase, again exponentially.

Note that in the parametric excitation, the excitation electrodes are identical with the trap electrodes, i.e. the

rf-excitation signal is applied with inversed polarities to the ring and the two endcaps. This excitation mode can thus be called axial quadrupolar. On the other hand, when only the radial terms are considered, this excitation corresponds to a "monopolar" (breathing) mode (see below).

For an axial dipolar excitation, the two polarities of the rf-signal are applied to the endcaps, on top of the appropriate trapping voltage. Similarly, for radial dipolar excitation, the ring is split into (at least two) pieces and rf-signals of opposite polarities are applied to opposing segments. As indicated in the introduction, for an azimuthal quadrupolar excitation two sets of pair-wise opposing ring segments are used, where rf-signals of opposite polarities are applied to the two sets.

Note that by "opposite polarities" we mean a phase shift of 180 degrees between the rf-signals. ("Quadrature excitation", where phase shifts of 90°, 180° and 270° are applied,[3,25,26] is not considered in this contribution.) Only in a hyperbolical Penning trap, including the two-electrode trap,[27] for a trapping potential as accurate as possible, the parametric excitation has "perfect" geometry, as it is identical with the equipotential lines of the trapping electrodes. In all other cases, for example, for cubic traps or for cylindrical traps, the excitation field is a superposition of multipoles with the dipolar or quadrupolar term being only the leading ones.

In particular, for the excitation modes of the radial motions applied to the ring segments, the coefficients of the multipole components can be calculated by a Fourier analysis of the potential at the electrodes as a function of the angle in cylindrical coordinates. This includes the parametric excitation as it corresponds to an offset of the voltage across the whole ring with respect to the trapping potential at the ring. Thus, in the following, the application of the standard excitation modes with four equally divided ring segments (corresponding to the set of four plates of a cubic cell) will be analyzed with respect

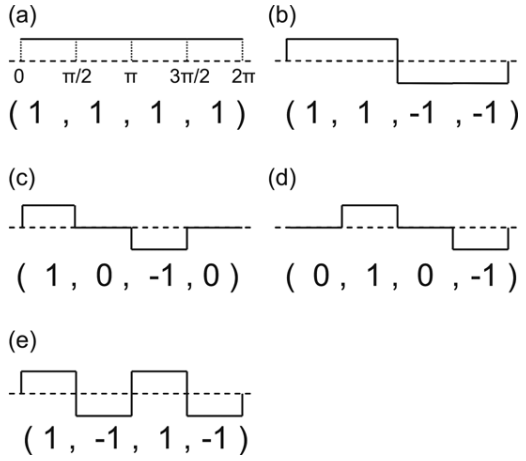

Figure 1. Excitation signal strength (and relative polarity) as a function of azimuthal angle along the ring electrode, (a) for parametric (monopolar), (b), (c) and (d) for azimuthal dipolar and (e) for quadrupolar geometries.

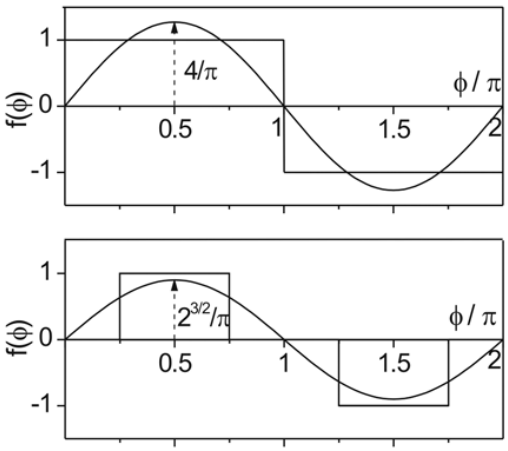

Figure 2. Excitation signal strength (and relative polarity) as a function of azimuthal angle along the ring electrode for "two-halve"-electrode (top) and "two-quarter"-electrode (bottom) dipolar excitation. For both configurations the respective dipolar Fourier components are plotted.

to the average signal at the ring electrode in order to deduce the parametric component.

Figure 1 shows the distribution of the excitation signal along the ring segments for the different excitation modes. Figure 1(a) would conventionally be associated with the parametric (monopolar), Figure 1(b) with the dipolar and Figure 1(e) with the quadrupolar excitation geometry. However, note that the configurations shown in (c) and (d) correspond to dipolar excitations as well, although of less electric-field strength as compared to the "two-halves" configuration of Figure 1(b). The ratio of the dipolar components of the Fourier transforms results in a factor of

$$\frac{\frac{1}{\pi}\int_{0}^{\pi}1\cdot\sin\varphi d\varphi+\frac{1}{\pi}\int_{\pi}^{2\pi}(-1)\cdot\sin\varphi d\varphi}{\frac{1}{\pi}\int_{\pi/4}^{3\pi/4}1\cdot\sin\varphi d\varphi+\frac{1}{\pi}\int_{5\pi/4}^{7\pi/4}(-1)\cdot\sin\varphi d\varphi}=\frac{\frac{4}{\pi}}{\frac{2\sqrt{2}}{\pi}}=\sqrt{2} \qquad (1)$$

between the arrangements (Figure 2). This small reduction is, in fact, traded for the convenience of having two further electrodes, which can be used, for example, as detection electrodes, as in the case of a cubic trap in FT-ICR MS.

For the following considerations, the arrangements (c) and (d) are more suitable than (b), as they can be considered as two basis vectors, $\mathbf{D_1}=(1,0,-1,0)$ and $\mathbf{D_2}=(0,1,0,-1)$, of a set of four, including the "monopole vector", $\mathbf{M}=(1,1,1,1)$, and the "quadrupole vector", $\mathbf{Q}=(1,-1,1,-1)$, which span a 4-dimensional vector space. The configuration of Figure 1(b) is then simply expressed by $\mathbf{D_1}+\mathbf{D_2}=(1,0,-1,0)+(0,1,0,-1)=(1,1,-1,-1)$.

With this vector representation and the results from Schweikhard *et al.*[3], the analysis of the resonances of the ion motion with respect to the signals applied to the ring segments reduces to a simple textbook exercise in linear algebra: given the signal strength and polarity at the four segments, what

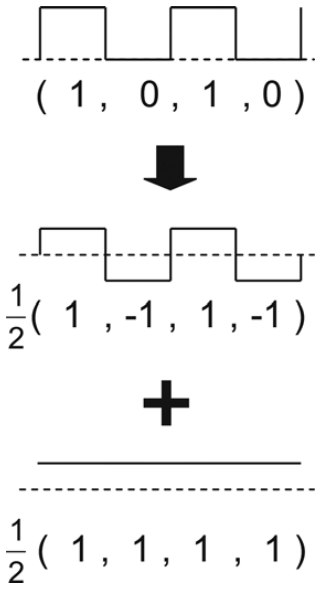

Figure 3. Excitation signal strength (and relative polarity) as a function of azimuthal angle along the ring electrode for two-electrode quadrupolar excitation (top). This excitation vector is achieved by combination of the "quadrupole vector" Q (middle) and the "monopole vector" M (bottom) with corresponding prefactors.

is the linear combination of the basis vectors that it can be decomposed to or—equivalently but in other words—that it can be synthesized from?

The case of the two-electrode quadrupolar excitation is shown graphically in Figure 3. This excitation geometry (top) can be decomposed to a combination of the "regular" quadrupolar and a parametric (monopolar) excitation of equal strengths, i.e.

$$(1,0,1,0) = \frac{1}{2}(1,-1,1,-1) + \frac{1}{2}(1,1,1,1) \qquad [2]$$
$$= \frac{1}{2}\mathbf{Q} + \frac{1}{2}\mathbf{M}$$

Although it is not needed for the present investigation of two-electrode quadrupolar excitation, let us also consider the excitation on a single quarter of the ring, i.e. only one of the segments, for example, (1,0,0,0). The basis set {(1,0,0,0), (0,1,0,0), (0,0,1,0), (0,0,0,1)} = {$\mathbf{E}_1$, $\mathbf{E}_2$, $\mathbf{E}_3$, $\mathbf{E}_4$} may look more familiar as {**M**, $\mathbf{D}_1$, $\mathbf{D}_2$, **Q**}, although the latter is the more "natural" for the present problem. On the other hand, the "single-segment excitation" is encountered when, for example, a lead to one of the excitation electrodes is broken during dipolar excitation, and it will be useful further below, when the excitation with two adjacent segments will be considered.

As graphically shown in Figure 4, the $\mathbf{E}_1$ configuration can be decomposed into a prominent dipolar term and both a monopolar and a quadrupolar additional term:

$$\mathbf{E}_1 = (1,0,0,0) = \frac{1}{4}\mathbf{M} + \frac{1}{2}\mathbf{D}_1 + 0\cdot\mathbf{D}_2 + \frac{1}{4}\mathbf{Q} \qquad [3(a)]$$

The other three base vectors can be analyzed with analog results:

$$\mathbf{E}_2 = (0,1,0,0) = \frac{1}{4}\mathbf{M} + 0\cdot\mathbf{D}_1 + \frac{1}{2}\mathbf{D}_2 - \frac{1}{4}\mathbf{Q} \qquad [3(b)]$$

$$\mathbf{E}_3 = (0,0,1,0) = \frac{1}{4}\mathbf{M} - \frac{1}{2}\mathbf{D}_1 + 0\cdot\mathbf{D}_2 + \frac{1}{4}\mathbf{Q} \qquad [3(c)]$$

$$\mathbf{E}_4 = (0,0,0,1) = \frac{1}{4}\mathbf{M} + 0\cdot\mathbf{D}_1 - \frac{1}{2}\mathbf{D}_2 - \frac{1}{4}\mathbf{Q} \qquad [3(d)]$$

(Note that the signs have almost no significance in the current context. Invertion of all signs corresponds to an inverted phase of the excitation.) For the present investigation, we will not dwell further on the method and only note a straightforward generalization: By segmentation into (*m*) smaller ring pieces (and calculations in correspondingly higher-dimensional vector spaces), higher multipoles can be addressed. In these cases, the use of the single-segment basis {$\mathbf{E}_1$, $\mathbf{E}_2$, $\mathbf{E}_3$, $\mathbf{E}_4$, ..., $\mathbf{E}_m$} might be even more helpful to deduce the corresponding multipoles.

Returning to the two-electrode quadrupolar excitation, according to Jackson *et al.*[22] one would expect that

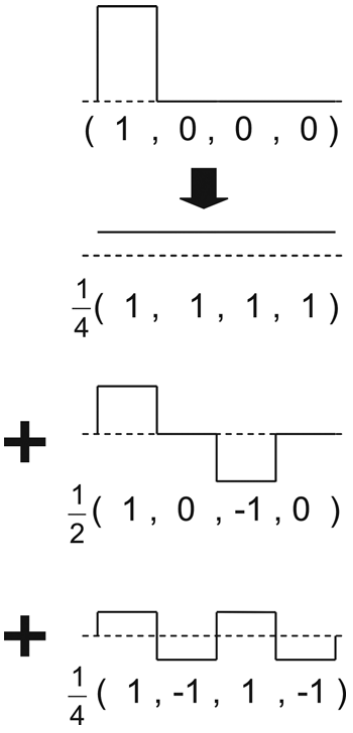

Figure 4. Excitation signal strength (and relative polarity) as a function of azimuthal angle along the ring electrode for excitation at one of four segments (top). This excitation vector is achieved by combination of the "monopole vector" M, the "dipole vector" D_1 and the "quadrupole vector" Q with corresponding prefactors (lines from top to bottom).

this excitation mode results in only 1/3 of the electric field strength as compared to a regular quadrupolar excitation with equal signal strengths at the two sets of excitation electrodes. In contrast, Equation (2) suggests a reduction by a factor of two. As shown in the attached appendix, the factor two is indeed correct.

Experimental set-up

The experiments have been conducted at the ClusterTrap set-up which has been described in some detail in previous publications.[23,28,29] In short, metal cluster ions are produced in an external source,[30] transferred by electrostatic ion–optical elements to a Penning trap, captured in flight and stored for further experiments. After the interactions of interest, which can be a sequence of manipulations, reactions and delay periods, the remaining ions are axially ejected and analyzed by time-of-flight (ToF) mass spectrometry.

In addition to single-bunch capturing, several ion bunches can be accumulated in the Penning trap in order to increase the number of ions for the subsequent experiments.[14] Such a scheme is also used in most of the experiments shown in the next section.

In contrast to the four-times-90° ring segmentation as analyzed above, the ClusterTrap ring is segmented into eight parts, including a set of two opposing segments of 80°, another set of two opposing segments of 40° and, finally, four segments each of 30° between the others.[31] However, this has no significant further influence on the current investigations since, for the measurements presented below, the rf-signal with the same polarity has been applied to a set of opposing segments, which effectively is the two-electrode quadrupolar excitation described above. Differences could only be due to contributions from higher multipoles, which have a small influence and can be neglected.

The present experiments have been performed with gold and aluminum clusters. Due to the high atomic mass of gold, even small clusters have a relatively low cyclotron frequency (at the magnetic field strength of $B = 5$ T). Thus, for the geometry parameter[28,31] $d^2 = 200\ \mathrm{mm}^2$ even trapping voltages of the order of $U_0 = 10$ V allow the effects on neighboring cluster sizes to be seen.[24] For the case of aluminum clusters, an example is shown (Figure 5), where both desired centering of clusters of one size and simultaneous ejection of two other cluster sizes (possibly unintended, for this demonstration on purpose), one by axial parametric and the other by radial parametric resonant excitation, have been observed.

Results and discussion

Figure 5 shows two ToF spectra of aluminum clusters Al_n^-. The cluster source generates a broad range of cluster sizes, not all of which are depicted here. The range of clusters transferred to the trap is determined by the transfer parameters

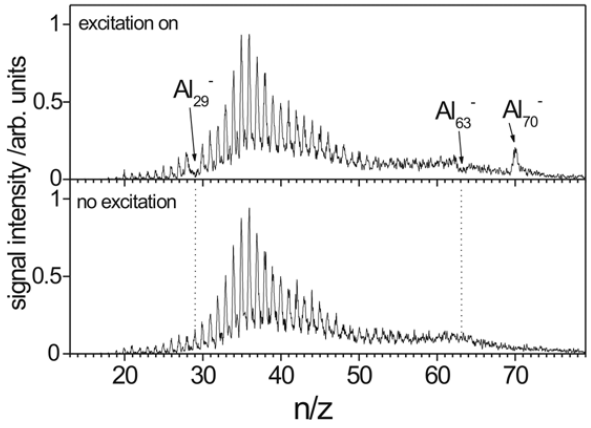

Figure 5. ToF mass spectra of aluminum cluster anions after accumulation (350 cycles) at trapping voltage $U_0 = 26$ V with (top) and without (bottom) axialization by application of argon buffer gas and two-electrode quadrupolar excitation at the cyclotron frequency of Al_{70}^-.

and chosen appropriately for the presentation of the effects described above, namely from size $n \approx 20$ to above $n = 70$.

The lower part of the figure shows a reference spectrum with the abundance pattern in the absence of any rf-manipulation of the ion motion. For the spectrum in the upper part, a two-electrode quadrupolar excitation at $\nu_c = 40.4$ kHz has been applied. This results in a strong enhancement of the cluster abundance around $n \approx 70$, as expected.

Note, that in a study of cluster properties, the clusters of interest would be chosen from the center of the distribution, or rather the distribution would be shifted accordingly.[28] The present situation is only chosen for the demonstration of the two-electrode quadrupolar excitation effects: while

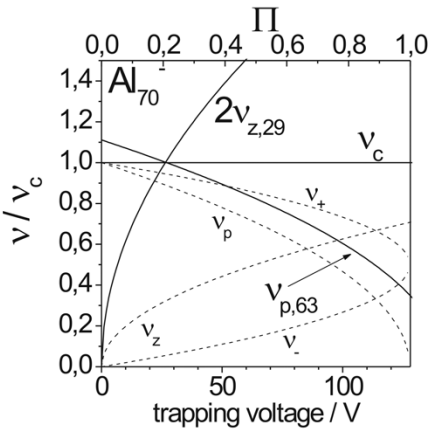

Figure 6. Comparison of the cyclotron frequency ν_c for $n = 70$ with the radial parametric frequency ν_p for $n = 63$ and with twice the axial oscillation frequency $2\nu_z$ for $n = 29$ (solid lines) as a function of the trapping voltage U_0 and the trap parameter Π for $n = 70$. For comparison ν_+, ν_-, ν_z and ν_p for $n = 70$ are plotted (dashed lines).

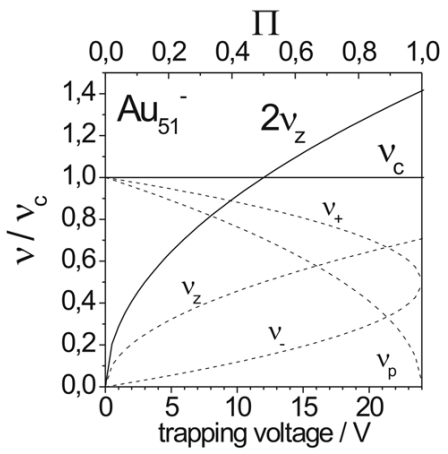

Figure 7. Comparison of the cyclotron frequency ν_c and twice the axial oscillation frequency $2\nu_z$ (solid lines) as a function of the trapping voltage, U_0 (for Au_{51}^- at ClusterTrap) and the trap parameter, Π. For comparison ν_+, ν_-, ν_z and ν_p are plotted (dashed lines).

the frequency of 40.4 kHz corresponds to ν_c at $n = 70$, it also coincides with $2\nu_z$ for $n \approx 29$ and with ν_p for $n \approx 63$. Indeed, the cluster abundance is observed to break down at exactly these two cluster sizes. This resonance condition can be described with the trap parameter Π of ICR traps,[32] as shown in Figure 6. The radial parametric frequency of $n = 63$ and the double axial frequency of $n = 29$ (both normalized to the cyclotron frequency of $n = 70$) are plotted as a function of the trapping voltage, U_0, and the trap parameter, Π, for $n = 70$.

In general, the cyclotron frequency ν_c is independent of the trapping voltage, in contrast to ν_p and $2\nu_z$. Of these two frequencies, the latter is strongly dependent on the trapping voltage. Thus, going to extremes, there will even be a "self ejection" of the axialized ions when the condition $2\nu_z = \nu_c$ is reached. In terms of the trap parameter, Π, this corresponds to $\Pi = 1/2$, as shown in Figure 7 for the example of the gold cluster, Au_{51}^-. In the case of the aluminum clusters, the trapping voltage is far away from "self-ejection" for the excited cluster size $n = 70$ (Figure 6).

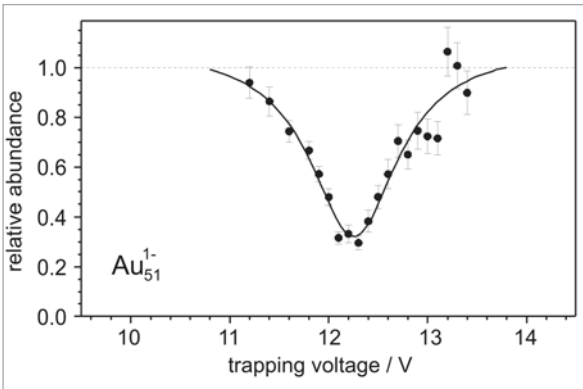

Figure 8. Abundance of Au_{51}^- after application of a quadrupolar rf-excitation ($\Delta t = 200$ ms) with frequency $\nu_c = 7639$ Hz as a function of the applied trapping voltage. The data is normalized to a reference cycle without a quadrupolar rf-excitation. The solid line is a fit of a Lorentzian to the data in order to guide the eye.

However, the situation of $2\nu_z = \nu_c$ can in fact be encountered experimentally, as shown in Figure 8. In this example a two-electrode quadrupolar excitation at $\nu_c = 7639$ Hz has been applied for the axialization of gold cluster ions, Au_{51}^-.

Note that this cluster has a mass-over-charge ratio exceeding 10,000. Thus, the condition $2\nu_z = \nu_c$ is already reached at relatively low trapping voltages, at least with respect to the voltages required for polyanion creation: for these studies, simultaneously stored electrons have to overcome the clusters' Coulomb barrier height to be able to form higher anionic charge states.[33–37]

Conclusion and outlook

The two-electrode quadrupolar excitation has been re-examined. The derivation of the resonance frequencies has been simplified in terms of an analysis of the multipolar components involved which can be reduced to a simple problem of linear algebra. Examples of ion ejection at ν_p and $2\nu_z$, the radial and axial parametric frequencies, respectively, have been given in the context of the simultaneous single-frequency axialization of cluster ions of a given size. In particular, it is shown that by the application of two-electrode quadrupolar excitation the ion species that is supposed to be axialized is rather ejected in the axial direction if its parametric-resonance frequency, $2\nu_z$, coincides with the applied axialization frequency, ν_c.

It should be noted that a "two-electrode excitation" does not necessarily need to unipolarly address two opposing electrodes. As another variation of excitation geometry, consider the use of two adjacent electrodes with rf-signals of opposite polarities, for example, segments one and two. Adding the corresponding base vectors results immediately in

$$\begin{aligned} \mathbf{E}_1 - \mathbf{E}_2 &= (1,-1,0,0) = \\ &= \left(\frac{1}{4} - \frac{1}{4}\right)\mathbf{M} + \frac{1}{2}(\mathbf{D}_1 - \mathbf{D}_2) + \left(\frac{1}{4} - \left[-\frac{1}{4}\right]\right)\mathbf{Q} \\ &= 0 \cdot \mathbf{M} + \frac{1}{2}(\mathbf{D}_1 - \mathbf{D}_2) + \frac{1}{2}\mathbf{Q} \end{aligned} \qquad (4)$$

By use of this "two-phase two-electrode quadrupolar excitation" the monopole term and, thus, the parametric resonances can be avoided! However, when the dipolar term is rewritten in the $\mathbf{E}_i$ base set,

$$\frac{1}{2}(\mathbf{D}_1 - \mathbf{D}_2) = \frac{1}{2}(1,-1,-1,1) \qquad (5)$$

it turns out to be equivalent to half of the signal strength of the two-halves configuration of Figure 1(b) (rotated by 90° along the ring).

Thus, unfortunately, this term of dipolar excitation leads to ejection for ions where the excitation frequency coincides with their ν_+. On the other hand, this may not be so bad after all, since ν_c is somewhat shifted from ν_+ and such a configuration allows a simultaneous application of axialization and off-resonance dipolar excitation. In essence, it looks like SORI (i.e. sustained off-resonance irradiation,[38,39] a well-known method of collision-induced dissociation) can be combined with a continuous re-axialization of the precursor ions. However, when applying this excitation scheme, keep in mind that the dipolar excitation has a resonance, and ensure it does not coincide with the dissociation product.

Acknowledgments

This work has been co-funded by the Collaborated Research Centre SFB652 of the Deutsche Forschungsgemeinschaft and the German Ministry for Education and Research (BMB) under the contract 06GF181I. F.M. thanks the Ernst-Moritz-Arndt-University of Greifswald and the International Max Planck Research School on Bounded Plasmas for support by a stipend. The authors thank the Max-Planck-Institute for Plasma Physics, Teilinstitut Greifswald, for its kind hospitality.

References

1. P.K. Ghosh, *Ion traps*. Oxford University Press, Oxford, UK (1995).
2. F.G. Major, V.N. Gheorghe and G. Werth, "Charged particle traps", Springer Verlag New Yor, USA (2005).
3. L. Schweikhard and A.G. Marshall, "Excitation modes for Fourier transform ion cyclotron resonance mass spectrometry", *J. Am. Soc. Mass Spectrom.* **4,** 433 (1993). doi: 10.1016/1044-0305(93)80001-F
4. M.B. Comisarow and A.G.Marshall, "Fourier transform ion cyclotron resonance spectroscopy", *Chem. Phys. Lett.* **25,** 282 (1974). doi: 10.1016/0009-2614(74)89137-2
5. A.G. Marshall and P.B. Grosshans, "Fourier transform ion cyclotron resonance mass spectrometry: the teenage years", *Anal. Chem.* **63,** 215A (1991).
6. A.G. Marshall and L. Schweikhard, "Fourier transform ion cyclotron resonance mass spectrometry: technique developments", *Int. J. Mass Spectrom. Ion Proc.* **118/119,** 37 (1992). doi: 10.1016/0168-1176(92)85058-8
7. A.G. Marshall, C.L. Hendrickson and G.S. Jackson, "Fourier transform ion cyclotron resonance mass spectrometry: A primer", *Mass Spectrom. Rev.* **17,** 1 (1998). doi: 10.1002/ (SICI)1098-2787(1998)17:1<1::AID-MAS1>3.0.CO;2-K
8. K. Blaum, "High-accuracy mass spectrometry with stored ions", *Phys. Rep.* **425,** 1 (2006). doi: 10.1016/ j.physrep.2005.10.011
9. L. Schweikhard and G. Bollen (Eds.), "Ultra-accurate mass spectrometry and related topics", *Int. J. Mass Spectrom.* (Special issue) **251,** (2006). doi: 10.1016/S1387-3806(06)00179-5
10. G. Bollen, R.B. Moore, G. Savard and H. Stolzenberg, "The accuracy of heavy-ion mass measurements using time-of-flight-ion cyclotron resonance in a Penning trap", *J. Appl. Phys.* **68,** 4355 (1990). doi: 10.1063/1.346185
11. G. Savard, St. Becker, G. Bollen, H.-J. Kluge, R.B. Moore, Th. Otto, L. Schweikhard, H. Stolzenberg and U. Wiess, "A new cooling technique for heavy ions in a Penning trap", *Phys. Lett. A* **158**, 247 (1991). doi: 10.1016/ 0375-9601(91)91008-2
12. L. Schweikhard, S. Guan and A.G. Marshall, "Quadrupolar excitation and collisional cooling for axialization and high pressure trapping of ions in Fourier transform ion cyclotron resonance mass spectrometry", *Int. J. Mass. Spectrom. Ion Proc.* **120,** 71 (1992). doi: 10.1016/0168-1176(92)80053-4
13. S. Guan, M.C. Wahl, T.D. Wood and A.G. Marshall, "Enhanced mass resolving power, sensitivity, and selectivity in laser desorption Fourier transform ion cyclotron mass spectrometry by ion axialisation and cooling", *Anal. Chem.* **65,** 1753 (1993). doi: 10.1021/ ac00061a019
14. H.-U. Hasse, St. Becker, G. Dietrich, N. Klisch, H.J. Kluge, M. Lindinger, K.Lützenkirchen, L. Schweikhard and J. Ziegler,"External-ion accumulation in a Penning trap with quadrupole excitation assisted buffer gas cooling", *Int. J. Mass Spectrom.* **132,** 181 (1994). doi: 10.1016/0168-1176(93)03924-B
15. C.L. Hendrickson and D.A. Laude Jr, "Quadrupolar axialization for improved control of electrosprayed proteins in FTICR mass spectrometry", *Anal. Chem.* **67,** 1717 (1995). doi: 10.1021/ac00106a011
16. A. Marshall, "Milestones in Fourier transform ion cyclotron resonance mass spectrometry technique development", *Int. J. Mass Spectrom.* **200,** 331 (2000). doi: 10.1016/S1387-3806(00)00324-9
17. J.A. Marto, S. Guan, A.G. Marshall and M.V. Buchanan, "Wide-mass-range axialization for high-resolution Fourier-transform ion cyclotron resonance mass spectrometry of externally generated ions", *Rapid Commun. Mass Spectrom.* **8**, 615 (2004). doi: 10.1002/ rcm.1290080809
18. M.L. Anderson, M.S. Ford, P.J. Derrick, T. Drewello, D.P. Woodruff and S.R. Mackenzie, "Nitric oxide decomposition on small rhodium clusters, $Rh_n^{+/-}$", *J. Phys. Chem. A* **110,** 10992 (2006). doi: 10.1021/jp062178z
19. J.P. Speir, G.S. Gorman, C.C. Pitsenberger, C.A. Turner, P.P. Wang and I.J. Amster, "Remeasurement of ions using quadrupolar excitation Fourier transform ion cyclotron resonance spectrometry", *Anal. Chem.* **65,** 1746 (1993). doi: 10.1021/ac00061a018
20. C.L. Hendrickson, J.J. Drader and D.A. Laude, Jr, "Simplified application of quadrupolar excitation in Fourier transform ion cyclotron resonance mass

spectrometry", *J. Am. Soc. Mass Spectrom.* **6,** 448 (1995). doi: 10.1016/1044-0305(95)00054-H

21. L. Schweikhard, M. Lindinger and H.-J. Kluge, "Parametric-mode excitation/dipole-mode detection FT-ICR", *Rev. Sci. Instrum.* **61,** 1055–8 (1990). doi: 10.1063/1.1141475

22. G.S. Jackson, C.L. Hendrickson, B.B. Reinhold and A.G. Marshall, "Two-plate vs. four-plate azimuthal quadrupolar excitation for FT-ICR mass spectrometry", *Int. J. Mass Spectrom. Ion Proc.* **165/166,** 327 (1997). doi: 10.1016/ S0168-1176(97)00188-2

23. L. Schweikhard, K. Hansen, A. Herlert, G. Marx and M. Vogel, "New approaches to stored cluster ions", *Eur. Phys. J. D* **24,** 137 (2003). doi: 10.1140/epjd/e2003-00181-x

24. L. Schweikhard, M. Breitenfeldt, A. Herlert, F. Martinez, G. Marx and N. Walsh, "Trap-based cluster research and cluster-based investigations of ion storage at ClusterTrap", *AIP Conf. Proc.* **862,** 264 (2006). doi: 10.1063/1.2387932

25. S. Guan, M.V. Gorshkov and A.G. Marshall, "Circularly polarized quadrature excitation for Fourier-transform ion cyclotron resonance mass spectrometry ", *Chem. Phys. Lett.* **198,** 143 (1992). doi: 10.1016/0009-2614(92)90062-R

26. L. Schweikhard, J.J. Drader, S.D.H. Shi, C.L. Hendrickson and A.G. Marshall, "Quadrature detection for the separation of the signals of positive and negative ions in Fourier transform ion cyclotron resonance mass spectrometry", *AIP Conf. Proc.* **606,** 647 (2002). doi: 10.1063/1.1454343

27. J.A. Marto, A.G. Marshall and L. Schweikhard, "A 2-electrode ion-trap for Fourier transform ion cyclotron resonance mass spectrometry", *Int. J. Mass Spectrom. Ion Proc.* **137,** 9 (1994). doi: 10.1016/0168-1176(94)85008-9

28. L. Schweikhard, St. Becker, K. Dasgupta, G. Dietrich, H.J. Kluge, D. Kreisle, S. Krückeberg, S. Kuznetsov, M. Lindinger, K. Lützenkirchen, B. Obst, C. Walther, H. Weidele and J. Ziegler, "Trapped metal cluster ions", *Phys. Scripta* **T59,** 236 (1995). doi: 10.1088/0031-8949/1995/T59/032

29. St. Becker, K. Dasgupta, G. Dietrich, H.J. Kluge, S. Kuznetsov, M. Lindinger, K. Lützenkirchen, L. Schweikhard and J. Ziegler, "A Penning trap mass spectrometer for the study of cluster ions", *Rev. Sci. Instrum.* **66,** 4902 (1995). doi : 10.1063/1.1146172

30. R. Weidele, U. Frenzel, T. Leisner and D. Kreisle, "Production of cold/hot metal cluster ions: a modified laser vaporization source", *Z. Phys. D* **20,** 411 (1991). doi: 10.1007/BF01544024

31. L. Schweikhard, M. Lindinger and H.J. Kluge,"Quadrupole-detection FT-ICR mass spectrometry" , *Int. J. Mass Spectrom. Ion Proc.* **98,** 25 (1990). doi: 10.1016/0168-1176(90)85045-4

32. L. Schweikhard, J. Ziegler, H. Bopp and K. Lützenkirchen, "The trapping condition and a new instability of the ion motion in the ion cyclotron resonance trap", *Int. J. Mass Spectrom. Ion Proc.* **141,** 77 (1995). doi: 10.1016/0168-1176(94)04092-L

33. A. Herlert, S. Krückeberg, L. Schweikhard, M. Vogel and C. Walther, "First observation of doubly charged negative gold cluster ions", *Phys. Scripta* **T80,** 200 (1999). doi: 10.1238/Physica.Topical.080a00200

34. A. Herlert, R. Jertz, J. Alonso Otamendi, A.J. González Martínez and L. Schweikhard, "The influence of the trapping potential on the attachment of a second electron to stored metal cluster and fullerene anions", *Int. J. Mass Spectrom.* **218,** 217 (2002). doi: 10.1016/S1387-3806(02)00723-6

35. A. Herlert and L. Schweikhard, "Production of dianionic and trianionic noble metal clusters in a Penning trap", *Int. J. Mass Spectrom.* **229**, 19 (2003). doi: 10.1016/S1387-3806(03)00251-3

36. A. Lassesson, N. Walsh, F. Martinez, A. Herlert, G. Marx and L. Schweikhard, "Formation of fullerene dianions in a Penning trap", *Eur. Phys. J. D* **34**, 73 (2005). doi: 10.1140/epjd/e2005-00122-9

37. N. Walsh, F. Martinez, G. Marx and L. Schweikhard, "Multiply negatively charged aluminium clusters. Production of Al_n^{2-} in a Penning trap", *Eur. Phys. J. D* **43,** 241 (2007). doi: 10.1140/epjd/e2007-00114-9

38. J.W. Gauthier, T.R. Trautman and D.B. Jacobson, "Sustained off-resonance irradiation for collision-activated dissociation involving Fourier transform mass spectrometry. Collision-activated dissociation technique that emulates infrared multiphoton dissociation", *Anal. Chim. Acta* **246,** 211 (1991). doi: 10.1016/S0003-2670(00)80678-9

39. L.A. McDonnell, P.J. Derrick, B.B. Powell and P. Double, "Sustained off-resonance irradiation collision-induced dissociation of linear, substituted and cyclic polyesters using a 9.4 T Fourier transform ion cyclotron resonance mass spectrometer", *Eur. J. Mass Spectrom.* **9,** 117 (2003). doi: 10.1255/ejms.530

Appendix

Comparison of the signal strength of two-electrode versus regular quadrupolar excitation

As derived by analysis in terms of a linear combination of the "natural" set of basis vectors (with respect to the different multipolar terms), the signal strength is reduced by a factor of two when the regular radial quadrupolar excitation is replaced by the two-electrode quadrupolar excitation. This is in contradiction to a statement by Jackson *et al.*[22] In the following the origin of this statement is traced back to a misleading decomposition of the "two-plate geometry". All citations and equation numbers refer to Reference 22:

While the rearrangement

$$\Phi_x(x,y,z) = V\left(\frac{\alpha}{2a^2}(x^2\text{-}y^2) + \frac{\alpha}{2a^2}(x^2\text{-}z^2)\right) \quad (4)$$

of the previously derived equation

$$\Phi_x(x,y,z) = V\left(\frac{\alpha}{2a^2}(2x^2 - y^2 - z^2)\right) \quad [2(a)]$$

is formally correct, it suggests that "for the $(x^2 - y^2)$ component of the 2-plate excitation potential, [...]

$$\left(\frac{3\alpha V_{p-p}}{2a^2}\right)$$

is replaced by

$$\left(\frac{\alpha V_{p-p}}{2a^2}\right)",$$

i.e. a reduction to one third of the potential (and field strength) of the regular quadrupolar excitation.

A closer look reveals that hidden in the remaining $(x^2 - z^2)$ term there is still a component of the quadrupolar ν_c-excitation mode as expressed explicitly in Equation (30). (Note in passing: In Equation (30) as given in Jackson *et al.*[22] there is also a factor of ½ missing for the first three summands.)

Nevertheless, and even though "intuition might suggest that twice as much voltage should be needed for 2-plate as for 4-plate quadrupolar excitation", the authors continue to conclude that Equation (4) and

$$\Phi_{q,ex}(x,y,z) = V\left(\frac{3\alpha}{2a^2}(x^2 - y^2)\right) \quad (3)$$

which follows from Equation [2(a)] and its equivalent for the *y*-direction, (see below), "suggest that three times as much voltage is needed to optimize 2-plate quadrupolar excitation".

The "apparent inconsistency" with the experimental value (of 87% for optimization of 2-plate vs 4-plate arrangement with no uncertainty figure) is later explained by the "limit of collisional damping with high-amplitude quadrupolar excitation"—which is not treated in the present contribution. Instead, we continue with the analysis of Equation [2(a)] in terms of the multipolar terms:

$$\Phi_x = V\left(\frac{\alpha}{2a^2}\frac{x^2 + y^2 - 2z^2}{2} + \frac{\alpha}{2a^2}\frac{3x^2 - 3y^2}{2}\right).$$

Obviously, in addition to the preceeding parametric term there is a quadrupolar part which is half as big as in the regular quadrupolar-excitation case [Equation (3)]. When the *y*-term, i.e. exchanging *x* and *y* and replacing *V* by *–V*,

$$\begin{aligned}\Phi_y &= -V\left(\frac{\alpha}{2a^2}(y^2 - x^2) + \frac{\alpha}{2a^2}(y^2 - z^2)\right) \\ &= -V\left(\frac{\alpha}{2a^2}\frac{x^2 + y^2 - 2z^2}{2} + \frac{\alpha}{2a^2}\frac{3y^2 - 3x^2}{2}\right)\end{aligned}$$

is added, Equation (3) is recovered, as intuition suggested all along.

Article III

International Journal of Mass Spectrometry 313 (2012) 30–35

Contents lists available at SciVerse ScienceDirect

International Journal of Mass Spectrometry

journal homepage: www.elsevier.com/locate/ijms

Lifting of the trapping potential during ion storage for multi-anion production in a Penning trap

Franklin Martinez, Steffi Bandelow, Christian Breitenfeldt, Gerrit Marx, Lutz Schweikhard, Frank Wienholtz, Falk Ziegler

Institut für Physik, Ernst-Moritz-Arndt-Universität, 17487 Greifswald, Germany

ARTICLE INFO

Article history:
Received 11 November 2011
Received in revised form
15 December 2011
Accepted 19 December 2011
Available online 28 December 2011

Keywords:
Multiply charged anions
Coulomb barrier
Penning trap
Trapping potential
Electron bath
Aluminum clusters

ABSTRACT

The attempts to produce higher and higher charge states of anionic metal clusters in Penning traps by attachment of simultaneously stored electrons run into a dilemma: On the one hand, the size of the clusters, which are initially only singly charged, has to be increased to accommodate additional electrons. On the other hand, in order to attach to already highly-charged particles, electrons have to overcome the respective Coulomb barriers. Thus, for the conventional electron-bath technique the electrons need to be created at correspondingly higher trapping potentials. This leads to a conflict as the "critical mass", above which the ion orbits are no longer stable, is inversely proportional to the trapping potential. However, as the critical mass is actually an upper limit of the mass-over-charge ratio, the introduction of a stepwise charging-up by repeated electron bathing after increase of the trapping potential allows one to reach higher and higher charge states.

© 2011 Elsevier B.V. All rights reserved.

1. Introduction

Multiply negatively charged species in the gas phase have been subject of experimental investigations over the years, and several methods for their production were developed. By sputtering [1], laser ablation [2–4] and electrospray ionization [5,6], doubly-charged anions can be formed in the ion source. Alternatively, mono-anionic species and electrons can be brought together to prompt electron attachment. The latter includes electron transfer reactions [7,8], and direct exposure of trapped mono-anions to an environment of quasi-free electrons, utilizing an electron beam [9,10] or an electron bath [11].

The electron bath uses the capability of Penning ion traps to store electrons and molecular anions, simultaneously. Thus, multiply-charged cluster anions were produced, ranging from di-anionic fullerenes [12,13], gold, silver, copper [11,12,14–17] and titanium [18] cluster di- and tri-anions, to aluminum cluster di-, tri- and tetra-anions [19–22].

On the way to even higher anionic charge states, the conventional electron-bath technique is reaching a limit, as discussed in Section 2. However, by introducing a variation of the trapping potential (Section 3), this limit has been bypassed. Changing the trapping potential during ion storage can be used as a method for the manipulation of the ion motion. This has been utilized, e.g. by adiabatic reduction of the trapping potential for ion cooling in Penning traps [23–25]. In contrast, in the experiments reported here the trapping potential is increased. This allows the creation and storage of electrons with kinetic energies higher than before the increase. As a result, higher charge states of anionic clusters can be produced as shown for the case of aluminum clusters (Section 4).

2. Multi-anion production in a Penning trap

The electron-bath technique for production of multiply charged cluster anions has been developed and applied at the Penning trap setup ClusterTrap [26–29]. In this section, the limitation of the electron-bath technique, caused by two opposing conditions, is discussed. In the first two parts, the Coulomb barrier and resulting trapping requirements for electron attachment to anionic clusters are reviewed. In the third part, the storage limitations of the Penning trap for charged clusters are considered.

2.1. The Coulomb barrier for electron attachment

For the production of multi-anionic cluster species, electrons are sequentially attached to already negatively charged cluster ions, $X_n^z + e^- \rightarrow X_n^{z-1}$. In the charged-metal-sphere model, the electrons

E-mail address: franklin.martinez@physik.uni-greifswald.de (F. Martinez).

1387-3806/$ – see front matter © 2011 Elsevier B.V. All rights reserved.
doi:10.1016/j.ijms.2011.12.009

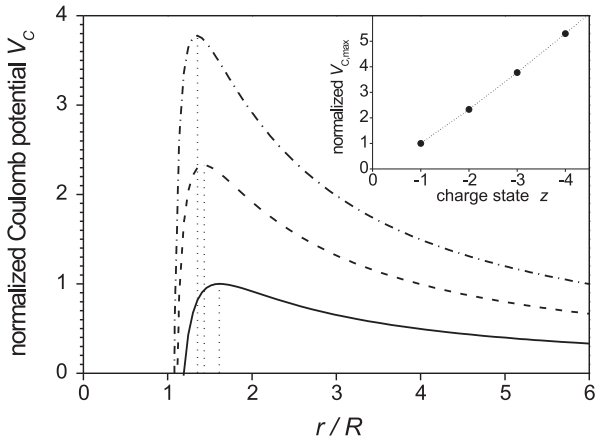

Fig. 1. Normalized Coulomb potential V_C of a cluster anion of radius $R = R(n)$, and charge state z = -1, -2 and -3 (solid, dashed, dash-dotted line, respectively). Inlet: normalized potential maxima $V_{C,max}$ as function of the charge state z.

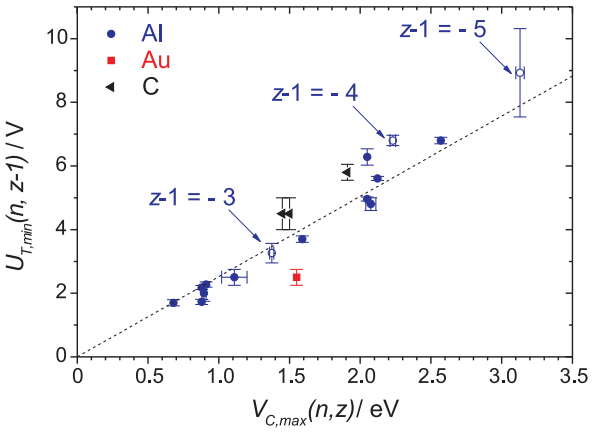

Fig. 2. Experimentally determined minimum trapping potential depths $U_{T,min}$ for production of X_n^{z-1} as function of the numerically calculated[1] Coulomb barrier heights $V_{C,max}$ of the precursor ions X_n^z (X = Al, Au, C). The dashed line is a linear fit through data from [12,13,19,21,22,35] (filled symbols) and zero. Data from present measurements (open symbols, Section 4) are not included in the fit.

have to overcome the repulsive force caused by the Coulomb potential barrier [30] (Fig. 1),

$$V_C(z, r, R) = \frac{e^2}{4\pi\varepsilon_0}\left(\frac{|z|}{r} - \frac{R^3}{2r^2(r^2 - R^2)}\right), \quad (1)$$

of the precursor cluster anion with charge state z and radius $R = R(n)$, given by the number of atoms in the cluster, n. In the following, the radius of a metal cluster is approximated by $R(n) = R_a n^{1/3}$, with R_a being the atomic radius.

The maximum height $V_{C,max}$ of the potential increases with increasing charge state z (Fig. 1, inlet). It determines the minimum energy which is required by an electron to overcome the barrier. Electrons with an energy too low to overcome the barrier are immediately repelled, causing very short interaction times. Thus, tunneling through the Coulomb barrier can be neglected for the process of electron attachment. This is in contrast to the reverse process of electron detachment from multi-anionic clusters: For cluster anions with negative electron affinities, an excess electron might yet be bound by the Coulomb barrier. However, such systems are meta-stable as the electron eventually escapes by tunneling through the barrier [14,16,19,20,22].

2.2. The Penning-trap well depth

The Penning trap consists of a combination of a homogeneous static magnetic field and an electrostatic quadrupolar field, for radial and axial ion confinement, respectively [31–33]. The electric field is generated by the trapping voltage, U_0, applied between a ring and two endcap electrodes. The axial trapping potential well depth

$$U_T = U_0 \frac{z_0^2}{2d_0^2} \quad (2)$$

is given by the geometry factor $d_0^2 = r_0^2/4 + z_0^2/2$, with r_0 and z_0 being the smallest distances of the ring and endcap electrodes to the center of the trap, respectively [12,26,31]. For asymptotically symmetric trap geometries ($z_0^2 = r_0^2/2$), as used at the ClusterTrap experiment, the axial potential well depth is $U_T = U_0/2$ [34].

Previous experimental results show an increase of the relative abundance of multiply charged anions after application of an electron bath as a function of the trapping voltage U_0 [12,13,17,19,21,22,35]. In particular, a minimum potential well depth $U_{T,min} = U_{0,min}/2$ is required to produce a multi-anionic charge state, reflecting the presence of the Coulomb barrier. In Fig. 2 experimentally determined minimum potential well depths $U_{T,min}(n, z-1)$ for the observation of cluster anions X_n^{z-1} (X = Al, Au, C) are plotted against the calculated[1] maxima $V_{C,max}(n, z)$ of the Coulomb barriers of the respective precursor anions, X_n^z (filled symbols). The linear fit to these data points through zero has a slope of $U_{T,min}/V_{C,max} = 2.52(2)$ V/eV. (The points with open symbols are not included in the fit, but are discussed in Section 4.) Fig. 2 shows that for the production of clusters X_n^{z-1}, the potential well depth has to fulfill the condition $U_T \geq U_{T,min}$, with

$$U_{T,min}(n, z-1)[V] \cong 2.5 \cdot V_{C,max}(n, z)[eV], \quad (3)$$

i.e. the trapping voltage $U_0 = 2U_T$ applied at ClusterTrap has to be at least five times higher than the Coulomb-potential maximum of the precursor cluster X_n^z. Eq. (3) can be understood in terms of the energy distribution of the trapped secondary electrons. An upper limit of their axial kinetic energy is given by the potential well depth eU_T. However, this limit is only valid for secondary electrons, that are generated close to the endcap electrodes. Electrons, which are generated closer to the trap center, gain less axial kinetic energy. Consequently, the mean kinetic energy of the trapped electron ensemble is considerably lower than the potential well depth.

2.3. The conflicting requirements for electron attachment to clusters in a Penning trap

Previous investigations of metal cluster (Au, Ag, Cu and Al) and fullerene multi-anions showed, that for the observation of each charge state, a minimum (appearance) cluster size is required [11,13–16,19,20,22]. In other words, to produce higher negative charge states, larger clusters have to be provided. By taking into account the electron affinity, the Coulomb barrier and tunneling effects, the appearance cluster sizes for particular charge states can be estimated [16,20,22,30] based on the charged-sphere model.

Starting point for the multi-anion production are mono-anionic clusters, that are captured in the Penning trap. However, for a given trapping voltage U_0 of the Penning trap, there is an upper limit of the mass-over-charge ratio of trapped ions [37],

$$\left(\frac{m_a n}{|ze|}\right)_{crit} = \frac{d_0^2 B^2}{2U_0}, \quad (4)$$

[1] R_a(Au)=0.159nm [36,12]; R_a(Al)=0.158nm [36]; $R(C_n)=R(C_{60})\sqrt{n/60}$ for n=78 and 84 [13], with $R(C_{60})$=0.42nm [7]; $R(C_{70})$=0.377nm [12].

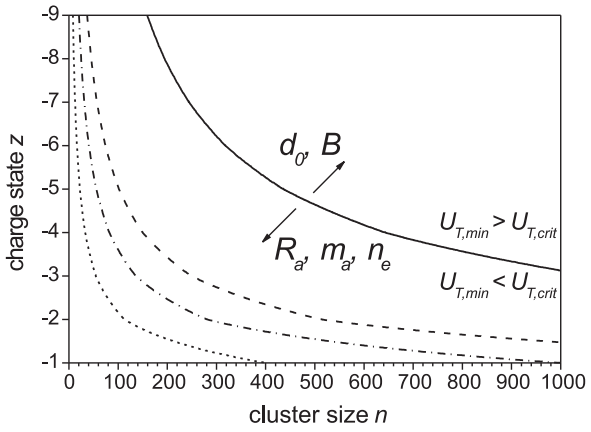

Fig. 3. Maximum charge state z of trapped cluster anions as function of the cluster size n, for which the relation $U_{T,\mathrm{crit}}(n,-1) = U_{T,\mathrm{min}}(n, z-1)$ is fulfilled (Eq. (3), B = 5 T, d_0^2 = 200 mm^2); for aluminum (solid line), copper (dashed line), silver (dash-dotted line) and gold (short-dashed line). As indicated, the curves shift upwards for increasing trap parameters d_0 and B, and downwards for increasing atomic radius R_a, atomic mass m_a and electron density n_e.

where B is the magnetic flux density, and m_a is the atomic mass of the element the cluster consists of. This limit corresponds to an upper limit $U_{0,\mathrm{crit}}$ of the trapping voltage (and potential well depth $U_{T,\mathrm{crit}}$, Eq. (2)) for a trapped cluster of size n and charge state z.

For cluster mono-anions that are stored together with many electrons, the axial trapping potential well depth U_T and the critical trapping voltage $U_{0,\mathrm{crit}}$ are shifted to lower values, as space–charge effects have to be considered. Assuming a space–charge density caused by electrons, $Q_{sc}n_{sc} = en_e$, the well depth and the critical trapping voltage can be estimated by [17,21,38]

$$U_T(n_e) = \frac{U_0 z_0^2}{2d_0^2} - \frac{d_0^2 e n_e}{6\varepsilon_0}, \tag{5}$$

$$U_{0,\mathrm{crit}}(n, z, n_e) = \frac{|ze| d_0^2 B^2}{2m_a n} - \frac{2d_0^2 e n_e}{3\varepsilon_0}. \tag{6}$$

In conclusion, for the production of multi-anionic clusters by application of the electron-bath technique in a Penning trap, two conditions need to be fulfilled: The trapping potential well depth U_T needs to be large enough to allow electron attachment, and at the same time needs to be low enough to store large cluster mono-anions, i.e. $U_{T,\mathrm{min}} < U_T < U_{T,\mathrm{crit}}$. In particular, $U_{T,\mathrm{min}}(n, z-1) < U_{T,\mathrm{crit}}(n, -1)$ must be fulfilled.

Based on this condition, the maximum charge states z of trapped cluster ions for which co-trapped electrons can overcome the Coulomb potential, are shown as a function of the cluster size n in Fig. 3. Note, that in Fig. 3, the stability of multi-anionic clusters, i.e. their size with respect to the appearance cluster size, is not taken into account. Electrons might overcome the Coulomb potential, but may not necessarily be stably bound to the cluster anion.

If one aimes for higher and higher negative charge states, which in turn require an increase of the cluster size, the condition $U_{T,\mathrm{min}} < U_{T,\mathrm{crit}}$ will eventually be violated, with the corresponding charge states and cluster sizes depending on the Penning trap parameters (Eqs. (2), (3) and (6), Fig. 3).

However, there is a solution to this dilemma: The multi-anion production can be performed stepwise, that is, the electron-bath technique has to be modified in such a way, that the trapping voltage U_0 is increased between application of consecutive electron baths. The experimental realization and results of such a procedure are presented in Section 3 and 4.

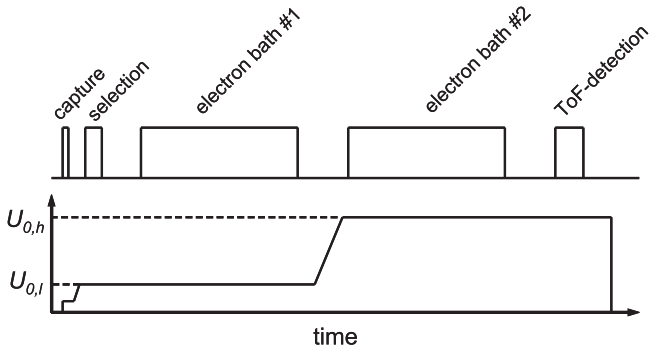

Fig. 4. Experimental sequence of the multi-anion production in the Penning trap. For most effective capture of mono-anions, the trapping voltage is kept at low values at the beginning of the sequence. It is then increased for size selection and application of the first electron bath. Then U_0 is further increased before application of a second electron bath. The product ions are analyzed by time-of-flight mass spectrometry.

3. Experimental setup and procedure

ClusterTrap is a 5-T Penning-trap setup developed for investigations of gas-phase cluster ions [26–29]. Cluster mono-anions are produced in a laser-ablation source [39], accumulated in a radio-frequency ion trap and transferred into the Penning trap. There, the cluster ions are centered by buffer-gas assisted quadrupolar radio-frequency excitation [40,41], size-selected, then subjected to one or several reaction steps, and subsequently the product ions are analyzed by time-of-flight (ToF) mass spectrometry.

The electron-bath [11,20–22] consists of trapped low-energetic secondary electrons, produced in the Penning trap for 200 ms by electron-impact ionization of argon gas. The gas is injected in several pulses from a pulsed leak valve. Each pulse causes a temporary pressure of up to 10^{-5} hPa in the trap, before being pumped away within tens of milliseconds [41]. The primary electron energy is about 110 eV. Variation by ±50 eV shows no significant changes in the experimental results. The subsequent reaction period of the clusters in the electron-bath is typically 1 s.

The procedure is repeated up to three times, for renewal of the electron bath. This renewal is needed due to Coulomb interaction between the electrons, which couples the axial and radial motion, where the latter enhances energy loss by synchrotron radiation [31,12,16,21,27].

In the present experimental scheme (Fig. 4), at the beginning of each cycle the trapping voltage U_0 is kept at 3 V, as capture of large clusters turned out to be most effective at low trapping voltages. For the selection step and the first electron bath U_0 is raised within 10 ms to $U_{0,l}$ = 10 V, and it is then ramped within typically 100 ms to a higher potential $U_{0,h}$, before application of the second electron bath. The variable trapping potential was realized by the output of an arbitrary function generator (SRS DS-345), which was further amplified by a factor of 10 by a voltage amplifier (CGC Instruments). To monitor the initial mono-anion number, a reference cycle was performed alternating with the measurement cycle [28,42]. In this cycle the cluster mono-anions were stored at $U_{0,l}$ = 10 V, without being subjected to the series of electron baths (not shown in Fig. 4).

4. Results

For the production of aluminum cluster anions Al_n^{2-}, Al_n^{3-}, and Al_n^{4-} [19–22] the condition $U_{0,\mathrm{min}}(n, z-1) \leq U_{0,\mathrm{crit}}(n, -1)$ has posed no problem. However, for the production of Al_n^{5-} where the expected required cluster-size range is $n \geq 445$ [43], the available U_0-range becomes critically narrow, as illustrated in Fig. 5. The thin lines indicate critical trapping voltages $U_{0,\mathrm{crit}}$ for aluminum cluster mono- and di-anions, for several electron densities n_e (Eq. (6)).

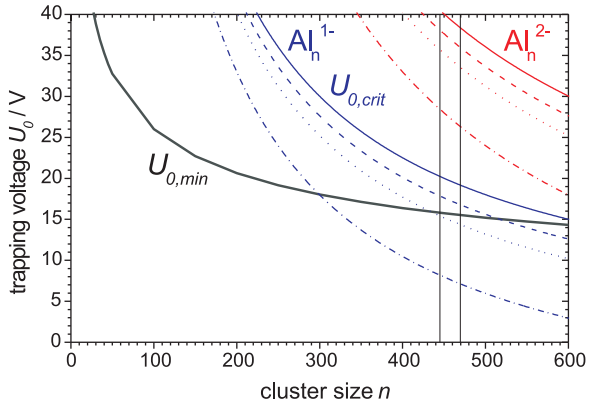

Fig. 5. Critical trapping voltage $U_{0,crit}$ of aluminum cluster mono- and di-anions as a function of the cluster size n, for different electron densities in the Penning trap (0, 1, 2 and 5×10^6 cm^{-3}, thin solid, dashed, dotted and dash-dotted lines, respectively, $B = 5$ T, $d_0^2 = 200$ mm^2). Expected minimum trapping voltage $U_{0,min}$ required for electron attachment to Al_n^{4-} to form Al_n^{5-} (thick solid line). The vertical lines mark the cluster size range, discussed in Section 4.

The thick line represents $U_{0,min}$ as required for electron attachment to Al_n^{4-}, for $n_e = 0$ (Section 2.2). Note, that for $n_e > 0$, the curve for $U_{0,min}$ is shifted upwards to higher voltages, further decreasing the available U_0-range (not shown).

Fig. 6 displays time-of-flight spectra of aluminum cluster anions ($n = 445$–470). The top spectrum shows a reference cycle, where mono-anions are trapped at low $U_{0,l} = 10$ V, without application of any electron bath (Fig. 6a). Due to the limited mass resolving power (≈70) the cluster sizes can not be resolved. While contaminations can not be excluded, nevertheless, bare aluminum clusters are assumed in the following. For the middle spectrum the electron bath has been applied twice at $U_{0,l} = 10$ V (Fig. 6b). Mono-anions remain trapped, but decrease in number, while di- and a few tri-anions appear in the spectrum. The left part of the spectrum is enhanced by a factor of 4, to match the scaling of the spectrum below. There, the trapping voltage has been raised to a high $U_{0,h} = 32$ V for the second electron bath (high-U_0 electron bath, Fig. 6c). Mono-anions leave the trap as their trajectories are unstable above $U_{0,crit} \approx 20$ V (Fig. 5). Di- and tri-anions formed at the $U_{0,l}$ electron bath remain trapped, and some are further converted to tetra- and penta-anions in the $U_{0,h}$ electron bath (Fig. 6c).

The multi-anion production has been investigated as a function of the trapping voltage $U_{0,h}$, making use of three independent

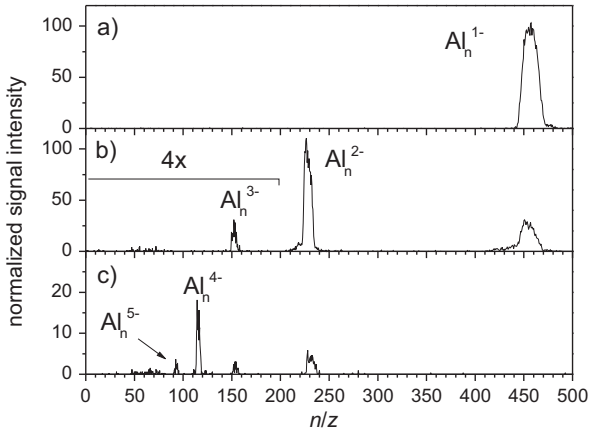

Fig. 6. Time-of-flight spectra of aluminum cluster anions Al_n^z, $n = 445$–470. (a) reference cycle without electron bath, $U_{0,l} = 10$ V, (b) application of two electron baths, both at $U_{0,l} = 10$ V, (c) cycle as in b) but with second electron bath at $U_{0,h} = 32$ V. A part of the spectrum in b) is enhanced to match the scale at c).

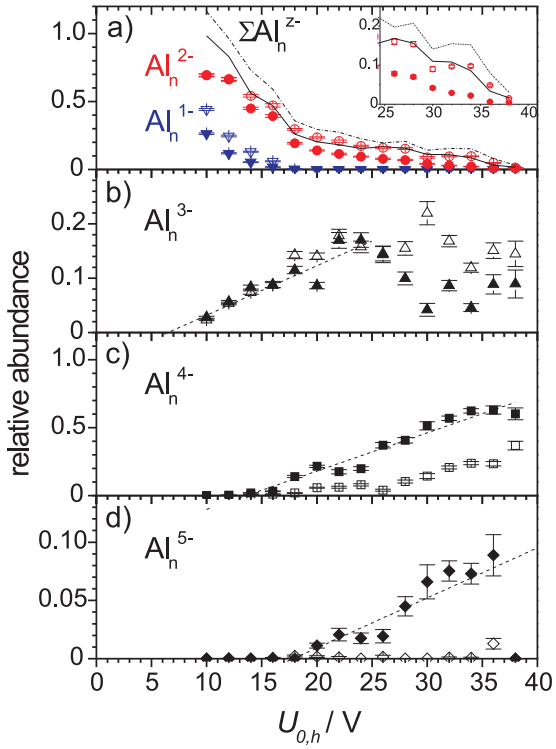

Fig. 7. Relative abundances of negatively charged aluminum clusters ($n = 445$–470) as a function of the trapping voltage $U_{0,h}$. At a first electron bath the trapping voltage was kept at $U_{0,l} = 10$ V, but was varied for a second electron bath, which was applied once (open symbols) and twice (filled symbols). (a) Abundances of Al_n^{1-}, Al_n^{2-} and all product ions Al_n^z (solid and dash-dotted lines) relative to the number of precursor mono-anions. (b–d) Abundances of Al_n^{3-}, Al_n^{4-} and Al_n^{5-}, respectively, relative to the sum of all multiply charged product ions, $\sum Al_n^z$, ($z = -2, \ldots, -5$). The dashed lines are linear fits to the rising edges.

experimental cycles (Fig. 7). The first cycle is the very same as described for Fig. 6c, but with variation of $U_{0,h}$ in the range between 10 and 38 V (open symbols, dashed line in Fig. 7). The second cycle was the same as the first one, except that the $U_{0,h}$ electron bath was applied twice (filled symbols, solid line). The third cycle is a reference cycle without electron bath, as described for Fig. 6a.

Fig. 7a shows the abundance of mono- and di-anions relative to the number of precursor mono-anions from the reference cycle. Additionally, the abundance of the sum of all detected anions ΣAl_n^z ($z = -1, \ldots, -5$) relative to the number of precursor mono-anions is indicated (solid and dashed line). An overall decrease in the total ion number is observed, which is independent of the number of applied electron baths. The decrease is steep up to $U_{0,h} = 18$ V, and than flattens. For the first data point ($U_{0,h} = 10$ V = $U_{0,l}$), where no change of the trapping potential occurs, the abundance of all product ions relative to the number of precursor mono-anions is close to 1 (Fig. 7a, solid and dashed lines). Apparently, the loss of ions is due to the ramping of the trapping potential, rather than to the application of the electron baths.

Most of the ions loss can be understood in terms of the critical mass-over-charge ratio (Section 2.3): The steep part of the decrease is due to the decreasing number of mono-anions; it stops, when the mono-anions fully disappear at $U_{0,h} \cong 18$ V, reaching their trapping limit. Comparison with Fig. 5 indicates an electron density of about $n_e \approx 1 \times 10^6$ cm^{-3}. Above $U_{0,h} = 34$ V, a further decrease is observed, in particular for the cycle with one $U_{0,h}$ electron bath, leading to almost zero in the abundances of all ions at $U_{0,h} = 38$ V (inset Fig. 7a). This again, indicates a trapping limitation, this time for the di-anions, and again at an electron densitiy of $n_e \approx 1 \times 10^6$ cm^{-3} (see

Table 1
Precursor Coulomb-barrier height $V_{C,max}$, experimentally determined minimum trapping voltage $U_{0,min}$, and calculated ratio $U_{T,min}/V_{C,max}$ (using Eq. (5)) of Al_n^z, n = 445–470, for n_e = 0 and 1×10^6 cm^{-3}.

z	$z-1$	$V_{C,max}(z)$ in eV	$U_{0,min}(z-1)$ in V	$U_{T,min}/V_{C,max}$, $n_e = 0$	$U_{T,min}/V_{C,max}$, $n_e = 1 \times 10^6$ cm^{-3}
-2	-3	1.38(2)	6.52(61)	2.37(5)	1.50(5)
-3	-4	2.23(2)	13.60(33)	3.05(1)	2.51(1)
-4	-5	3.13(3)	17.9(2.8)	2.85(20)	2.47(20)

Fig. 5). Electron densities in the same order of magnitude have already been observed at ClusterTrap, earlier [21].

The space charge in the trap might be reduced, and thus the critical trapping potential increased, by removal of the electrons after the first electron bath. As mentioned in Section 3, trapped electrons loose energy over time, and at some point do not contribute to the multi-anion production any longer. If the potential of one or both endcaps is lowered for about 1 μs, the electrons leave the trap, while the slower cluster ions remain trapped (suspended trapping, [44]). Alternatively, axial dipolar radio-frequency excitation is suitable to remove only the electrons from the Penning trap [21].

Fig. 7b–d shows the abundances of product ions Al_n^{3-}, Al_n^{4-} and Al_n^{5-}, respectively, relative to the number of all multiply charged product ions, $\sum Al_n^z$, $z = -2, \ldots, -5$. Up to $U_{0,h} \cong$ 14 V, only di- (Fig. 7a) and tri-anions are observed, showing about the same relative ratios after one (open symbols) and two $U_{0,h}$ electron baths (filled symbols). Above $U_{0,h} \cong$ 14 V, tetra-anions are formed, and in this range, the repeated application of the $U_{0,h}$ electron bath effects also the relative abundances, reducing the amount of di- and tri-anions, and increasing the number of tetra-anions, as compared to single application. Above $U_{0,h} \cong$ 18 V, penta-anions appear, but only after two applications of the $U_{0,h}$ electron bath.

The multi-anion distributions are dominated by di-anions up to $U_{0,h}$ = 25 V, and by tetra-anions for higher trapping voltages (see also Fig. 6). The tri-anion abundance is strikingly low (note the different scales in Fig. 7b–d), even for low $U_{0,h}$, where no tetra-anions are formed, yet. In contrast, for some measurements (spectra not shown) with two $U_{0,h}$ electron baths no penta-anions are observed, while at the same time, the tri-anion abundance is comparable to the tetra-anion abundance. There is as yet no explanation for this observation.

The considerable ion loss (i.e. from 70 down to 10% for the di-anions, Fig. 7a) is affecting the total multi-anion yield. While the penta-anion yield relative to all multi-anions is about 7% in the range $U_{0,h}$ = 30 to 34 V (Fig. 7d), the total multi-anion yield is only 10% relative to the initial mono-anion number (Fig. 7a). This results in a total penta-anion yield of 0.7% with respect to the initial mono-anion number. At about 300 mono-anions per experimental cycle, this results in only 2 penta-anions detected per cycle. Centering of the ions before ramping, and a slower ramping rate might reduce the ion loss in future experiments.

Minimum trapping voltages $U_{0,min}$ have been determined from linear fits (dashed lines in Fig. 7b–d), and are given in Table 1. They increase with the charge state, again reflecting the increasing height of the Coulomb barrier (Fig. 1, Table 1). For calculation of the respective ratios $U_{T,min}/V_{C,max}$, the space–charge effect of the electron cloud at the corresponding trapping potential well depth $U_{T,min}$ should be taken into account (Eq. (5)). For the data presented here, the electron density is estimated from the shift of the critical trapping voltage $U_{0,crit}$ (Fig. 5), to be $n_e \approx 1 \times 10^6$ cm^{-3}. Its consideration for the calculation of U_T results in ratios $U_{T,min}/V_{C,max}$ as presented in Table 1. But, as no electron densities were known for the data in Fig. 2 (filled symbols), those potential well depths U_T were calculated according to Eq. (2). For comparison, the ratios for n_e = 0 from Table 1 have been added to the data points in Fig. 2 (open symbols). While the ratio for the production of tri-anions and penta-anions is in agreement with the expected value of 2.52(2) V/eV (Section 2.2), the ratio of the tetra-anions is somewhat higher. However, it is still within the scattering of the previous data. This scattering is probably due to variations of the electron bath parameters in the different measurements, in particular the poorly known electron density.

5. Conclusion

The production of multi-anionic metal clusters in a Penning trap by the electron-bath method has been investigated with respect to the trapping voltage U_0. Analysis of previous measurements suggest that at ClusterTrap a minimum trapping voltage of at least five times the height of the Coulomb barrier potential of an anionic cluster is required for the attachment of a further electron. In the case of aluminum clusters the minimum trapping potential, required for production of Al_n^{5-}, is similar to the upper limit of the trapping potential for the cluster sizes required for production of penta-anions.

This conflict has been solved by increasing the trapping potential between two electron baths while the cluster ions have been kept stored. Thus, penta-anionic clusters $Al_{445-470}^{5-}$ have been produced, and minimum trapping voltages $U_{0,min}$ for the production of tri-, tetra- and penta-anions have been determined. The respective ratios $U_{T,min}/V_{C,max}$ follow the trend of previous measurements.

Besides supporting the production of multi-anionic species, increasing of the trapping voltage might be a useful technique for selection of high charge states. The critical trapping potential is inversely proportional to the mass-over-charge ratio. Thus lower charge states of a given cluster size can be removed from the trap by raising the trapping potential.

Acknowledgments

The project was supported by a Collaborative Research Center of the DFG (SFB 652-TP A03). F. Martinez and S. Bandelow have received postgraduate stipends from the state of Mecklenburg-Vorpommern (Landesgraduiertenförderung) in the framework of the International Max Planck Research School on Bounded Plasmas.

Appendix A.

The potential maximum $V_{C,max}$ of the Coulomb barrier is calculated from its relative position $r_{C,max}/R$, by use of Eq. (1). While for $z = -1$, the relative maximum position can be calculated analytically, resulting in the golden ratio $(\sqrt{5}+1)/2 = 1 + (\sqrt{5}-1)/2$ [14], for higher charge states, $z = -2, -3, \ldots$, numerical calculations are required.

For an estimation of $V_{C,max}$, the numerically calculated maximum position (Fig. 8a, open squares) has been fitted as a function of the charge state z by

$$\frac{r_{C,max}}{R}(z) = 1 + \frac{\sqrt{5}-1}{2} \cdot |z|^{\alpha}, \tag{7}$$

(solid line). The only free fit parameter α has been determined from the range $z = -1, \ldots, -9$, yielding the value $\alpha = -0.5378(8)$. In Fig. 8b the relative deviation of the fit function (Eq. (7)) from the

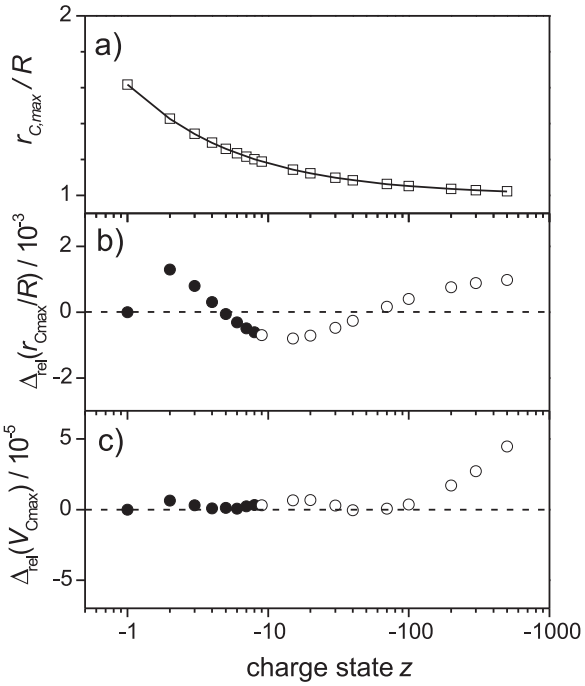

Fig. 8. (a) Relative position $r_{C,max}/R$ of the Coulomb potential maximum $V_{C,max}$ as calculated numerically from Eq. (1) (open squares), and fitted with Eq. (7) (solid line) for $z = -1, \ldots, -9$. (b) Relative deviation of the fitted function for $r_{C,max}/R$ and (c) for $V_{C,max}$. (b) and (c): filled symbols for fitted data, open symbols for extrapolated data.

numerically determined values for $r_{C,max}/R$ is plotted. The correspondingly approximated values for $V_{C,max}$ (Eqs. (1) and (7)) deviate from the numerical values by less than 1×10^{-5} even beyond the fitted range (filled circles) up to $z = -100$ (Fig. 8c, open circles, note the logarithmic scaling).

References

[1] S.N. Schauer, P. Williams, R.N. Compton, Phys. Rev. Lett. 65 (1990) 625.
[2] P.A. Limbach, L. Schweikhard, K.A. Cowen, M.T. McDermott, A.G. Marshall, J.V. Coe, J. Am. Chem. Soc. 113 (1991) 6795.
[3] R.L. Hettich, R.N. Compton, R.H. Ritchie, Phys. Rev. Lett. 67 (1991) 1242.
[4] C. Stoermer, J. Friedrich, M.M. Kappes, Int. J. Mass Spectrom. 206 (2001) 63.
[5] X.-B. Wang, L.S. Wang, W.R. Wiley, Phys. Rev. Lett. 83 (1999) 3402.
[6] O. Hampe, M. Neumaier, M.N. Blom, M.M. Kappes, Chem. Phys. Lett. 354 (2002) 303.
[7] B. Liu, P. Hvelplund, S. Brøndsted Nielsen, S. Tomita, Phys. Rev. Lett. 92 (2004) 168301.
[8] P. Hvelplund, B. Liu, S. Brøndsted Nielsen, S. Tomita, Eur. Phys. J. D 43 (2007) 133.
[9] K. Leiter, W. Ritter, A. Stamatovic, T.D. Märk, Int. J. Mass Spectrom. Ion Process. 68 (1986) 341.
[10] J. Hartig, M.N. Blom, O. Hampe, M.M. Kappes, Int. J. Mass Spectrom. 229 (2003) 93.
[11] A. Herlert, S. Krückeberg, L. Schweikhard, M. Vogel, C. Walther, Phys. Scr. T 80 (1999) 200.
[12] A. Herlert, R. Jertz, J. Alonso Otamendi, A.J. Gonzalez Martinez, L. Schweikhard, Int. J. Mass Spectrom. 218 (2002) 217.
[13] A. Lassesson, N. Walsh, F. Martinez, A. Herlert, G. Marx, L. Schweikhard, Eur. Phys. J. D 34 (2005) 73.
[14] L. Schweikhard, A. Herlert, S. Krückeberg, M. Vogel, C. Walther, Philos. Mag. B 79 (1999) 1343.
[15] A. Herlert, L. Schweikhard, M. Vogel, Eur. J. Phys. D 16 (2001) 65.
[16] A. Herlert, L. Schweikhard, Int. J. Mass Spectrom. 229 (2003) 19.
[17] L. Schweikhard, A. Herlert, G. Marx, AIP Conf. Proc. 692 (2003) 203.
[18] A. Herlert, K. Hansen, L. Schweikhard, M. Vogel, Hyperfine Interactions 127 (2000) 529.
[19] N. Walsh, F. Martinez, G. Marx, L. Schweikhard, Eur. Phys. J. D 43 (2007) 241.
[20] N. Walsh, F. Martinez, G. Marx, L. Schweikhard, F. Ziegler, Eur. Phys. J. D 52 (2009) 27.
[21] N. Walsh, A. Herlert, F. Martinez, G. Marx, L. Schweikhard, J. Phys. B 42 (2009) 154024.
[22] N. Walsh, F. Martinez, G. Marx, L. Schweikhard, F. Ziegler, J. Chem. Phys. 132 (2010) 014308.
[23] S.L. Rolston, G. Gabrielse, Hyperfine Interactions 44 (1988) 233.
[24] G.-Z. Li, R. Poggiani, G. Testera, G. Werth, Z. Phys. D 22 (1991) 375.
[25] G.-Z. Li, R. Poggiani, G. Testera, G. Werth, Hyperfine Interactions 76 (1993) 281.
[26] S. Becker, K. Dasgupta, G. Dietrich, H.J. Kluge, S. Kuznetsov, M. Lindinger, K. Lützenkirchen, L. Schweikhard, J. Ziegler, Rev. Sci. Instrum. 66 (1995) 4902.
[27] L. Schweikhard, K. Hansen, A. Herlert, G. Marx, M. Vogel, Eur. Phys. J. D 24 (2003) 137.
[28] L. Schweikhard, S. Becker, K. Dasgupta, et al., Phys. Scripta T59 (1995) 236.
[29] F. Martinez, G. Marx, L. Schweikhard, A. Vass, F. Ziegler, Eur. Phys. J. D 63 (2011) 255.
[30] J.D. Jackson, Classical Electrodynamics, 3rd ed., Wiley, New York, USA, 1998.
[31] L.S. Brown, G. Gabrielse, Rev. Mod. Phys. 58 (1986) 233.
[32] P.K. Gosh, Ion traps, Oxford University Press, Oxford UK, 1995.
[33] F.G. Major, V.N. Gheorghe, G. Werth, Charged Particle Traps, Springer Verlag, New York, USA, 2005.
[34] R.D. Knight, Int. J. Mass Spectrom. Ion Phys. 51 (1983) 127.
[35] N. Walsh, Multiply-negatively charged aluminium clusters and fullerenes, PhD thesis, Greifswald, Germany (2008).
[36] Ch. Kittel, Einführung in die Festkörperphysik, 14th ed., Oldenbourg Wissenschaftsverlag, London UK, 1994.
[37] L. Schweikhard, J. Ziegler, H. Bopp, K. Lützenkirchen, Int. J. Mass Spectrom. Ion Process. 141 (1995) 77.
[38] J.B. Jeffries, S.E. Barlow, G.H. Dunn, Int. J. Mass Spectrom. Ion Processes 54 (1983) 169–187.
[39] R. Weidele, U. Frenzel, T. Leisner, D. Kreisle, Z. Phys. D 20 (1991) 411.
[40] G. Savard, St. Becker, G. Bollen, H.-J. Kluge, R.B. Moore, Th. Otto, L. Schweikhard, H. Stolzenberg, U. Wiess, Phys. Lett. A 158 (1991) 247.
[41] H.-U. Hasse, St. Becker, G. Dietrich, N. Klisch, H.-J. Kluge, M. Lindinger, K. Lützenkirchen, L. Schweikhard, J. Ziegler, Int. J. Mass Spectrom. 132 (1994) 181.
[42] F. Ziegler, D. Beck, H. Brand, H. Hahn, G. Marx, L. Schweikhard, submitted for publication.
[43] F. Martinez, S. Bandelow, C. Breitenfeldt, G. Marx, L. Schweikhard, F. Wienholtz, F. Ziegler, in preparation.
[44] D.A. Laude, S.C. Beu, Anal. Chem. 61 (1989) 2422.

Article IV

EPJ manuscript No.
(will be inserted by the editor)

Appearance size of poly-anionic aluminum clusters, Al_n^{z-}, $z = 2-5$

Franklin Martinez, Steffi Bandelow, Christian Breitenfeldt, Gerrit Marx, Lutz Schweikhard, Frank Wienholtz, and Falk Ziegler

Institut für Physik, Ernst-Moritz-Arndt-Universität, 17487 Greifswald, Germany, e-mail: martinez@physik.uni-greifswald.de

Received: date / Revised version: date

Abstract. The production of poly-anionic metal clusters by simultaneous storage of electrons and cluster anions in a Penning trap has been extended to the fifth charge state. The minimum cluster size, required to attach a fifth excess electron, has been experimentally determined for aluminum clusters. A new data evaluation method is proposed, redefining the appearance size with respect to the delayed electron emission. It has been applied to the penta-anions as well as to previous data of poly-anionic aluminum clusters. In addition, new measurements of aluminum di-anions have revealed a lower minimum appearance size than reported earlier. Comparison of the experimental results with predictions by the conducting-sphere model for the di-, tri-, tetra- and penta-anions show deviations, that are probably due to thermal excitation of the cluster anions. The abundance spectra of the poly-anionic aluminum clusters can be reproduced by a thermionic-electron-emission approach with an effective Coulomb barrier.

1 Introduction

The ability of atomic clusters to carry a certain amount of excess charges is determined by their size, i.e. the number of atoms n [1,2]. In particular, an element-specific minimum cluster size is required to access a certain negative charge state. The appearance size was determined in theoretical investigations [1,3–5] and previous experiments, for cluster ions $Au_n^{2-,3-}$ [6–11], $Ag_n^{2-,3-}$ [9,11,12], $Pb_n^{2-,3-}$ [10], $Cu_n^{2-,3-}$ [11] and recently for $Al_n^{2-,3-,4-}$ [13–15]. In the case of aluminum cluster anions, a simple approach based on the conducting-sphere model, taking into account the Coulomb potential and the electron spill-out, gave fair predictions of the appearance sizes. In the present work the appearance size of the fifth charge state for aluminum clusters is reported. Furthermore, the appearance size for aluminum di-anions has been measured again, as suggested previously [15]. A new evaluation method for the determination of the experimental appearance sizes is proposed, and the experimental results are compared to the model prediction.

2 Multi-anion formation and stability

In this section, the formation of multiply negatively charged metal clusters by sequential attachment of electrons is described. Likewise, the stability of the poly-anionic clusters with respect to the reverse process, the electron detachment, is considered. In particular, the electron affinity and the Coulomb "barrier" potential of the precursor cluster anion determine the appearance size of a poly-anionic cluster.

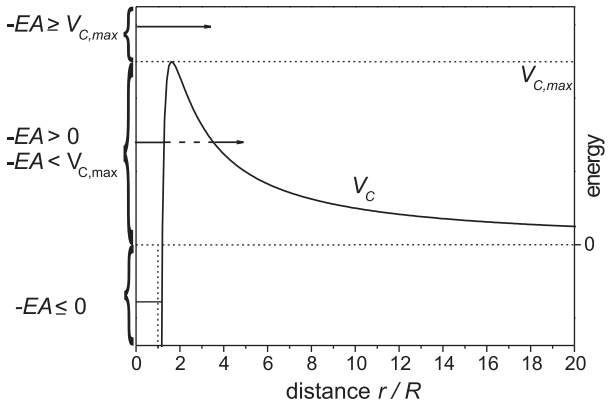

Fig. 1. Coulomb potential V_C and excess electron binding energies, given by the negative electron affinity $-EA$.

A cluster with a number of z excess electrons ($z > 0$) is formed by attachment of an electron to a precursor cluster already charged with $z-1$ excess electrons. Note, that in this notation the charge of the cluster is given by $q = -ze$, i.e. the charge state is described by $-z$.
In the conducting-sphere model the electron affinity of the precursor cluster is approximated by [2]

$$EA(R, z-1) = W - \left((z-1) + \frac{1}{2}\right) \frac{e^2}{4\pi\varepsilon_0 R} \quad , \qquad (1)$$

with the (bulk) work function W (for aluminum W=4.28 eV [17]). The cluster radius $R = R_a n^{1/3}$ is approximated by the atomic radius R_a, such that the volume of the cluster is given by the sum of the volumina of the constituents (for aluminum R_a=0.158 nm [16]). If the precursor cluster is

Table 1. Predicted "appearance sizes" n_{EA}, n_{ET}, and n_{V_C} for Al_n^{z-}, calculated for $t = 1$ s, the typical time range in the experiments, and no electron spill-out. See text for details.

z	n_{EA}	n_{ET}	n_{V_C}
2	33	29	10
3	151	109	23
4	414	248	40
5	880	445	61

sufficiently large, its electron affinity is positive ($EA > 0$) and an additional electron is stably bound to the cluster anion (Fig. 1). By equating the electron affinity (Eq. (1)) with zero, the corresponding cluster size n_{EA} is obtained from

$$n_{EA}^{1/3}(z) = \frac{e^2}{4\pi\varepsilon_0 W R_a}\left(z - \frac{1}{2}\right) \quad . \tag{2}$$

However, if the precursor cluster is already negatively charged, the next electron to be attached has to overcome the Coulomb potential (as a function of the distance r from the center of the cluster) [18]

$$V_C(R, z-1, r) = \frac{e^2}{4\pi\varepsilon_0}\left(\frac{z-1}{r} - \frac{R^3}{2r^2(r^2 - R^2)}\right) \quad , \tag{3}$$

(Fig. 1). In turn, the Coulomb potential prevents the excess electron - once attached - from immediate escape, even if the electron affinity is slightly negative ($EA \lesssim 0$), as in the case of clusters with $n \lesssim n_{EA}$. In the classical picture, the critical value for the (negative) electron affinity with respect to electron emission is then given by the height of the Coulomb potential, $-EA = V_{C,max}$ (Fig. 1), corresponding to a size n_{V_C} with

$$n_{V_C}^{1/3}(z) = \frac{e^2}{4\pi\varepsilon_0 W R_a}\left(z - \frac{1}{2} - \frac{z-1}{\rho} + \frac{1}{2\rho^2(\rho^2 - 1)}\right) \tag{4}$$

where the relative position $\rho = r_{C,max}/R$ of the Coulomb-potential maximum $V_{C,max}$ depends only on the charge state of the (precursor) cluster [19]. However, as the Coulomb potential represents a barrier of finite width, for anions with (negative) electron affinities in the range $0 < -EA < V_{C,max}$, the electron will eventually leave the cluster by tunneling through the barrier (Fig. 1). The respective lifetime for electron tunneling of those metastable poly-anionic clusters can be calculated by means of the Wentzel-Kramers-Brillouin (WKB) approximation [11,14,15].

The electron-tunneling lifetime $\tau_{ET}(n, z)$ of a poly-anionic cluster depends on its size and charge state. As a consequence, the definition of an appearance size n_{ET}, which takes into account the electron tunneling, has to be specified by a corresponding lifetime τ_{ET}. Because both above-mentioned sizes, n_{EA} and n_{V_C}, correspond to the limits zero and infinity of the tunneling lifetime, respectively, the relation $n_{V_C} \leq n_{ET} \leq n_{EA}$ holds for all τ_{ET} [7, 13–15] (Tab. 1). In contrast to n_{EA} and n_{V_C}, an explicit formula for n_{ET} can not be given. However, the lifetime

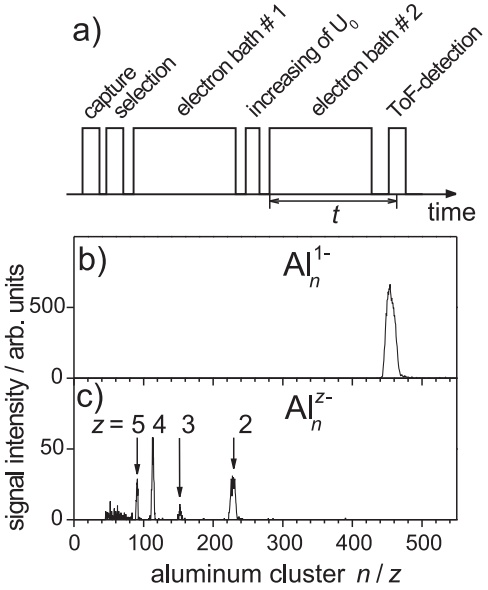

Fig. 2. (a) Temporal structure of the experimental cycle in the Penning trap. (b) Mass-spectrum of Al_n mono-anions after capture and selection (n = 440 - 470, U_0 = 15 V). (c) Mass spectrum of Al_n poly-anions after application of two electron baths with intermediate increase of the trapping voltage U_0 from 15 to 30 V. See text for details.

τ_{ET} can be calculated numerically as a function of the cluster size. The appearance size $n_{ET}(z)$ is then determined as the smallest cluster size, for which the lifetime is equal to or larger than τ_{ET}.

3 Experimental setup

Penta-anionic aluminum clusters have been produced at the ClusterTrap setup [20,21], by a modified electron-bath technique. A detailed description of this method has been published, recently [19]. In short, mono-anionic clusters are produced by a laser-vaporization source [22], accumulated in a linear radio-frequency quadrupole ion trap and then transferred into a Penning trap. There, the mono-anionic clusters are stored together with secondary electrons, produced by electron-impact ionization of argon gas in the Penning trap. Additionally, the argon gas causes thermalization of the clusters to room temperature. The poly-anionic reaction products are analyzed by ejection from the trap and time-of-flight (ToF) mass spectrometry.

In Figure 2a the experimental sequence in the Penning trap is indicated. After capture of the mono-anions, selection of a cluster size range is realized by removal of unwanted ions, using the SWIFT-method with dipolar ion-cyclotron-resonance excitation [23,24] (Fig. 2b). Application of two electron baths, with an intermediate increase of the trapping voltage U_0 from 15 V to 30 V, leads to the formation of di- , tri-, tetra-, and penta-anions (Fig. 2c). The observation time t for penta-anions is given by the reaction time in the second electron bath (Fig. 2a).

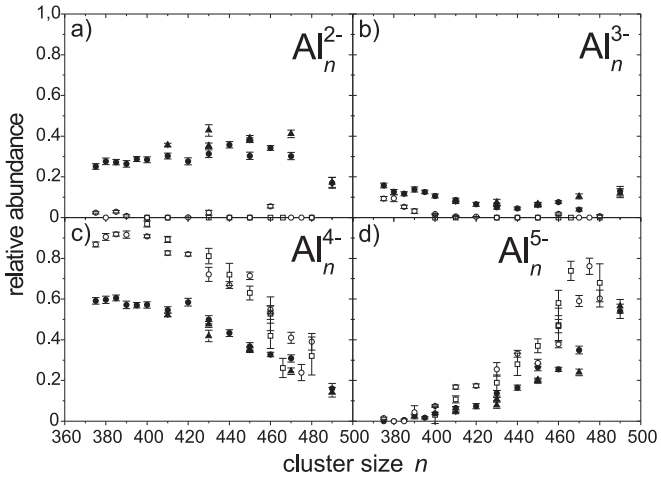

Fig. 3. Abundance of aluminum cluster di-(a), tri-(b), tetra-(c) and penta-anions (d), relative to the sum of all poly-anions, as a function of the cluster size, after application of two electron baths at $U_0 = 15$ V and 30 V, respectively. Different symbols (circles, squares and triangles) indicate different independent measurements. Data are from measurements with (open symbols) and without (filled symbols) removal of di- and trianions before application of the second electron bath.

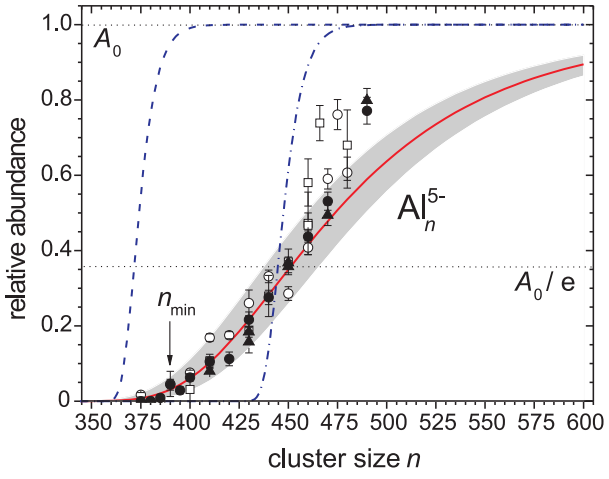

Fig. 4. (colored online) Abundance of penta-anionic aluminum clusters, relative to the sum of tetra- and penta-anions as a function of the cluster size. Data are from measurements with (open symbols) and without (filled symbols) removal of di- and trianions before application of the second electron bath. Expected abundances due to Eq. (5), without (dash-dotted line) and with inclusion of the electronic spill-out are indicated ($\delta = 0.7$ Å, dashed line). The solid line and the gray-shaded area mark the region of abundance for a modified Richardson-Dushman law ($T = 300$ K for $\alpha = 0.347(3)$). Details are given in Sect. 6.

The intermediate increase of the trapping potential is necessary due to two opposing effects [19]: On the one hand, high-mass mono-anions delivered from the cluster source require a low trapping voltage U_0 to be trapped, according to an upper limit of the mass-over-charge ratio of ions that can be trapped at a given U_0 [25]. On the other hand, a minimum U_0 is required to trap electrons with sufficient energy to overcome the Coulomb potential of poly-anionic clusters for further electron attachment [19,26].

4 Experimental Results

4.1 Penta-anionic aluminum clusters

For the investigation of penta-anionic aluminum clusters mono-anions in the size range $n = 375$ to 490 have been studied. Due to the low count rates, cluster ranges covering 10 sizes, rather than a single cluster size, were selected corresponding to a relative size range of about ±1.3%. The selected cluster mono-anions were exposed to two electron baths, as described in Sec.3.

In Figure 3 the abundances of di-anions (a), tri-anions (b), tetra-anions (c) and penta-anions (d) relative to the sum of all detected poly-anions are shown as function of the cluster size n. In the size range monitored, aluminum cluster di-, tri- and tetra-anions are produced.

In one set of measurements, all poly-anions formed in the first electron bath were exposed to the second electron bath (filled symbols). Di- and trianions show a constant abundance of about 30% and 10%, respectively (filled symbols in Fig. 3a and b). Up to $n = 420$, tetra-anions show a constant relative abundance of 60%, before dropping to 15% with increasing cluster size (filled symbols in Fig. 3c). This decrease is accompanied by the appearance of penta-anions, which increase from 0 to about 50 % at around $n \approx 490$ (filled symbols in Fig. 3d).

In another set of measurements, the tetra-anions were selected, i.e. di- and trianions were removed from the trap, before the application of the second electron bath. These data of tetra- and penta-anions (open symbols in Fig. 3 c and d) show qualitatively the same behavior as the first set of measurements.

For comparison of both sets of measurements, the abundance of penta-anions relative to the sum of tetra- and penta-anions is plotted in Fig. 4 (open and filled symbols). Both data sets overlap, confirming that the penta-anion production is governed by the tetra-anion abundance in the two cases. The smallest aluminum cluster penta-anion, Al_n^{5-}, for which a signal peak was distinguished from noise in the ToF-spectra is $n_{min} = 390 \pm 5$.

4.2 Di-anionic aluminum clusters revisited

The appearance size of di-anionic aluminum clusters Al_n^{2-} for an electron-tunneling lifetime of $\tau_{ET} = 1$ s is expected at $n_{ET} = 29$. The smallest size observed in previous experiments, $n_{min} = 34$ [13], was above the predicted value, although it was later suggested to be smaller [15]. Figure 5 shows the relative abundance of aluminum cluster di-anions of recent sets of measurements (marked by different symbols). The di-anion yield increases with cluster size up to 60% in the size range from $n = 26$ to 34. The

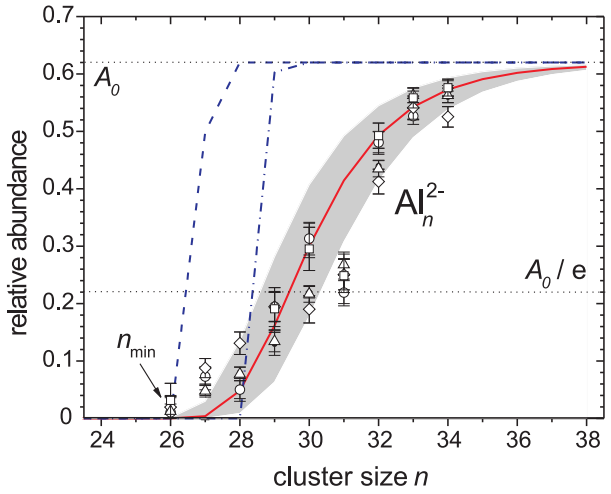

Fig. 5. (colored online) Abundance of di-anionic aluminum clusters, relative to the sum of mono- and di-anions as a function of the cluster size. Data are from different measurements (circles, squares, triangles and diamonds). Expected abundances due to Eq. (5), without (dash-dotted line) and with inclusion of the electronic spill-out ($\delta = 0.1$ Å, dashed line) are indicated. The solid line and the gray-shaded area mark the region of abundance for a modified Richardson-Dushman law for $T = 300$ K, $\alpha = 0.515(10)$. Details are given in Sect. 6.

smallest aluminum cluster di-anion, Al_n^{2-}, for which a signal peak was distinguished from noise in the ToF-spectra is $n_{min} = 26$.

5 Data evaluation

Previously, the calculated appearance sizes n_{ET} for tunneling lifetimes $\tau_{ET} = 1$ s of aluminum cluster di-, tri- and tetra-anions were directly compared to the respective smallest cluster anions observed in experiment [13–15]. This method was based on the assumption that any metastable cluster species detected after an observation time of $t = 1$ s has a lifetime $\tau_{ET} \geq t$. The smallest sizes observed for Al_n^{3-} and Al_n^{4-} were smaller than the calculated n_{ET} [14,15]. To match the model predictions with the experimental findings, an electron spill-out [27] was included in the calculations. It accounts for an exponential decrease of the valence electron density beyond the cluster radius, yielding an increased effective cluster radius $R_{eff} = R_a n^{1/3} + \delta$, and a decreasing predicted appearance size n_{ET} [14,15].

In the following, a different approach is used for the comparison between calculation and experiment. From the lifetime $\tau(n, z)$ of a poly-anionic cluster species, its (relative) abundance $A(t)$ expected at the observation time t after production can be approximated by the decay law

$$A(t, n, z) = A_0 e^{-t/\tau(n,z)} \quad , \qquad (5)$$

with the initial abundance $A_0 = A(t = 0)$. In particular, anions with lifetimes that are smaller than the observation time, $\tau < t$, may still be observed, although with decreased abundance.

In the experiments, the observation time was fixed at $t = 1$ s. With this fixed t, the ion abundance depends on the cluster size n via the size-dependent lifetimes $\tau(n, z)$ as given in Eq. 5.

The multi-anion abundance $A(n)$ is measured as a function of the cluster size n. Following Eq. (5), the observed appearance size n_{exp} is determined by its abundance being $A(n_{exp}) = A_0/e$, satisfying the condition $\tau(n_{exp}) = t$. The initial multi-anion abundance A_0 depends on experimental conditions (e.g. multi-anion production parameters like the electron density and the reaction time in an electron bath). In the following it is approximated by extrapolating the abundance of larger clusters, whose lifetimes $\tau(n)$ exceed the observation time t, i.e. $\tau(n, z) \gg t$ in Eq. (5) and thus $A(n) \to A_0$.

6 Discussion

6.1 Penta-anion abundance

The observed relative penta-anion abundance (Fig. 4) shows a slower rise than the abundance calculated with Eq. (5) for $t = 1$ s (normalized to the experimental A_0-value, dash-dotted line). In particular, the smaller clusters ($n \leqslant 440$) appear in higher abundance than expected from the model, indicating higher lifetimes, which correspond to lower-lying energy levels.

As discussed in Sect. 5, inclusion of the electron spill-out will increase the expected tunneling lifetimes τ_{ET} and thus shift the calculated abundance curve towards smaller clusters. While the spill-out factor was reported to be almost independent of the cluster radius, with a value of about $\delta = 0.7...0.8$ Å for aluminum [27,28], polarizability measurements indicate that δ is close to zero for a range of smaller aluminum clusters ($19 < n < 38$) [28]. For the larger penta-anionic clusters considered here, $\delta = 0.7$ Å has been assumed, which provides an adequate shift of the calculated abundances (dashed line in Fig. 4).

As for the shallower slope of the observed abundances, two possible explanations can be considered:

(i) The abundance curves are calculated under the assumption that A_0 is equal for all investigated cluster sizes, i.e. the probability for electron attachment in the electron bath is equal for all n. This assumption may not be valid. Assuming geometrical cross sections of spherical clusters, larger cluster should rather show an enhanced abundance than a depleted one. An experimental confirmation would require to determine A_0 for each n at several shorter observation times. For the time being it is assumed that A_0 is constant with respect to the cluster size.

(ii) The conducting-sphere model does not include any effect due to the finite cluster temperature, which might cause reduced lifetimes, and thus reduced abundances. Therefore, thermionic emission of electrons is considered for data analysis, as discussed in the following section.

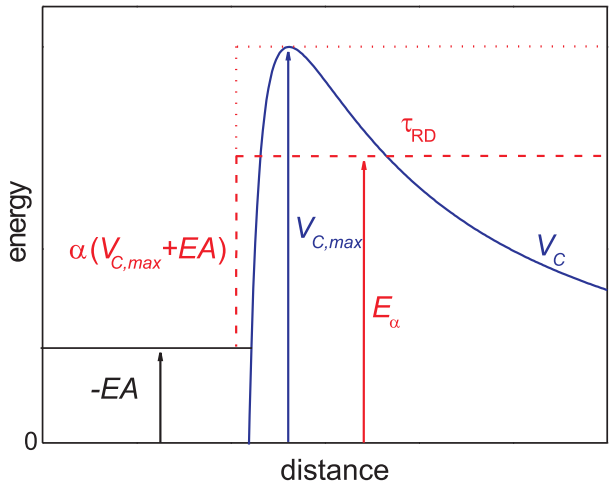

Fig. 6. (colored online) Potential as assumed for thermionic emission. See text for details.

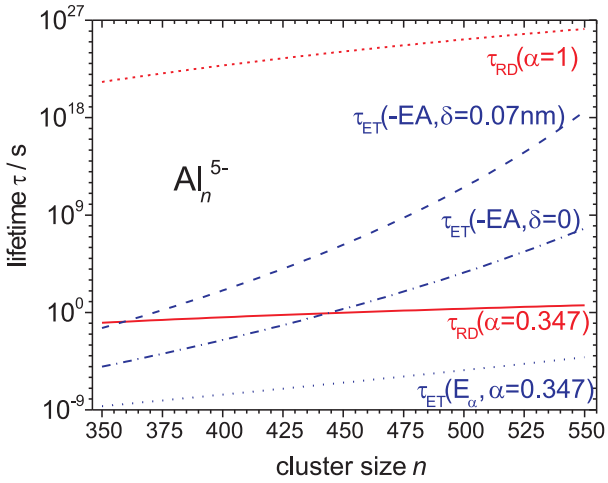

Fig. 7. (colored online) Calculated lifetimes of Al_n^{5-} for: electron tunneling through the Coulomb barrier (blue lines) for the electronic state $-EA$ with $\delta = 0.7$ Å (dashed line) and with $\delta = 0$ (dash-dotted line), and for the virtual state E_α ($\alpha = 0.347$, dotted line); and for thermionic emission (Eq. 6, red lines) at $T = 300$ K with $\alpha = 1$ (short-dashed line) and $\alpha = 0.347$ (solid line, corresponding roughly to the observed lifetimes). See text for details.

6.2 Thermionic emission

For the present approximation, lifetimes of cluster anions with respect to thermionic electron emission are calculated by the current density of emitted electrons as described by the Richardson-Dushman equation for bulk matter [29]. The corresponding emission rate for a spherical cluster,

$$\frac{1}{\tau_{RD}} = \frac{2\pi m_e (k_B T)^2}{h^3} \cdot 4\pi R_a^2 n^{2/3} \cdot exp\left[-\frac{\Phi}{k_B T}\right] \quad , \quad (6)$$

is given by means of a respective lifetime τ_{RD}, with k_B being the Boltzmann constant. The clusters are assumed to have an energy distribution given by room temperature, $T = 300$ K, according to the experimental conditions.
If the potential height is chosen as $\Phi = V_{C,max} + EA$ (Fig. 6, dotted lines, $\alpha = 1$), including the spill-out correction, the calculated rate for electron emission is by orders of magnitude too low to describe the observed abundances (Fig. 7, red short-dashed line). This ansatz leads in the $T = 0$K - limit to the appearance size n_{V_C}, as described in Sect. 2, including the spill-out. However, the data are well described (red solid line and shaded area in Fig. 4), if the potential is reduced to an effective height $\Phi = \alpha(V_{C,max} + EA)$ (Fig. 6, dashed line), with a barrier scaling factor $\alpha = 0.347(3)$, that is independent of the cluster size n.
The description of the experimental data by introducing an effective potential height in the Richardson-Dushman formula (Eq. 6) compensates the neglect of electron tunneling through the Coulomb potential. The energy level $E_\alpha = \alpha(V_{C,max} + EA) - EA$, which corresponds to the effective potential height (Fig. 6b), is not to be interpreted as a real electronic state, but as a qualitative measure of the thermal excitation of the cluster. The corresponding electron-tunneling lifetimes $\tau_{ET}(E_\alpha)$ for the actual barrier at that energy (Fig. 7, blue dotted line) are by orders of magnitude below the observed lifetimes (red solid line). The ratio of both, $P_\alpha = \tau_{ET}(E_\alpha)/\tau_{RD}(\alpha)$, may be interpreted as a mean probability for an electron to statistically access a (virtual) state at $E_\alpha$due to the temperature T. However, no explicit expression for P_α, nor a detailed discussion can be given here, as this would exceed the scope of this report.

6.3 Di-anion abundance

A situation similar to that of the penta-anions is found for the relative abundances of the di-anions. However, for a shift of the calculated abundance curve ($\delta = 0$, blue dash-dotted line in Fig. 5) towards smaller cluster sizes, a spill-out factor of only $\delta = 0.1$ Å is required (blue dashed line), in agreement with earlier reports [28] (Sect. 6.1). Again, thermal excitation of the room-temperature clusters is assumed to reconstruct the di-anion abundance curve. Application of the Richardson-Dushman formula (Eq. 6) with an effective potential height reproduces the observed abundances (for $\alpha = 0.515(10)$, red solid line and gray-shaded area in Fig. 5).

6.4 Comparison to model predictions

The new evaluation method has been applied to the aluminum penta- and remeasured di-anions, as well as to previous data sets of aluminum tri- and tetra-anions, which where obtained by the electron bath technique at ClusterTrap, with observation times of $t \approx 1$ s, too [14,15]. In Table 2 the relevant cluster sizes are listed as a function of the number of excess electrons z.
As described in Sect. 5, in previous investigations the smallest observed cluster sizes, n_{min}, were identified as the measured appearance sizes and directly compared to

Table 2. Predicted appearance size n_{ET} for electron spill-out δ, smallest observed cluster size n_{min}, appearance size n_{exp} (of Al_n^{z-}-clusters for $t = 1$ s), and barrier scaling factor α (Sect. 6.2).

z	δ/Å	n_{ET}	n_{min}	n_{exp}	α
2	0.1	27	26	30	0.515(10)
3	0.2	101	103	113	0.560(10)
4	0.5	212	215	250	0.366(2)
5	0.7	372	390(±5)	450(±5)	0.347(3)

the sizes n_{ET}, predicted for electron-tunneling with a lifetime of $\tau_{ET} = 1$ s, including the spill-out δ [13–15]. In fact, the smallest cluster sizes observed, n_{min}, are numerically close to the respective sizes n_{ET} (Tab. 2). However, they do not match the condition $A = A_0/e$ for an abundance that indicates a lifetime of 1 s (Sect. 5). Furthermore, the predictions refer to cold clusters ($T = 0$ K), whereas the experimental data are collected for room-temperature clusters, which meet the A_0/e-condition at sizes n_{exp}, that are 10 to 20% above the predicted n_{ET} (Tab. 2). This deviation is considered to be due to the thermal excitation of the cluster anions, as indicated by the description of the cluster abundance curves by means of thermionic emission with a barrier scaling factor α (Tab. 2), which is in good agreement with the experimental data (Figs. 4 and 5).

7 Conclusion and outlook

Anionic aluminum clusters in the gas phase with up to five excess electrons have been produced in a Penning trap. The relative abundances have been investigated as a function of the cluster size. The appearance size of Al_n^{-5} for a lifetime of 1 s has been determined experimentally to be $n_{exp} = 450(\pm 5)$, following a new evaluation procedure, taking into account the influence of the observation time on the abundances of the anions. This new method has also been applied to re-measured aluminum di-anions, yielding $n_{exp} = 30$, and to previously published data of aluminum tri- and tetra-anions.

The conducting-sphere approximation in combination with WKB-calculations for electron tunneling through the Coulomb potential has been used to estimate appearance sizes for poly-anionic metal clusters. However, this simple approach is neglecting internal energies. The observed appearance sizes are larger than the predicted ones, probably due to thermal excitation of the room-temperature cluster-anions. This assumption is supported by inclusion of thermionic electron emission into the data analysis, which roughly reproduces the observed ion abundances.

In summary, for the determination of the appearance size of poly-anionic clusters, the metastable character of these species has to be considered. Thus, statements on the appearance size require a specification of the lifetime or the observation time, as well as consideration of thermal excitation of the clusters. An extension of the measurements by systematic variations of the observation times and cluster temperatures would be helpful to get further experimental information on the stability of poly-anionic clusters with respect to electron emission. Likewise, it would be desirable to replace the simplified present approach of thermionic electron emission from a classical potential well of a reduced Coulomb barrier by a convolution that combines thermal excitation and tunneling through the barrier.

The project was supported by a Collaborative Research Center of the DFG (SFB 652-TP A03). F. Martinez and S. Bandelow acknowledge postgraduate stipends from the state of Mecklenburg-Vorpommern (Landesgraduiertenförderung) in the framework of the International Max Planck Research School on Bounded Plasmas.

References

1. Y. Ishii, Solid State Commun. **61**, (1987) 227.
2. J.P. Perdew, Phys. Rev. B **37**, (1988) 6175.
3. C. Yannouleas, and U. Landman, Chem. Phys. Lett. **210**, (1993) 437.
4. M. Seidl, J.P. Perdew, M. Brajczewska, and C. Fiolhais, J. Chem. Phys. **108**, (1998) 8182.
5. C. Yannouleas, and U. Landman, Phys. Rev. B **61**, (2000) R10 587.
6. A. Herlert, S. Krückeberg, L. Schweikhard, M. Vogel, C. Walther, Phys. Scr. **T 80**, (1999) 200.
7. L. Schweikhard, A. Herlert, S. Krückeberg, M. Vogel, and C. Walther, Philos. Mag. B **79**, (1999) 1343.
8. C. Yannouleas, U. Landman, A. Herlert, and L. Schweikhard, Eur. Phys. J. D **16**, (2001) 81.
9. C. Yannouleas, U. Landman, A. Herlert, and L. Schweikhard, Phys. Rev. Lett. **86**, (2001) 2996.
10. C. Stoermer, J. Friedrich, and M.M. Kappes, Int. J. Mass Spectrom. **206**, (2001) 63.
11. A. Herlert and L. Schweikhard, Int. J. Mass Spectrom. **229**, (2003) 19.
12. A. Herlert, L. Schweikhard, and M. Vogel, Eur. J. Phys. D **16**, (2001) 65.
13. N. Walsh, F. Martinez, G. Marx, and L. Schweikhard, Eur. Phys. J. D **43**, (2007) 241.
14. N. Walsh, F. Martinez, G. Marx, L. Schweikhard and F. Ziegler, Eur. Phys. J. D **52**, (2009) 27.
15. N. Walsh, F. Martinez, G. Marx, L. Schweikhard, and F. Ziegler, J. Chem. Phys. **132**, (2010) 014308.
16. Ch. Kittel, *Einführung in die Festkörperphysik*, 14th ed. (Oldenbourg Wissenschaftsverlag, London UK 1994).
17. M. Astruc-Hoffmann, G. Wrigge, and B. v.Issendorff, Phys. Rev. B **66**, (2002) 041404(R).
18. J. D. Jackson, *Classical Electrodynamics*, 3rd ed. (Wiley, New York 1998), pp. 5762.
19. F. Martinez, S. Bandelow, C. Breitenfeldt, G. Marx, L. Schweikhard, F. Wienholtz, and F. Ziegler, Int. J. Mass Spectrom. **313**, (2012) 30.
20. L. Schweikhard, K. Hansen, A. Herlert, G. Marx, and M. Vogel, Eur. Phys. J. D **24**, (2003) 137.
21. F. Martinez, G. Marx, L. Schweikhard, A. Vass, and F. Ziegler, Eur. Phys. J. D **63**, (2011) 255.
22. R. Weidele, U. Frenzel, T. Leisner, and D. Kreisle, Z. Phys. D **20**, (1991) 411.

23. A.G. Marshall, T.-C.L. Wang, T.L. Ricca, J. Am. Chem. Soc. **107**, (1985) 7893.
24. S. Guan, A.G. Marshall, Anal. Chem. 65, (1993) 1288.
25. L. Schweikhard, J. Ziegler, H. Bopp, and K. Lützenkirchen, Int. J. Mass Spectrom. Ion Process. **141**, (1995) 77.
26. A. Herlert, R. Jertz, J. Alonso Otamendi, A. J. Gonzalez Martinez, and L. Schweikhard, Int. J. Mass Spectrom. **218**, (2002) 217.
27. D. R. Snider, and R. S. Sorbello, Phys. Rev. B **28**, (1983) 5702.
28. W.A. de Heer, P. Milani, and A. Châtelain, Phys. Rev. Lett. **63**, (1989) 2834.
29. S. Dushman, Phys. Rev. **21**, (1923) 623.

8 Publications

2012:
Appearance size of poly-anionic aluminum clusters, Al_n^{z-}, $z = 2 - 5$
F. Martinez, S. Bandelow, C. Breitenfeldt, G. Marx, L. Schweikhard, F. Wienholtz, F. Ziegler, submitted to *Eur. Phys. J. D* (2012)

Lifting of the trapping potential during ion storage for multi-anion production in a Penning trap
F. Martinez, S. Bandelow, C. Breitenfeldt, G. Marx, L. Schweikhard, F. Wienholtz, F. Ziegler, *Int. J. Mass Spectrom.* **313**, 30-35 (2012)

2011:
The new ClusterTrap setup
F. Martinez, G. Marx, L. Schweikhard, A. Vass, F. Ziegler, *Eur. Phys. J. D* **63**, 255-262 (2011)

2010:
First observation of a tetra-anionic metal cluster, Al_n^{4-}
N. Walsh, F. Martinez, G. Marx, L. Schweikhard, F. Ziegler, *J. Chem. Pys.* **132**, 014308 (2010)

2009:
Atomic clusters in a Penning trap: investigation of their properties and utilization as diagnostic tools
N. Walsh, A. Herlert, F. Martinez, G. Marx, L. Schweikhard, *J. Phys. B* **42**, 154024 (2009)

Multiply negatively charged aluminium clusters II: Production of Al_n^{3-}
N. Walsh, F. Martinez, G. Marx, L. Schweikhard, F. Ziegler, *Eur. Phys. J. D* **52**, 27-30 (2009)

Unintended parametric ejection of ions from ion cyclotron resonance trap by two-electrode axialization
F. Martinez, A. Herlert, G. Marx, L. Schweikhard, N. Walsh, *Eur. J. Mass Spectrom.* **15**, 283-291 (2009)

Comparison of the low-energy decay mechanisms of C_{70}^+ and C_{70}^-
N. Walsh, A. Lassesson, F. Martinez, G. Marx, L. Schweikhard, *Vacuum* **83**, 761-767 (2009)

2008:
The elliptical Penning trap: Experimental investigations and simulations
M. Breitenfeldt, S. Baruah, K. Blaum, A. Herlert, M. Kretzschmar, F. Martinez, G. Marx, L. Schweikhard, N. Walsh, *Int. J. Mass Spectrom.* **275**, 34-44 (2008)

2007:
Multiply negatively charged aluminium clusters: Production of Al_n^{2-} in a Penning trap
N. Walsh, F. Martinez, G. Marx, L. Schweikhard, *Eur. Phys. J. D* **43**, 241-245 (2007)

2006:
Trap-based Cluster Research and Cluster-based Investigations on Ion Storage at ClusterTrap
L. Schweikhard, M. Breitenfeldt, A. Herlert, F. Martinez, G. Marx, N. Walsh
in "NON-NEUTRAL PLASMA PHYSICS VI", eds.: M. Drewsen, U.I. Uggerhoj, H. Knudsen, *AIP Conf. Proc.* **862**, p. 264-273, ISBN 978-0-7354-0360-4

2005:
Formation of fullerene dianions in a Penning ion trap
A. Lassesson, N. Walsh, F. Martinez, A. Herlert, G. Marx, L. Schweikhard, *Eur. Phys. J. D* **34**, 73-77 (2005)

2004:
Entwicklung und Test neuer Ionenquellen für die Clusterfalle
F. Martinez, *diploma thesis*, Universität Greifswald (2004)

9 Presentations

Talks

First Observation of Penta-Anionic Metal Clusters
Int. Conf. on Correlation Effects in Radiation Fields (CERF), Rostock, Sept. 2011

Preparation of Size and Charge-State Selected Trapped Cluster Ions
SFB 652 Workshop, Plau am See, September 2010

Parametric Excitation of Ions in an ICR-Trap by Axialisation using 2 Electrodes
DPG spring meeting, Hamburg, March 2009

Production of multiply negatively charged Aluminum clusters in a Penning trap
DPG spring meeting, Hamburg, March 2009

Investigation of Aluminum Cluster Anions in a Penning Trap
Clustertreffen, Berlin, September 2007

Investigations of atomic clusters in Penning traps
8. Eur. Fourier Transf. Mass Spectrometry (FTMS) Conf., Moscow, Aug. 2007

Photoactivation of Multiply Negatively Charged Aluminum Clusters
DPG spring meeting, Düsseldorf, March 2007

News from ClusterTrap: Investigation of Cluster Ions in a Penning Trap
39. Tagung der Dt. Gesell. für Massenspektrometrie (DGMS), Mainz, March 2006;
DPG spring meeting, Frankfurt, March 2006

Posters

Dependence of Multianion Production on the Trapping Voltage in a Penning Trap
DPG spring meeting, Stuttgart, March 2012

Penta-anionic aluminum clusters observed at ClusterTrap
DPG spring meeting, Dresden, March 2011

The New ClusterTrap Setup
XV. Int. Symp. Small Partic. & Inorg. Clusters (ISSPIC), Oaxaca, Sept. 2010

Modification of the ClusterTrap setup
Clustertreffen, Herzogenhorn, October 2009

Parametric Excitation of Ions in an ICR-Trap by Axialisation using 2 Electrodes;
Modification of the Penning-trap setup ClusterTrap;
News from the ClusterTrap
18th Int. Mass Spectrometry Conference (IMSC), Bremen, September 2009

News from the ClusterTrap
XIV. Int. Symp. Small Partic. & Inorg. Clusters (ISSPIC), Valladolid, Sept. 2008;
Int. Conf. on Correlation Effects in Radiation Fields (CERF), Rostock, Sept. 2008;
DPG spring meeting, Darmstadt, March 2008

Production and Laser Excitation of Multiply Negatively Charged Aluminium Cluster
DPG spring meeting, Düsseldorf, March 2007

Investigations of and with Fullerene Ions in a Penning Trap
International Conference on Clusters at Surfaces (ICCS), Warnemünde, May 2006

Investigation of Fullerene Ions in a Penning Trap
Clustertreffen, Bad Herrenalb, September 2005

Investigations of and with Fullerene Ions in a Penning Trap
12th Euro Summer School on Exotic Beams, Mainz, August 2005

Production of Fullerene Dianions in a Penning Trap
DPG spring meeting, Berlin, March 2005

Investigation of Cluster Ions in a Paul Trap
Symposium on Size Selected Clusters (S^3C), Brand, March 2005

Erklärung

Hiermit erkläre ich, dass diese Arbeit bisher von mir weder an der Mathematisch-Naturwissenschaftlichen Fakultät der Ernst-Moritz-Arndt-Universität Greifswald noch einer anderen wissenschaftlichen Einrichtung zum Zwecke der Promotion eingereicht wurde.
Ferner erkläre ich, daß ich diese Arbeit selbständig verfasst und keine anderen als die darin angegebenen Hilfsmittel und Hilfen benutzt und keine Textabschnitte eines Dritten ohne Kennzeichnung übernommen habe.

Greifswald, den 15. Juni 2012

Danksagung

Zum Abschluß möchte ich es nicht versäumen, all jenen Leuten zu danken, die zum Gelingen dieser Arbeit beigetragen haben.

Vorneweg gilt mein Dank Prof. Lutz Schweikhard und Dr. Gerrit Marx für die geduldige Betreuung, für den wertvollen Erfahrungsaustausch in vielen Gesprächen und Diskussionen, für zahlreiche Möglichkeiten zur Konferenzteilnahme, und für die vielen Gelegenheiten selbst tätig zu werden und dabei ordentlich zu lernen.

Ebenso danke ich allen Kollegen der Arbeitsgruppe für hilfreiche Hände und Köpfe, für zahlreiche Hinweise auf wichtige Kleinigkeiten, aber auch für die Vielfalt an sowohl sinnvollen als gelegentlich auch erholsam sinnfreien Gesprächen. Besonderer Dank gilt sämtlichen früheren und derzeitigen Kollegen des ClusterTrap-Teams, insbesondere Falk Ziegler, weiterhin Noelle Walsh, Steffi Bandelow, Albert Vass, Christian Breitenfeldt, Martin Breitenfeldt und Frank Wienholtz. Ebenso zu erwähnen seien die außer-häuslichen Kollegen Katja Fricke und Christian Brandt. Vielen Dank auch der treuen Kollegin K. Feepause die mit Keksen, Kuchen und Eis die Arbeitsgruppe bei Laune hielt.

Physiker-Kollegen können zwar (fast) alles erklären, aber (nur knapp) nicht alles selber machen, daher auch großer Dank für fachkräftige Unterstützung durch die Werkstatt und die Haustechnik, im Besonderen seien Erhardt Eich und Frank Scheffter zu nennen, sowie den Kolleginnen von Sekretariat und Verwaltung für die Abwicklung von Mengen an Bestellvorgängen und Dienstreiseformalitäten.

Gelegentliche Ausflüge in die Welt außerhalb der Physik ... ... -Institutswände wurden durch viele Freunde gewissenhaft begleitet. An alle jene herzlichen Dank für gemeinsame Erlebnisse wie Mittags-Mensa, Tatort-gucken, Mittendrin, Geokeller, und für jede einzelne "festliche Veranstaltung im privaten oder halböffentlichen Rahmen" [wikipedia.de], sowie zahlreiche andere soziale Geselligkeiten.

Großer Dank natürlich auch meiner großen Familie in Nah und Fern, insbesondere der Frau Mutter, allein schon aus kausalen Gründen.